The Abdus Salam
International Centre for Theoretical Physics

United Nations
Educational, Scientific
and Cultural Organization

International Atomic
Energy Agency

SMR/1758-9

"Workshop on Ion Beam Studies of Nanomaterials:
Synthesis, Modification and Characterization"

26 June - 1 July 2006

Ion Beam Applications in Defects and Strain Studies of Nano-Sized Structures

Anand P. Pathak
School of Physics
University of Hyderabad
India

ICTP Workshop on Ion Beam Studies of NanoMaterials:
Syntheis, Modification and Characterization
26 June - 1 July 2006

Ion Beam Applications in Defects and Strain Studies of Nano-Sized Structures

Anand P Pathak

School of Physics

University of Hyderabad, INDIA

Collaborators

Past

Dr V Harikumar
Dr AM Siddiqui
Dr LNS Prakash Goteti
Dr S.V.S. Nageswara Rao

Present

S Dhamodaran
N Sathish
J George
N Srinivas Rao

Collaborating Indian Institutes in Experimental work

Nuclear Science Centre, New Delhi (DK Avasthi)

Institute of Physics, Bhubaneswar (BN Dev)

Solid State Physics Laboratory, Delhi (R Muralidharan)

IGCAR Kalpakkam (KGM Nair)

Ion Beams in Materials Science

Motivation

- Introduce atoms into solid-state matter without constraints of equilibrium thermodynamics
- Production of novel materials and states of matter
- Doping of semiconductors : device development
- Development of materials for reactors
- Basic Physics : To understand processes involving bound atoms/ions, molecules and clusters------→ Inter-atomic Potentials

The stopping power of solids for energetic charged particles occupies central role in all the fundamental as well as application oriented studies. The low velocity region and high velocity region are well understood by now but the medium velocity region is most difficult because none of the approximations of low or high velocity theories are applicable.

IN ADDITION; ONE HAS TO CONSIDER CHANNELING EFFECTS for CRYSTALLINE SOLIDS; WHICH REDUCE THE TOTAL STOPPING:

Ion Solid Interactions

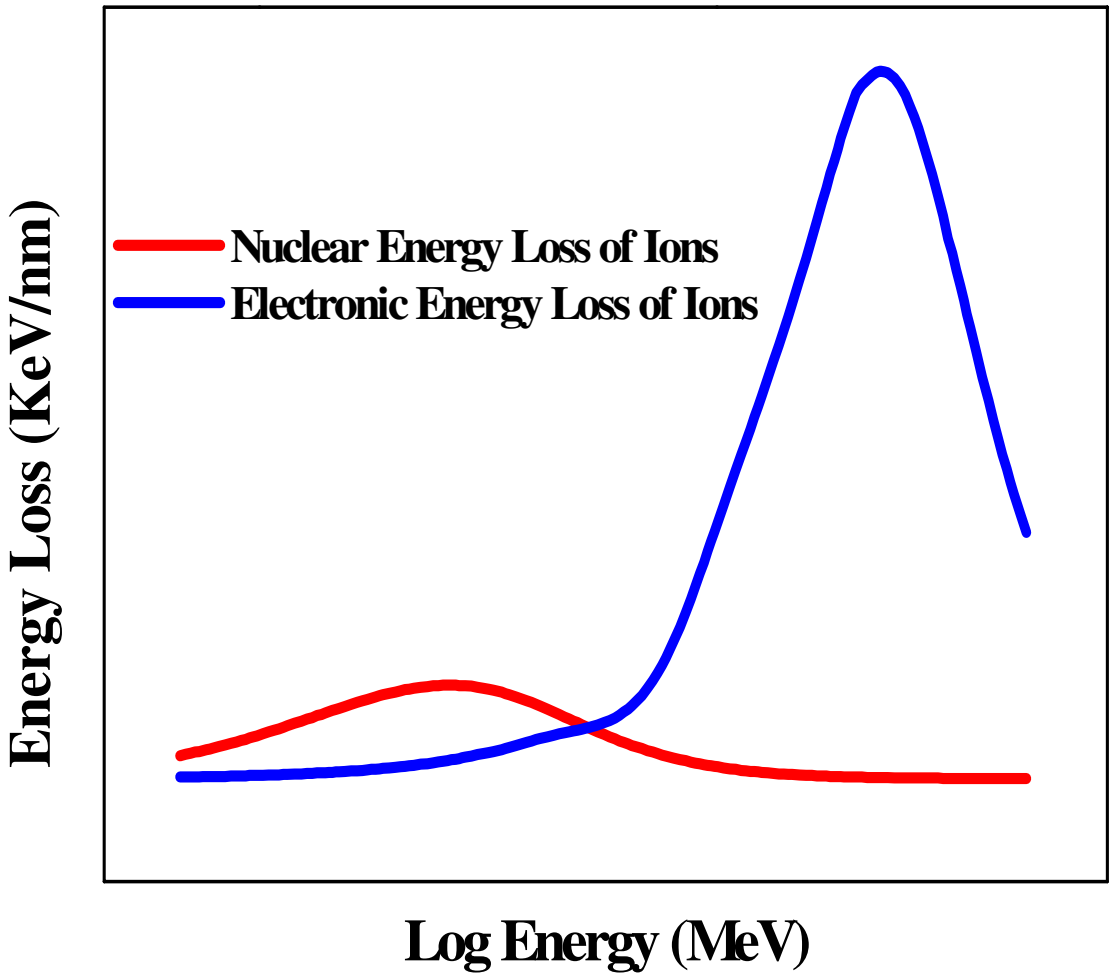

Example: Energy loss of Ag Ions in GaAs

Energy loss and range of energetic ions in matter

Electronic stopping: Energy loss from electron-ion and electron-electron interactions

- **Excitation and ionization**
- **Capture, loss and charge exchange**
- **Other processes: Autoionization, Auger**
- **Binary encounter electron model**
- **Solid state effects: Transport, electronic structure**
- **Secondary electron induced effects**

The Nuclear Stopping reduces further under channeling conditions and one has to worry only about ELECTRONIC STOPPING except at very low velocities i.e at the end of the projectile trajectory.

This last part of trajectory is seriously affected by the straggling and creation of damage and displacements of the target atoms;

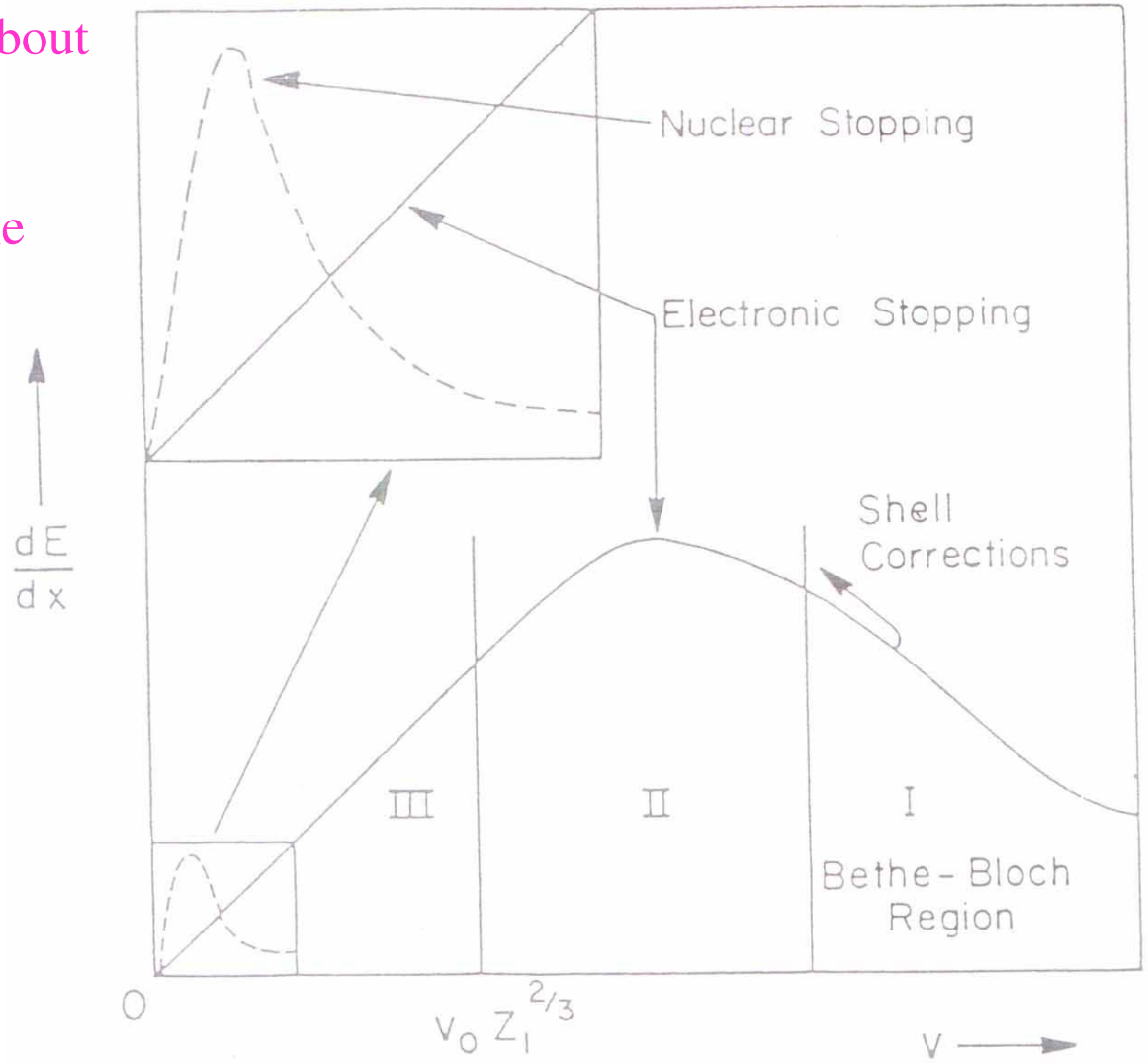

Nuclear Energy loss

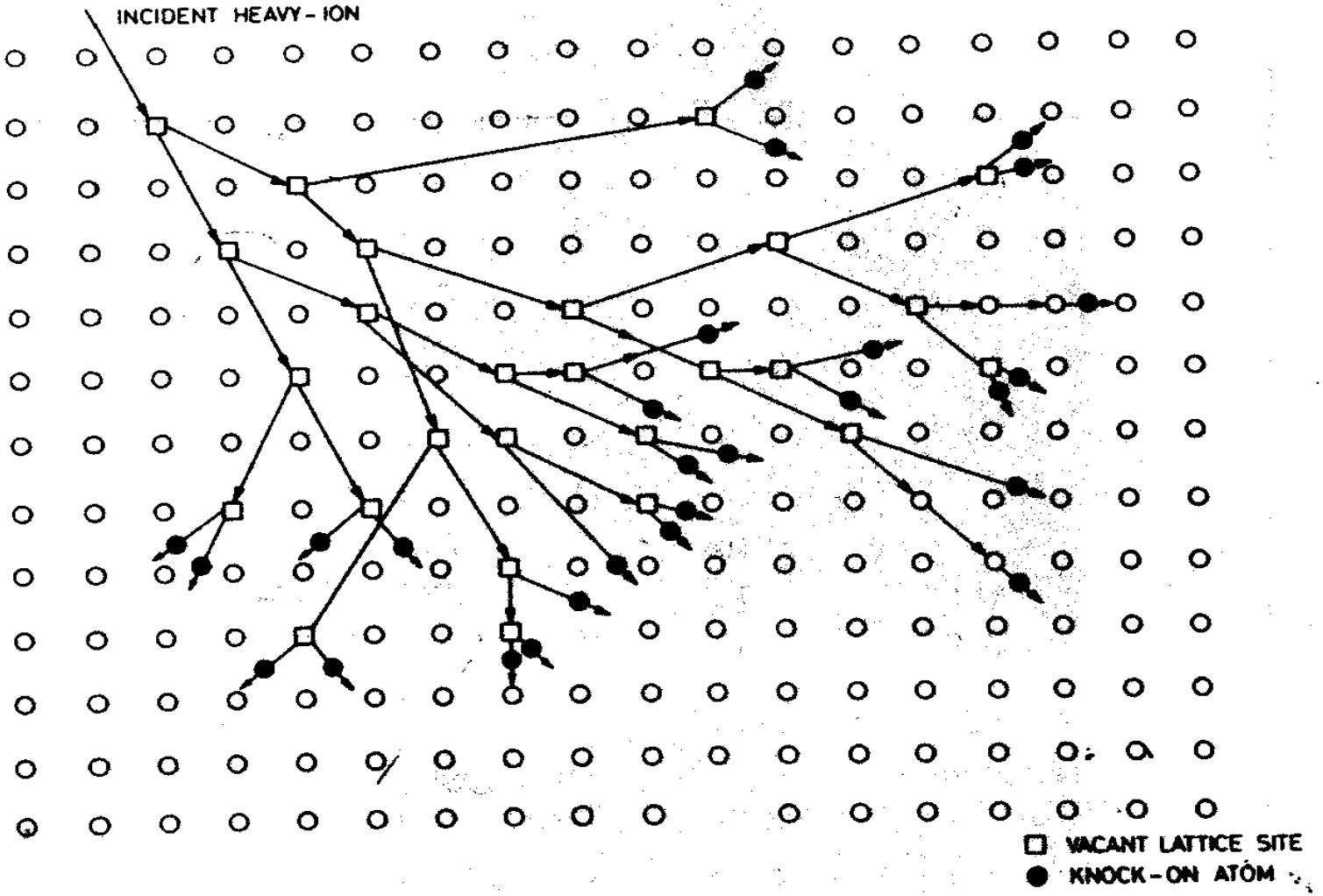

The Techniques: RBS & ERDA

Rutherford's α – scattering experiment was the first successful attempt to study the structure of atom. Since then, energetic ion beams have been used as probes to study the structure of atom, nucleus and SOLIDS.

The ultimate goal of the subject is to understand the basic principles of ion – solid interactions and then to apply those principles in the development of modern technology.

Ion beams can be used to synthesize, characterize and / or engineer the materials properties[down to Nano scale]

Ion Beam Characterization ……..

RBS

Rutherford backscattering spectrometry (RBS) detects the energies and amount of the backscattered ions from a solid target. The incident probe is a mono-energetic light ion beam. The scattered particles from the target are energy analyzed by a particle detector positioned at a specified backscattered angle with respect to the incident ion beam (typically ranging from 100-170 depending on the specific analysis).

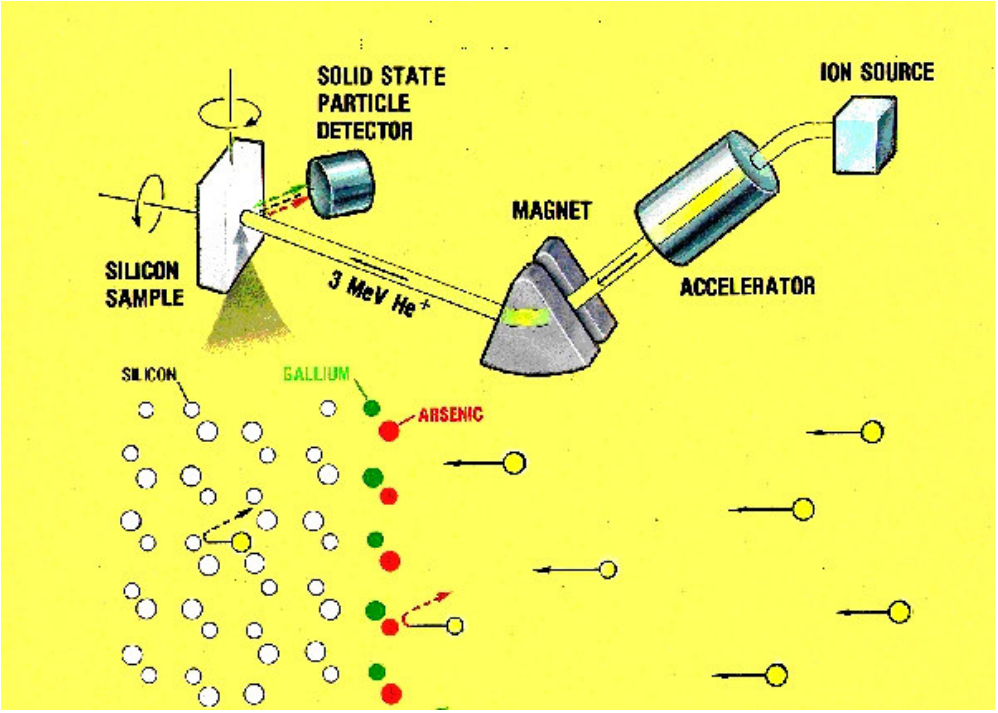

Kinematical Factor

$$K_{rbs} = \frac{E_s}{E_p} = \left[\frac{\left(M_t^2 - M_p^2 \sin^2\theta\right)^{1/2} + M_p \cos\theta}{M_p + M_t} \right]^2$$

$$Y = \sigma \Omega Q N_s$$

ERDA

The sensitivity of RBS is overcome by its complimentary technique ERDA where the recoils emerging from a tilted target sample are detected in forward direction at an angle larger than the tilt angle. Instead of light particles, heavier projectiles are employed from heavy ion accelerators. Scattered ions and unwanted heavy recoils will be stopped in a stopping foil placed in front of the detector.

Kinematical Factor

$$K_{erda} = \frac{E_r}{E_p} = \frac{4M_pM_t}{(M_p + M_t)^2}\cos^2\phi$$

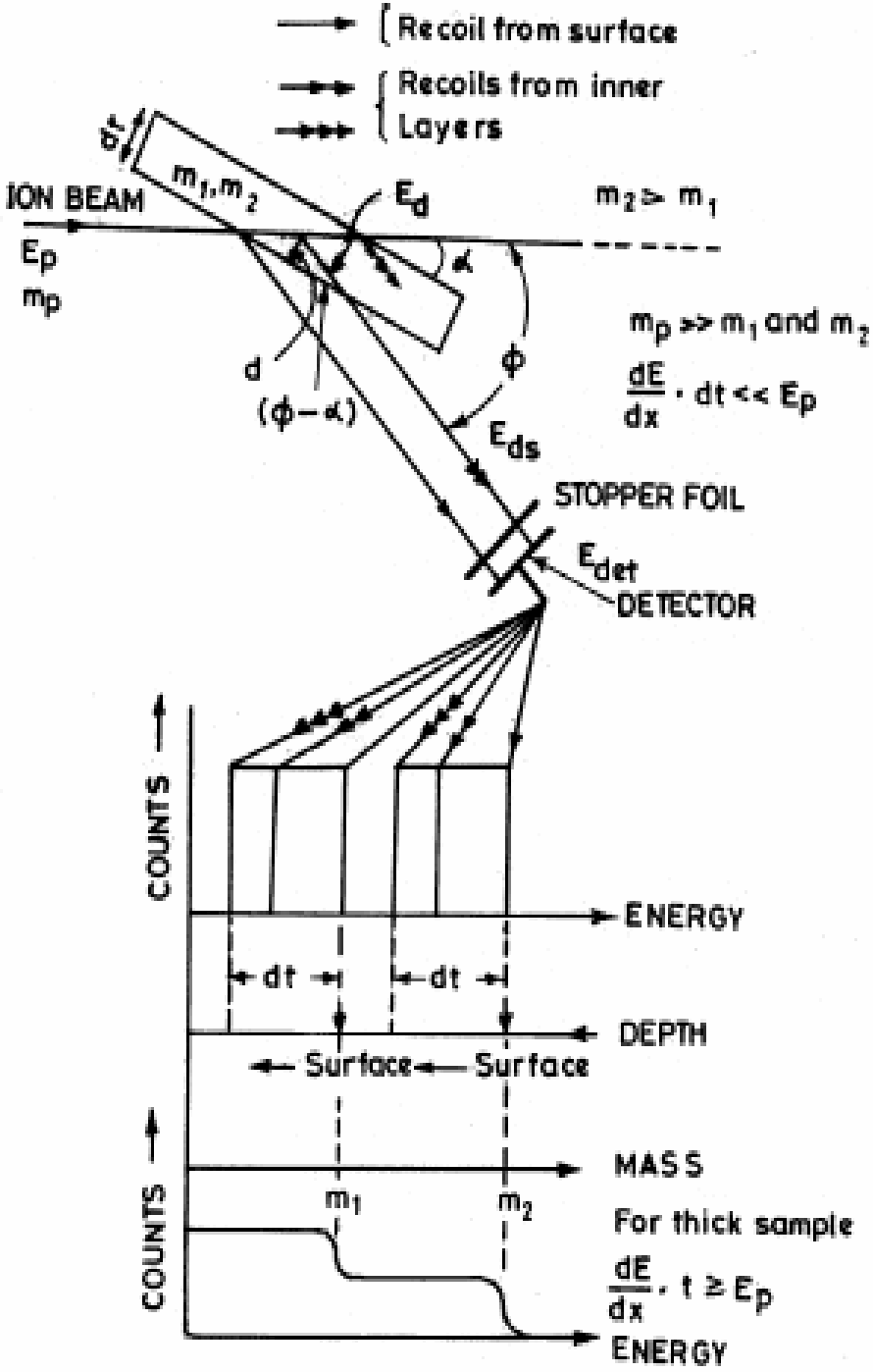

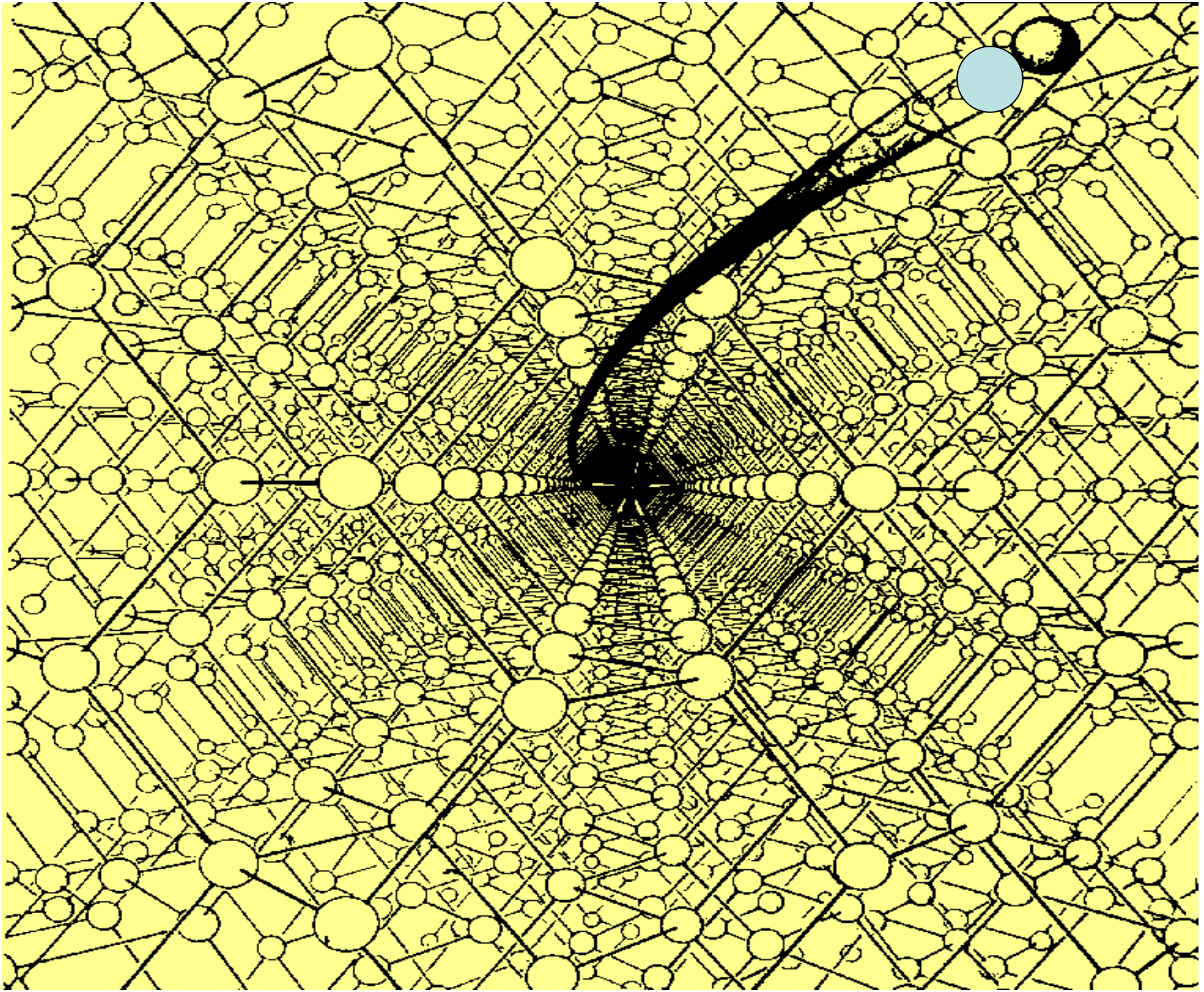

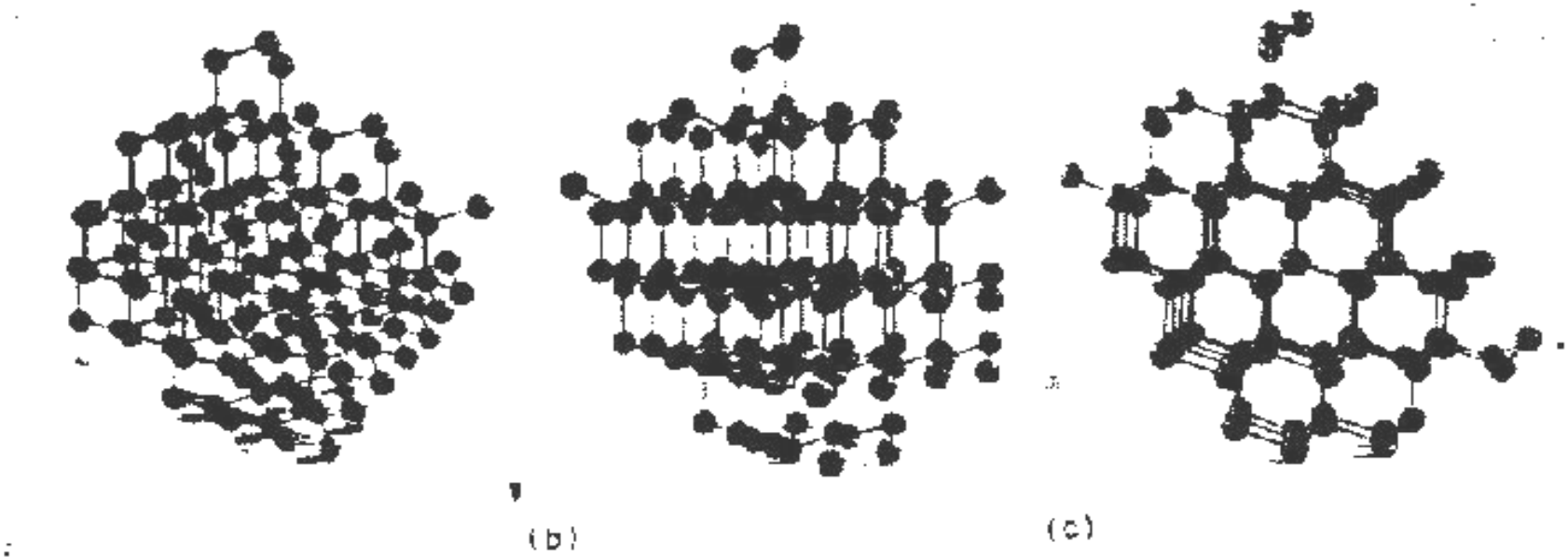

Fig. 8.1 Model of lattice atoms showing the atomic configuration in the diamond-type lattice viewed along (a) random, (b) planar, or (c) axial directions.

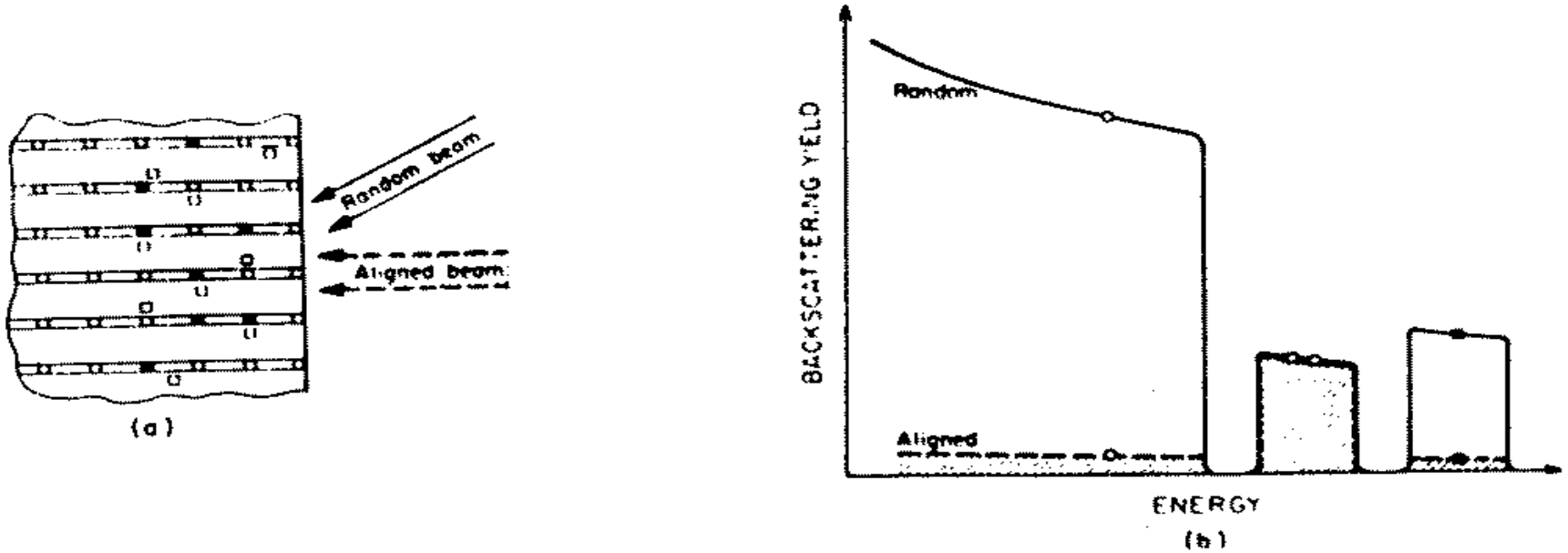

Ion Channeling

Ion channeling occurs in single crystals. There exists void space between crystal planes and rows called channel. When an energetic particle is aligned to such channels, it will be steered in the channel by the small angle gentle collisions with atoms sitting on the channel walls. The probability of large angle scattering like RBS will be decreased drastically. This results in a great reduction in the yield of RBS (up to 95%). Any defect in the crystal will immediately affect the channeling condition.

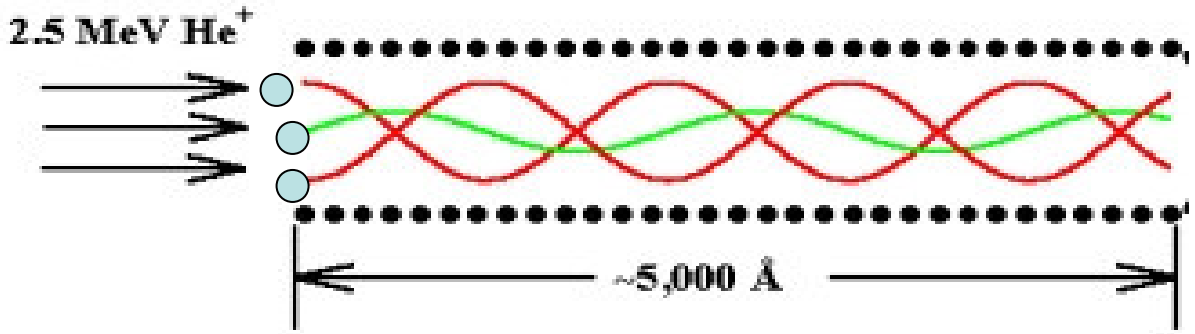

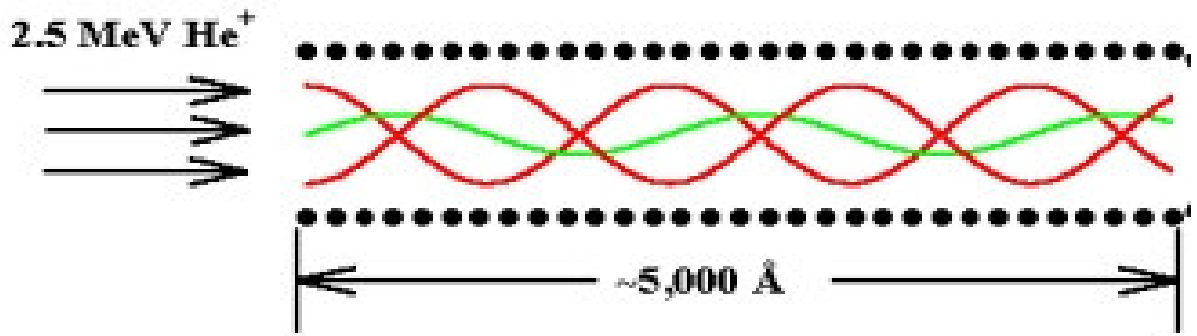

Ion channeling distinguishes between directions in a crystal

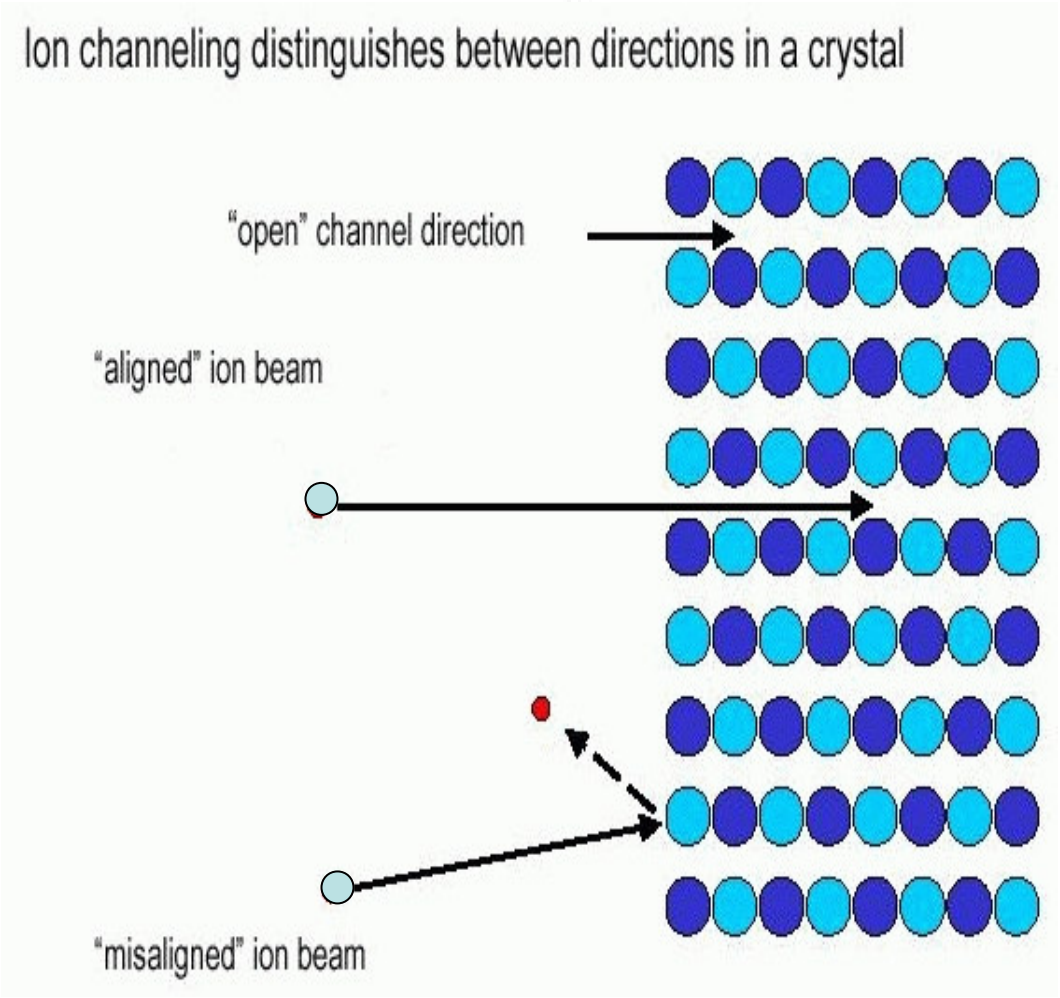

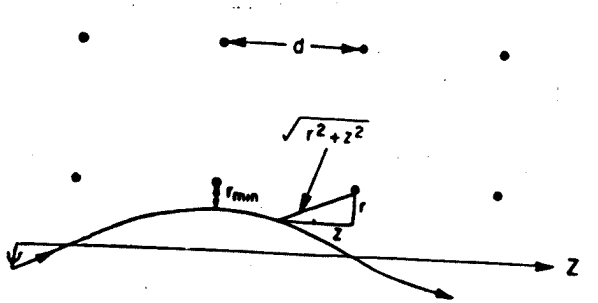

$$\frac{r_{\min}}{v \sin \psi} > \frac{d}{v \cos \psi}$$

$$\psi_1 \propto E^{-\frac{1}{2}}$$

$$\frac{r_{\min}}{v\sin\psi} > \frac{d}{v\cos\psi}$$

$$U(r) = \int_{-\infty}^{\infty} \frac{dz}{d} V\left(\sqrt{z^2 + r^2}\right)$$

$$V_{Li}(R) = Z_1 Z_2 e^2 \left[\frac{1}{R} - \frac{1}{\sqrt{R^2 + C^2 a^2}}\right]$$

$$U(r) = \frac{Z_1 Z_2 e^2}{d} \ln\left[\left(\frac{Ca}{r}\right)^2 + 1\right]$$

$$\psi < \psi_1 = \sqrt{2 Z_1 Z_2 e^2 / dE} \qquad E > E_1 = 2 Z_1 Z_2 e^2 d / a^2$$

$$\psi < \psi_2 = \sqrt{Ca\psi_1 / d\sqrt{2}} \qquad \mathbf{E < E_1}$$

$$\psi_p = \sqrt{2\pi N_p Z_1 Z_2 e^2 a / E}$$

Lattice strain measurement using channeling

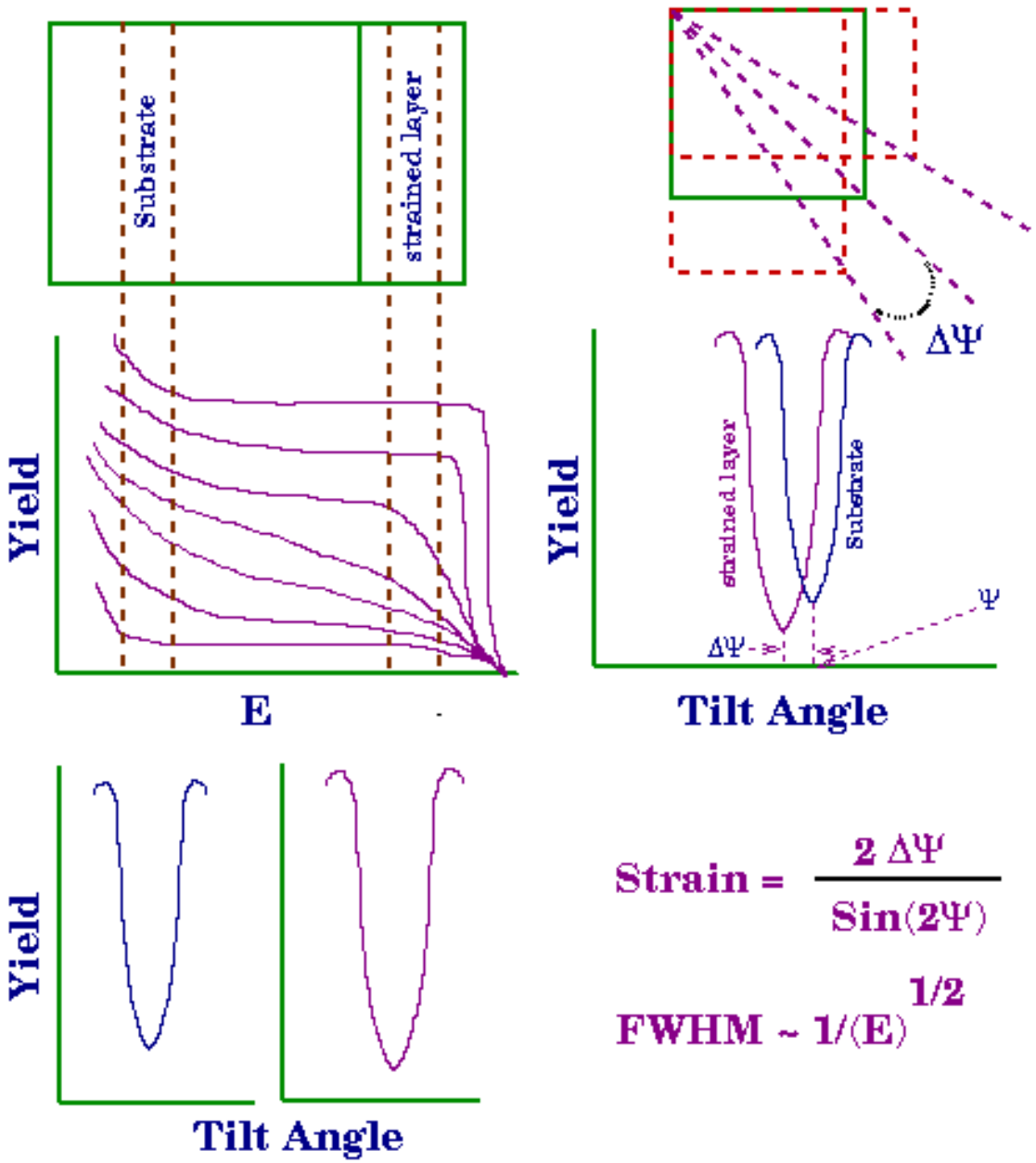

$$\text{Strain} = \frac{2\,\Delta\Psi}{\text{Sin}(2\Psi)}$$

$$\text{FWHM} \sim 1/(E)^{1/2}$$

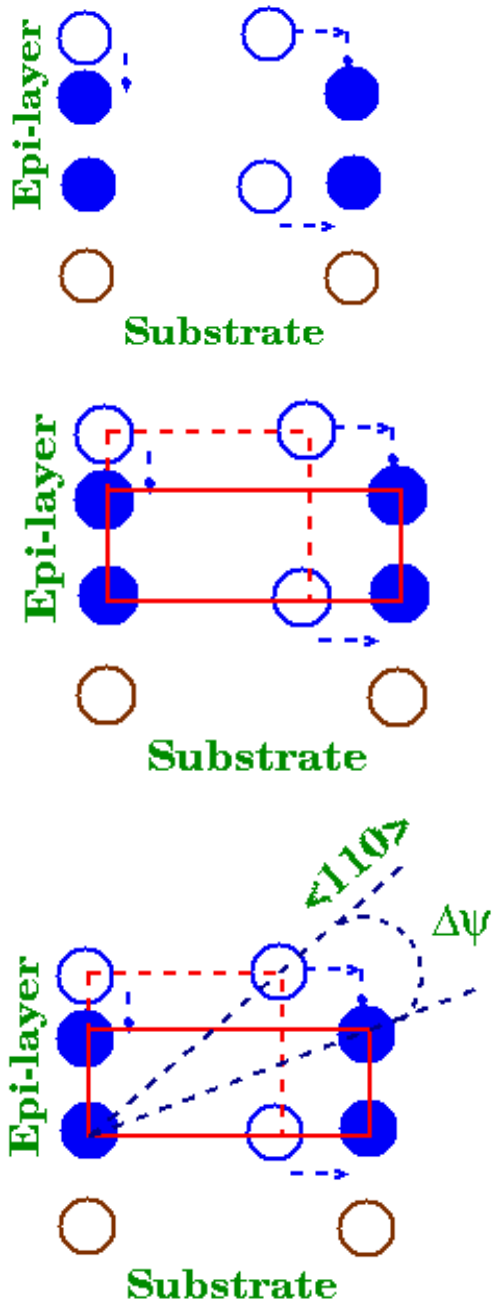

High Resolution X-Ray Diffraction

- **HRXRD is an essential and versatile tool to characterize heteroepitaxial structures. It gives a measure of the crystalline and interface quality. The thickness and composition of the period of the superlattice can be estimated.**

- **It is very sensitive to the lattice strain with a sensitivity of about 10^{-5}.**

- **The data are X-ray intensity distributed in the vicinity of a reciprocal lattice point, which is integrated over the direction normal to the diffraction plane by scanning with a detector wide open in that direction to obtain the reflection pattern.**

- **The width of the substrate peak gives the angular resolution.**

- **The shift ($\Delta\theta$) in the center of the satellite peak system w.r.t the substrate peak determines the strain [$(\Delta d/d)_{\perp} = \mathit{cot}\theta\Delta\theta$ for the Bragg angle θ].**

Low Velocity Stopping Power

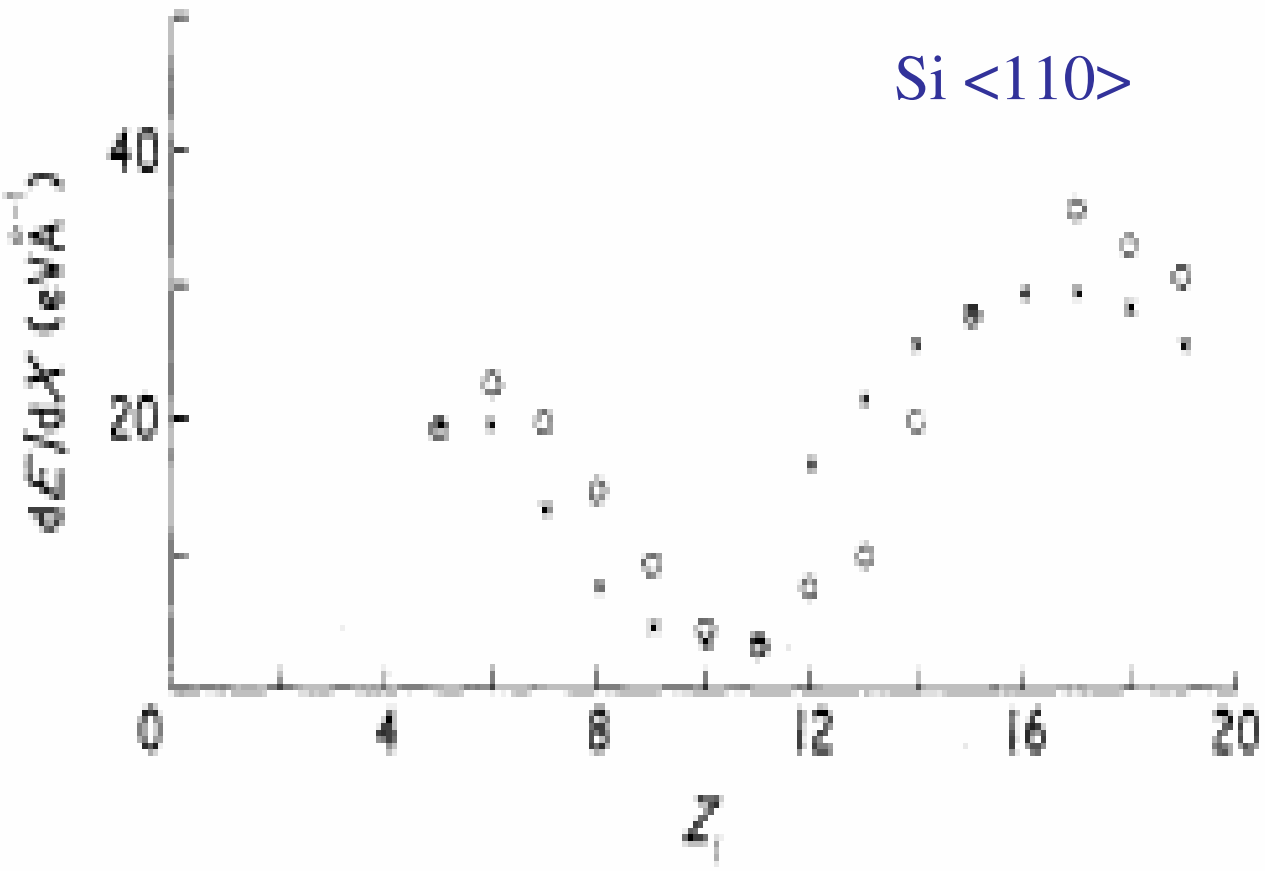

Figure 2. The stopping power of silicon for heavy ions channelled along the ⟨110⟩ direction. ○ experiment of Eisen; × theory.

A P Pathak

Au <110>

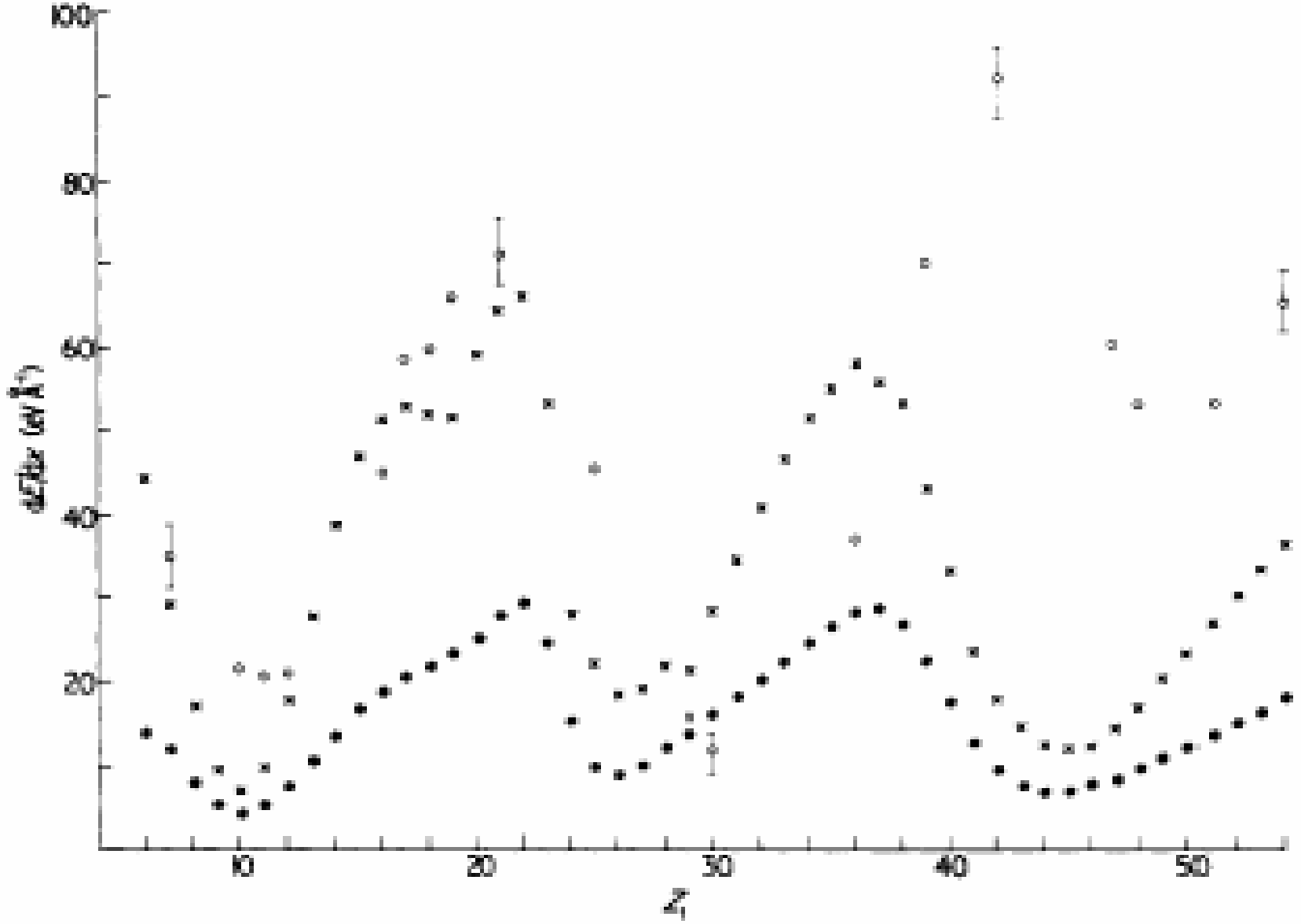

W<100>

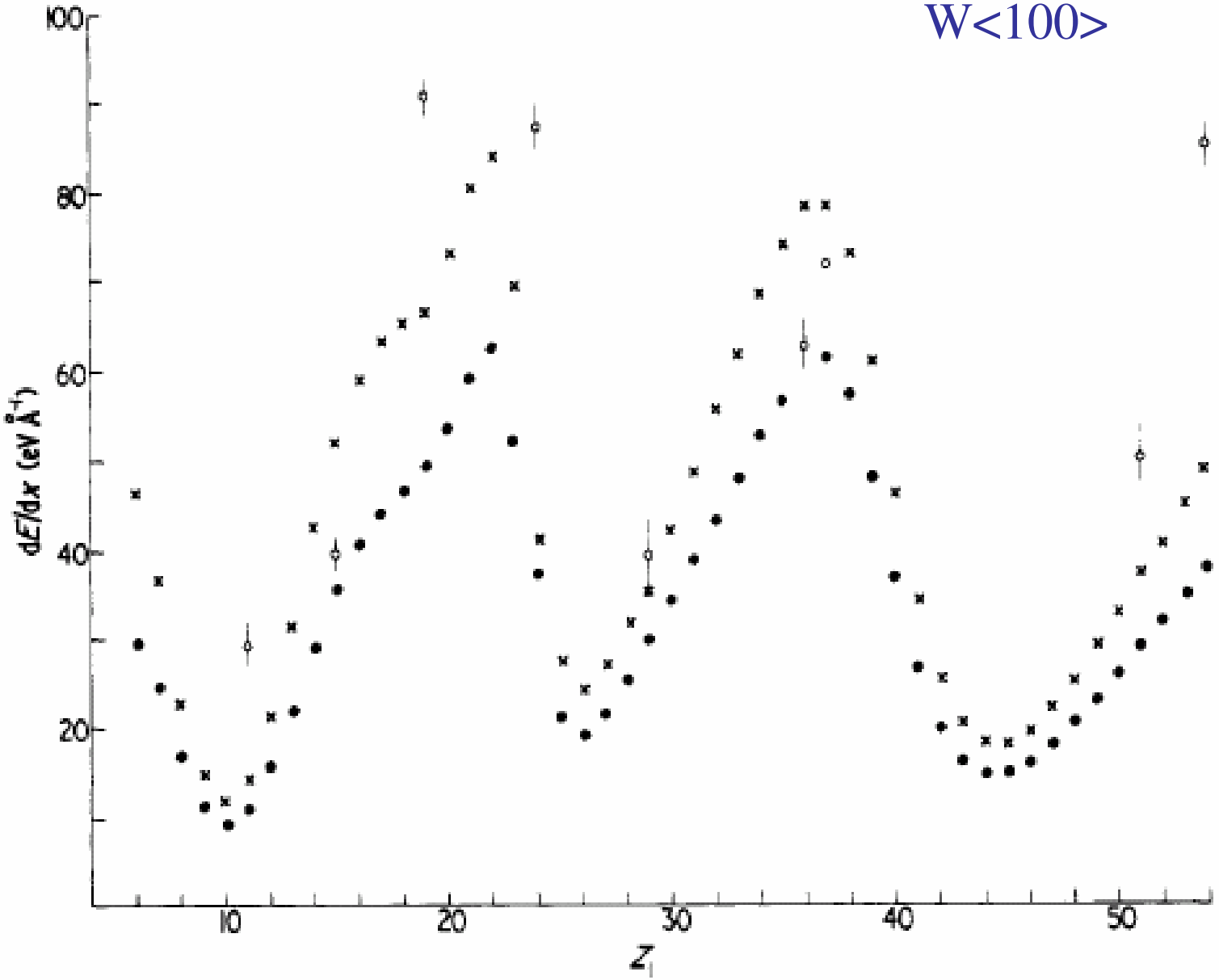

Figure 2. Stopping power of tungsten for heavy ions channelled along ⟨100⟩ direction. ○Experiment (Eriksson *et al* 1967); × theory (total contribution of 6s and 5d electrons); ● contribution of 6s electrons.

The mean energy lost by an ion of velocity v to an electron gas of density n is given by[7]

$$-\frac{dE}{dX} = nmv^2 Q_d \quad , \tag{1}$$

where m is the electronic mass and Q_d the momentum-transfer cross section, given by

$$Q_d = \frac{4\pi}{k^2} \sum_l (l+1) \sin^2(\eta_l - \eta_{l+1}) \quad . \tag{2}$$

Using atomic units, these two equations [(1) and (2)] can be combined to read

$$-\frac{dE}{dX} = 4\pi n \bar{Q}_d = 4\pi n \sum_l (l+1) \sin^2(\eta_l - \eta_{l+1}) \quad . \tag{3}$$

The magnitude of the phase shift η_l is then determined by the competition between the attractive potential $U(r)$ and repulsive centrifugal potential $l(l+1)/r^2$ and as such is computed by finding the shift of nodes of the solution (5) with respect to the corresponding node of the Bessel function (6) for large r.

The atomic field $U(r)$ in which the target electrons are scattered is taken to be statistical Thomas-Fermi potential. For use in the numerical calculations, this was fitted to a sum of screened Coulomb form (i.e., Moliere type)

$$U(r) = \frac{1}{r} \sum_{i=1}^{3} a_i \exp(-b_i r) \quad . \tag{7}$$

Here, η_l is the lth partial-wave phase shift and has been determined by solving the radial part of the Schrödinger equation

$$\frac{d^2G_l}{dr^2}+\left[k^2+U(r)-\frac{l(l+1)}{r^2}\right]G_l=0 \quad . \tag{4}$$

As is well known, for $U(r)$ varying faster than $1/r$, the asymptotic form of the solution G_l of Eq. (4) is

$$G_l(r)\sim\sin(kr-\tfrac{1}{2}l\pi+\eta_l) \quad . \tag{5}$$

and without atomic field $[U(r)=0]$, Eq. (4) gives the Bessel function solution whose asymptotic form is

$$G_l(r)\sim j_l(kr)\overset{r\to\infty}{\longrightarrow}\sin(kr-\tfrac{1}{2}l\pi) \quad . \tag{6}$$

The square bracket in eq. (4) is actually [$k^2 - U_{eff}(r)$] of usual radial Sch. Eqn. where:

$$U_{eff}(r) = -U(r) + l(l+1)/r^2$$

Here the first term is Z_1 dependent attractive potential responsible for atomic binding and second term is the centrifugal potential (repulsive). For a given l, as Z_1 increases, U_{eff} becomes negative for some Z_1 and can support a BOUND state of that l^{th} partial wave, according to Levinson's theorem, corresponding phase shift undergoes a sudden phase change of π

Partial wave contributions to Momentum Transfer Cross sections

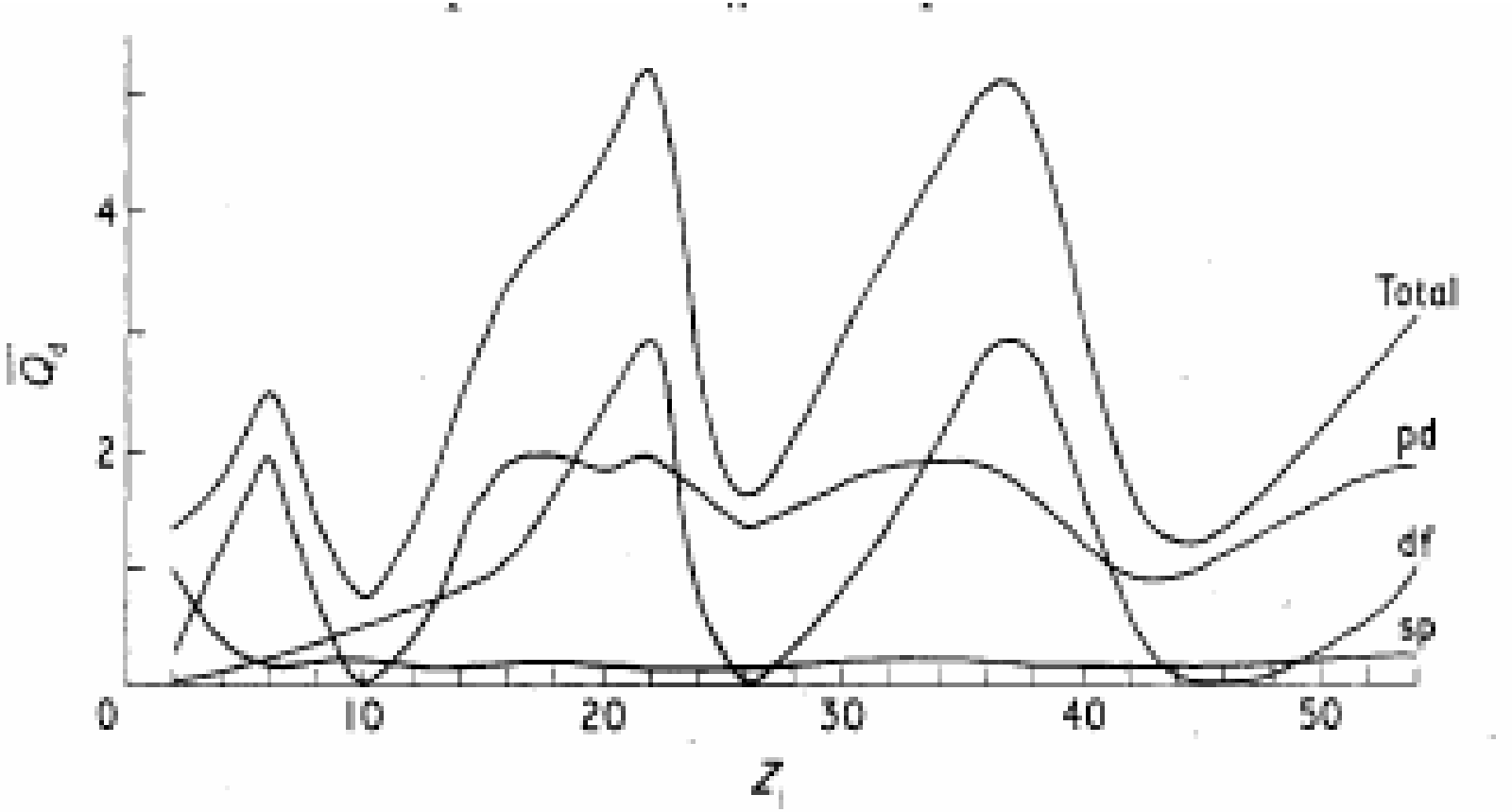

Figure 1. The quantity $(k^2/4\pi)\,Q_l$ against Z_1 for $k = 0{\cdot}75$ au. The curves labelled sp, pd, df are the partial contributions from terms with $l = 0, 1, 2$ respectively in equation (2).

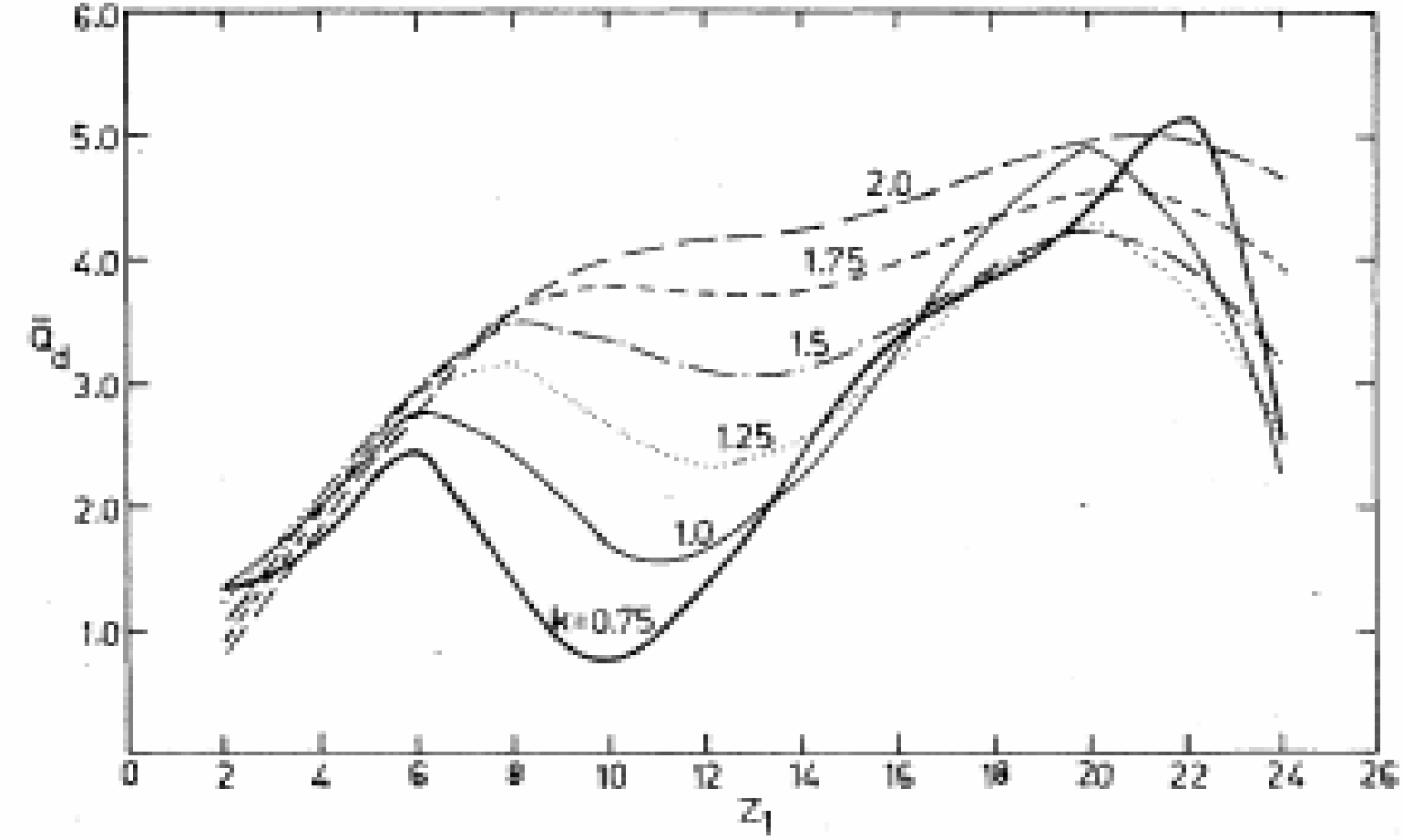

FIG. 1. The variation of the momentum-transfer cross section $\bar{Q}_d$ with the projectile atomic number Z_1 for various values of projectile velocity given in atomic units, by $k = 0.75$, 1.0, 1.25, 1.5, 1.75, and 2.0. The stopping power is obtained through Eq. (3).

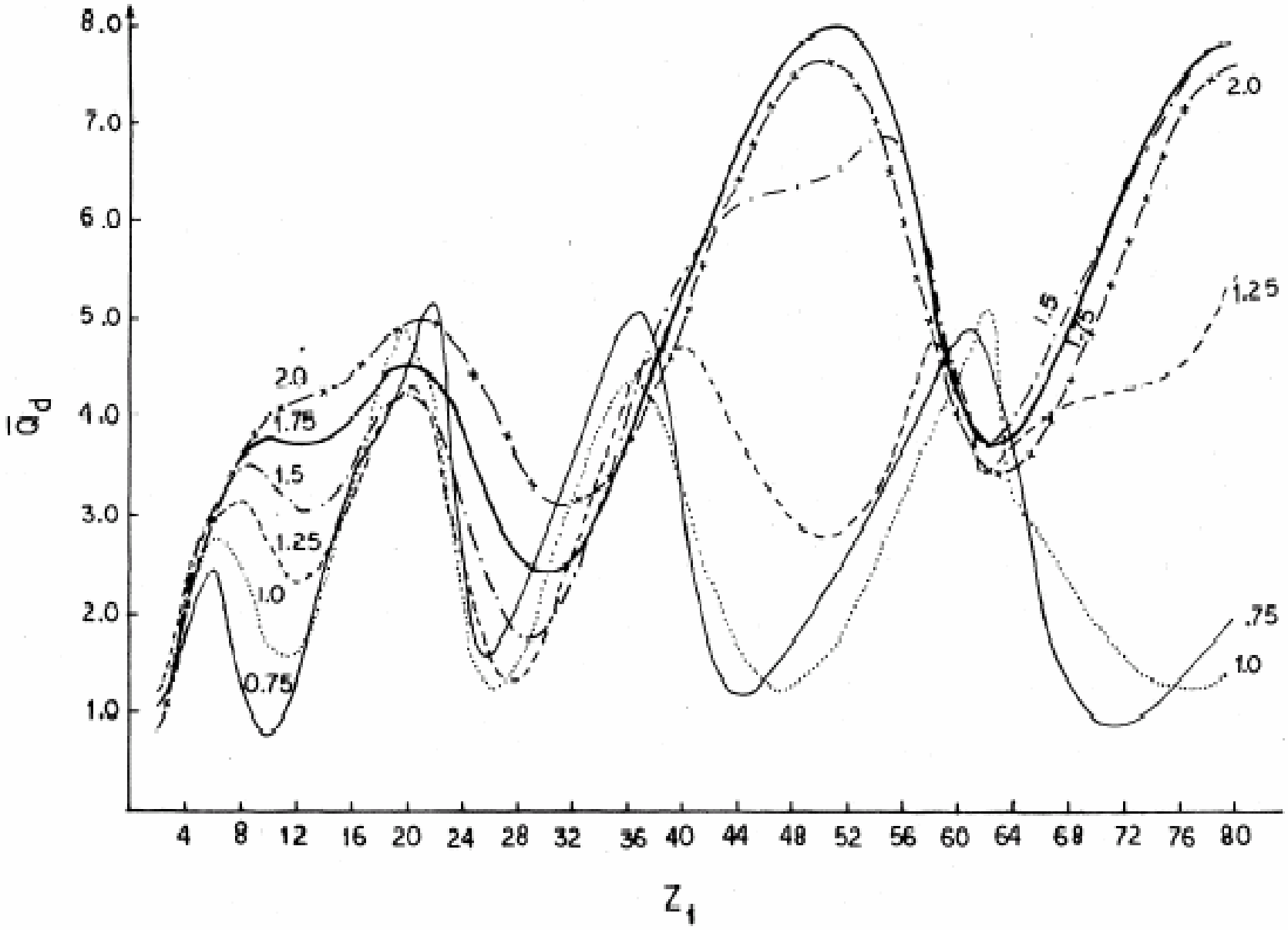

FIG. 1. Variation of momentum-transfer cross section Q_d with the projectile atomic number Z_1 for various values of projectile velocity given in atomic units by $k = 0.75$, 1.0, 1.25, 1.5, 1.75, and 2.0. The stopping power is obtained through Eq. (1).

Ion Implantation

- **Implantation terminology**
  - **Dose Φ --> *no. of projectiles (atoms/cm^{2}Sec)***
  - **Beam current $I = (\Phi\, q_i\, A) / t$**

    q_i --> charge per ion A --> beam area

    t --> implantation time
  - **Projected range and projected straggle**

    Range: Total distance travelled by ion before stopping

    Projected range R_p : Projection of range // ion beam

    Projected straggle : Statistical fluctuation of R_p

Ion Implantation

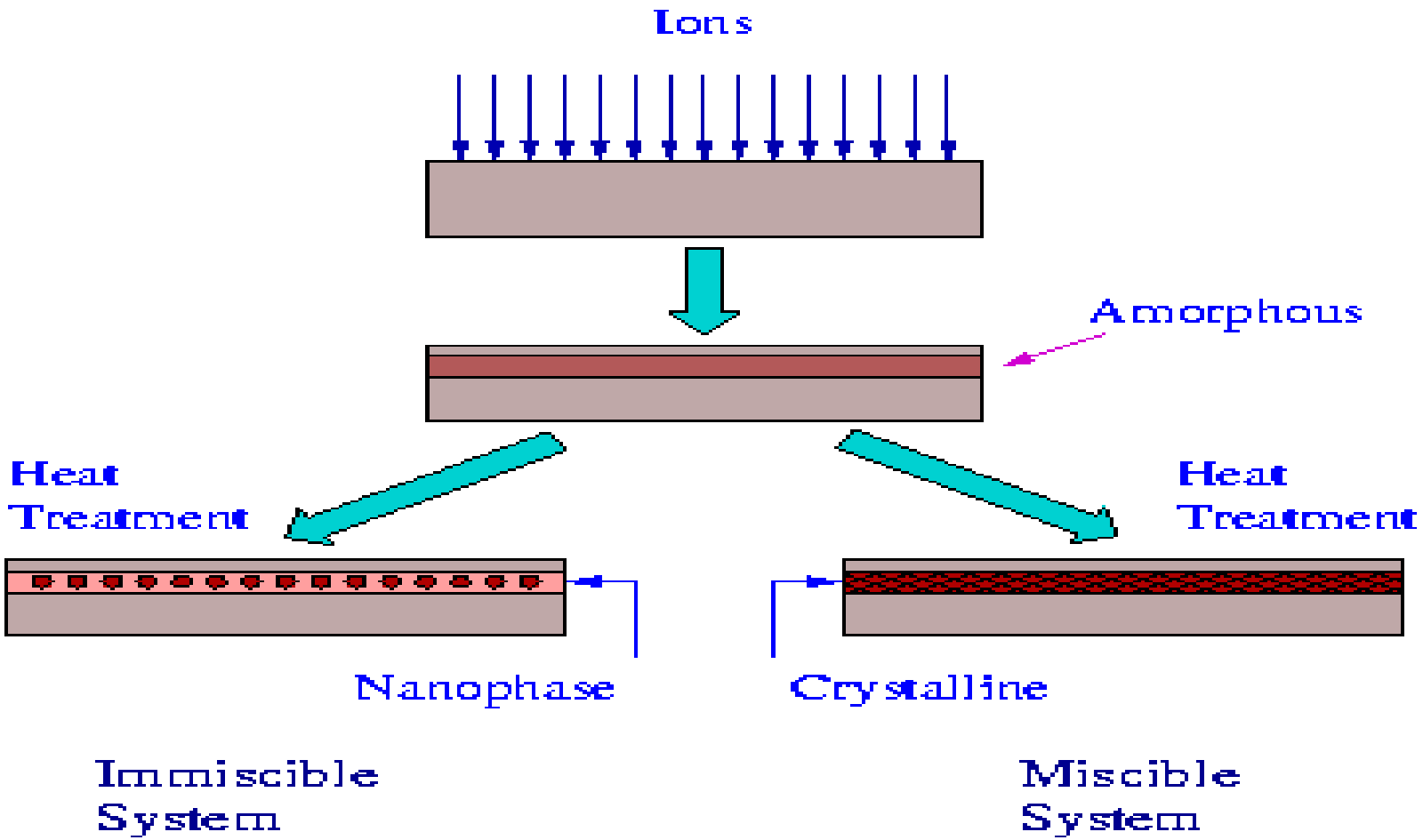

CHANNELING STOPPING POWER

The position dependent stopping power is calculated using the well-known Bethe-Bloch based expression

$$S(x) = \frac{4\pi Z_1^2 e^4}{m\mathrm{v}^2} \sum_{i=1}^{5} \rho_i(x) \ln\left(\frac{2m\mathrm{v}^2}{\mathrm{I_i}}\right)$$

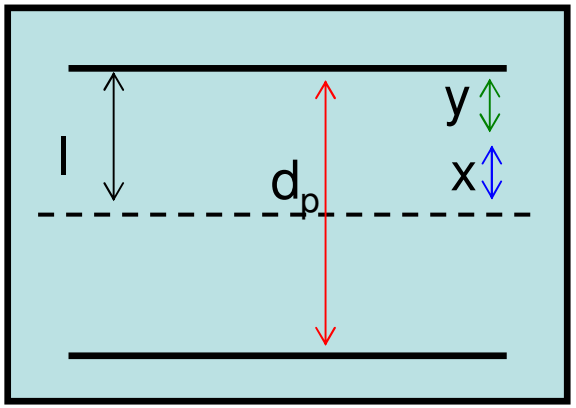

$$\rho_i(x) = \rho_i^{(1)}(l-x) + \rho_i^{(1)}(l+x)$$

$$\rho_i^{(1)}(y) = 2\pi N d_p N_i e^{-2\xi_i y}\left[\sum_{k=0}^{2n_i-1} \frac{(2n_i-1)!\, y^{2n_i-k-1}}{(2n_i-k-1)!(2\xi_i)^{k+1}}\right.$$

$$\left. -\frac{1}{R}\sum_{k=0}^{2n_i} \frac{(2n_i)!\, y^{2n_i-k}}{(2n_i-k)!(2\xi_i)^{k+1}}\right]$$

The position and energy dependences of energy loss have been separated by Robinson et al, to explain their experimental results of planar channeling stopping.

$$\sigma(x) = \frac{\mathrm{d}}{\mathrm{d}x}\left(\frac{2}{V_2''(0)}\left[V_2(x) - V_2(0)\right]\right); \qquad 0 \leqq x \leqq l\,,$$

where x is measured from the midpoint between the two pla primes denote differentiation with respect to x. The total elec given by

$$S(x) = s_0 + s_1(\sigma(x) - 1)\,,$$

All the energy dependence is contained i

S_0 and S_1

For example their functional forms depend on projectile and target parameters and the energy range. For low velocity we have velocity proportional increase and Lindhard and Bohr formulas. For high velocity, Bethe formula with appropriate logrithmic dependence on ionization energies for atomic target and dielectric function for electron gas in metals and in channeling situations.

$$V_2(x) = 2\pi Z_1 Z_2 e^2 N_p C a^2 \left(\frac{1}{l + a - x} + \frac{1}{l + a + x} \right),$$

where C is a constant ($= \sqrt{3}$), Z_1 and Z_2 are charge numbers atoms, respectively, $N_p (= 2lN)$ is the planar density of atom sity), and a is the usual Thomas-Fermi screening radius give

$$a = 0.8853 \frac{a_0}{(Z_1^{2/3} + Z_2^{2/3})^{1/2}}$$

with a_0 as the Bohr radius. This planar potential has been sh just a mathematical approximation and corresponds to an in power law screening,

$$V(r) = \frac{Z_1 Z_2 e^2}{r} \frac{Ca^2}{(r + a)^2},$$

where r is the interatomic separation. The planar potential (:

$$\sigma(x) = \frac{(l + a)^3}{[(l + a)^2 - x^2]^{3/2}}.$$

$$S(x) = \frac{4\pi Z_1^2 e^4}{mv^2} \sum_j \varrho_j(x) \ln \frac{2mv^2}{I_j},$$

where v is the velocity of the projectile, m t
the j-th shell of the target (silicon), I_j the c
silicon has no free electrons, the individual
for each electronic orbit.

As in the case of continuum potentials,
culate the effective planar charge density fr
trons density

$$\varrho(r) = \frac{1}{4\pi r^2} \sum_j \omega_j r^2 N_j^2 R_j^2 ,$$

Assuming Si <110> as a regular hexagon, the effective charge density can be calculated for use in the energy loss formula.

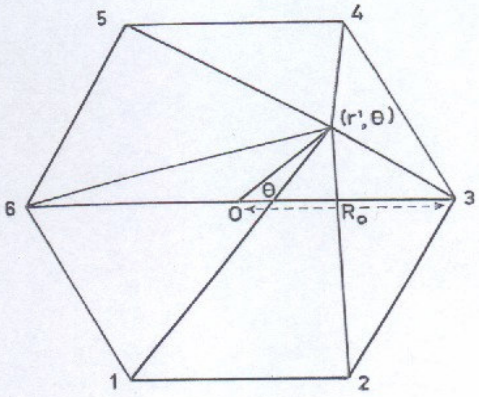

Fig. 1. Approximate ⟨110⟩ axial channel in diamond structure crystals. Each of the corners represents a string perpendicular to the plane of drawing

density of target atoms seen by the projectile inside ⟨110⟩ axial channel of silicon is taken to be given by the phenomenological expression for the number density

$$n_e(r', \theta) = \frac{1}{\pi d} \sum_{p=1}^{6} \frac{1}{(r' + R_0^2 - 2r'R_0 \cos(p\pi/3 - \theta))} \tag{5}$$

and therefore the effective valence electron density at any point inside the channel is

$$\varrho_v(r', \theta) = 4n_e(r', \theta) \tag{6}$$

and the corresponding Fermi velocity

$$v_F(r', \theta) = (3\pi^2/\varrho_v(r', \theta))^{1/3} \quad \text{(in at. units)}, \tag{7}$$

i.e., the valence electron contributions to the stopping power due to plasma oscillations is position dependent.

Using this electronic charge density variation with distance r' for the ⟨110⟩ axial case, we calculated the electronic stopping power [4 to 6] by

$$S_e(r', \theta) = \frac{4\pi z_1^2 e^2}{mv^2} \left[\varrho_c \ln \frac{2mv^2}{\hbar\omega_p} + \varrho_v \ln \frac{v}{v_F} + \varrho_{loc}(r', \theta) \ln \frac{2mvv_F}{I} + \sum_j \varrho_j(r', \theta) \ln \frac{2mv^2}{I_j} \right], \tag{8}$$

where z_1 is the charge number of the projectile atom, e the electronic charge, m the electronic mass, v the ion velocity, ϱ_c the contribution to stopping due to conduction electrons, ϱ_{loc} the local electron density, $\varrho_j(r', \theta)$ the axial average of the electron density due to j-th shell, $\hbar\omega_p$ the plasmon energy due to conduction electrons of uniform electron density ϱ_c, and I_j the binding energy of the j-th shell. The agreement with earlier more detailed numerical calculation [14] which do not yield usable analytical expressions, was found to be good as

GaAs based materials

Direct bandgap & High mobility

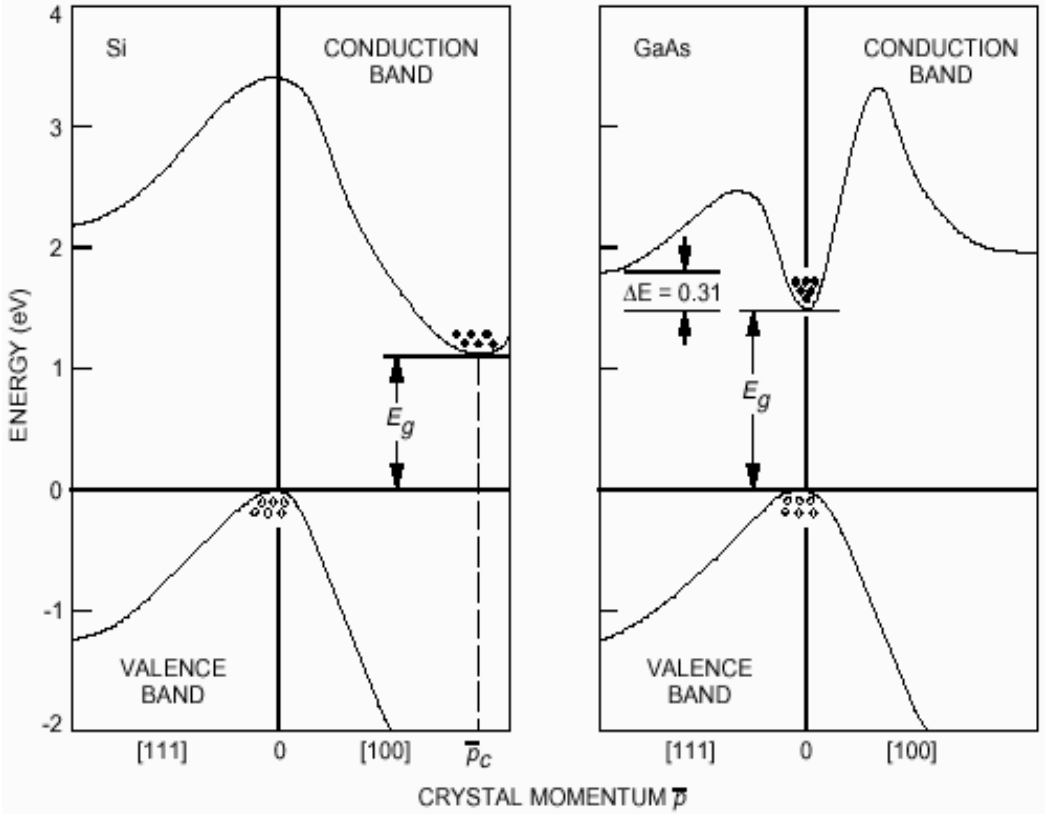

Figure 3-3. Energy band structure of Si and GaAs.

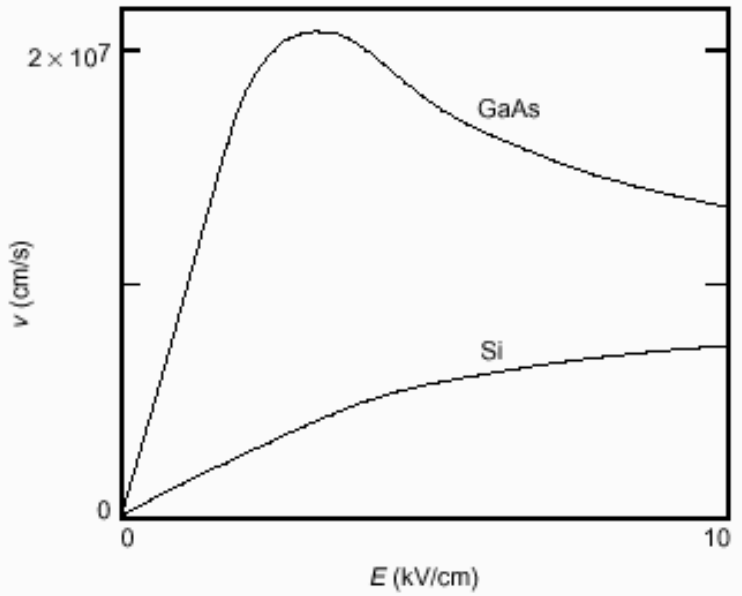

Figure 3-4. Drift velocity of electrons in GaAs and Si as a function of the electric field.

III - V Compounds
GaAs

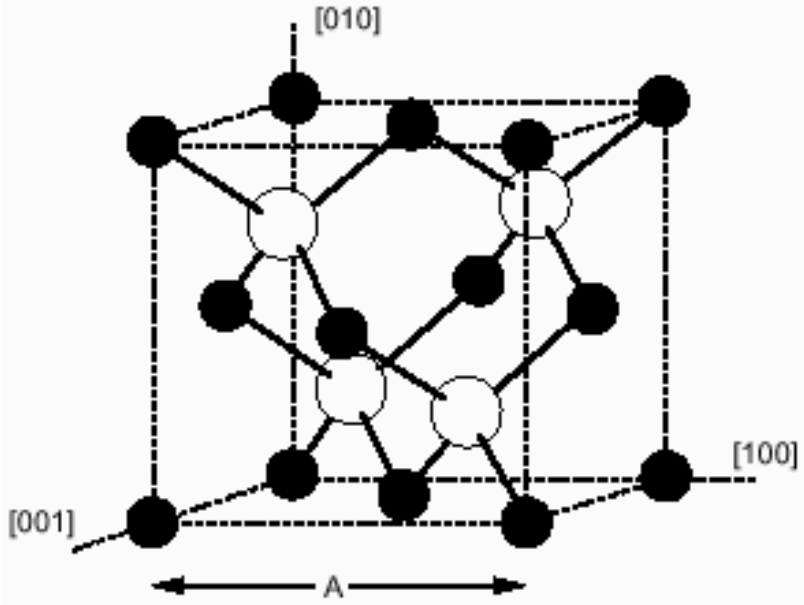

Figure 3-1. Unit cube of GaAs crystal lattice.

Table 3-1. Room-temperature properties of GaAs.

Property	Parameter
Crystal structure	Zinc blende
Lattice constant	5.65 Å
Density	5.32 g/cm^3
Atomic density	4.5×10^{22} atoms/cm^3
Molecular weight	144.64
Bulk modulus	7.55×10^{11} dyn/cm^2
Sheer modulus	3.26×10^{11} dyn/cm^2
Coefficient of thermal expansion	5.8×10^{-6} K^{-1}
Specific heat	0.327 J/g-K
Lattice thermal conductivity	0.55 W/cm-°C
Dielectric constant	12.85
Band gap	1.42 eV
Threshold field	3.3 kV/cm
Peak drift velocity	2.1×10^7 cm/s
Electron mobility (undoped)	8500 cm^2/V-s
Hole mobility (undoped)	400 cm^2/V-s
Melting point	1238°C

Band gap tailoring

band gap Vs Lattice constant

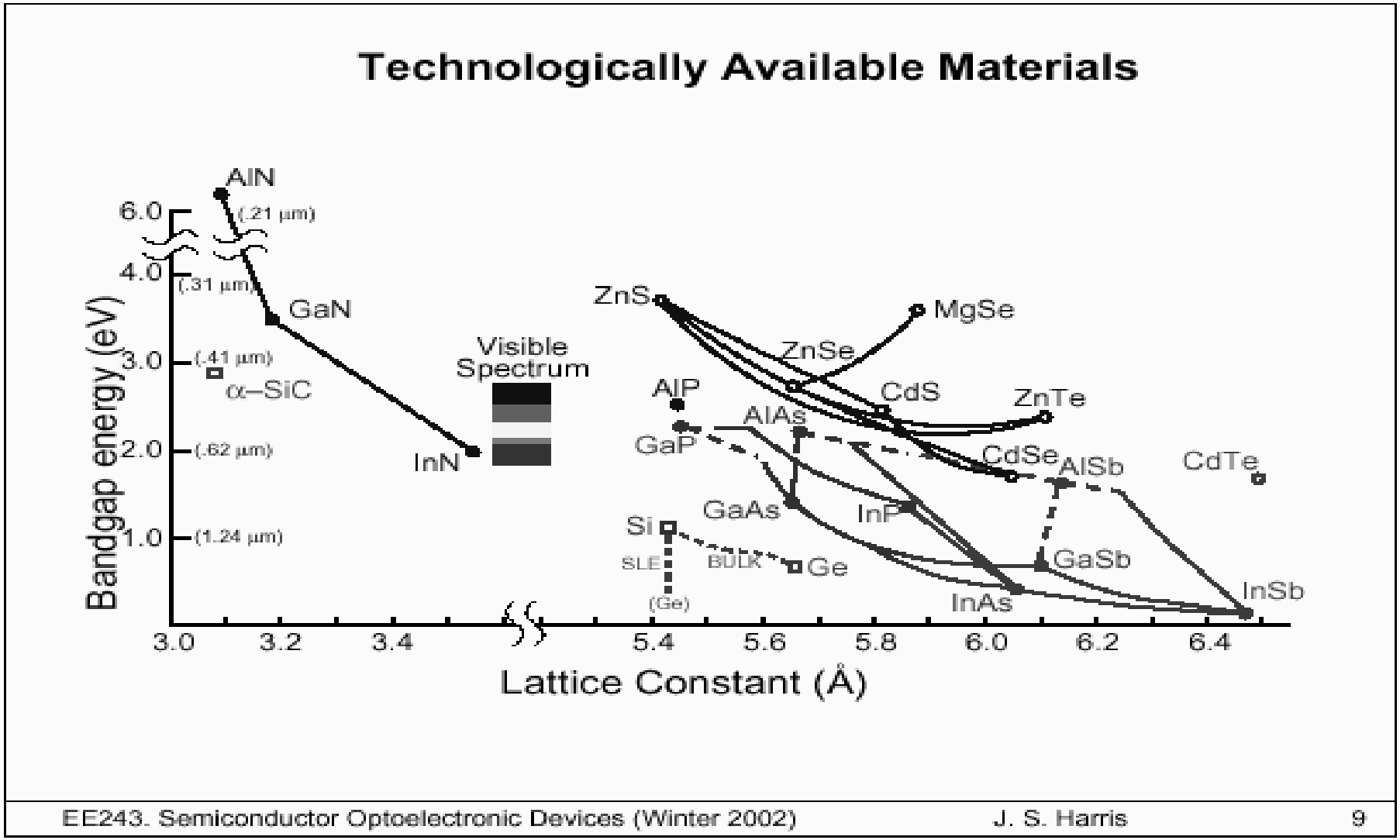

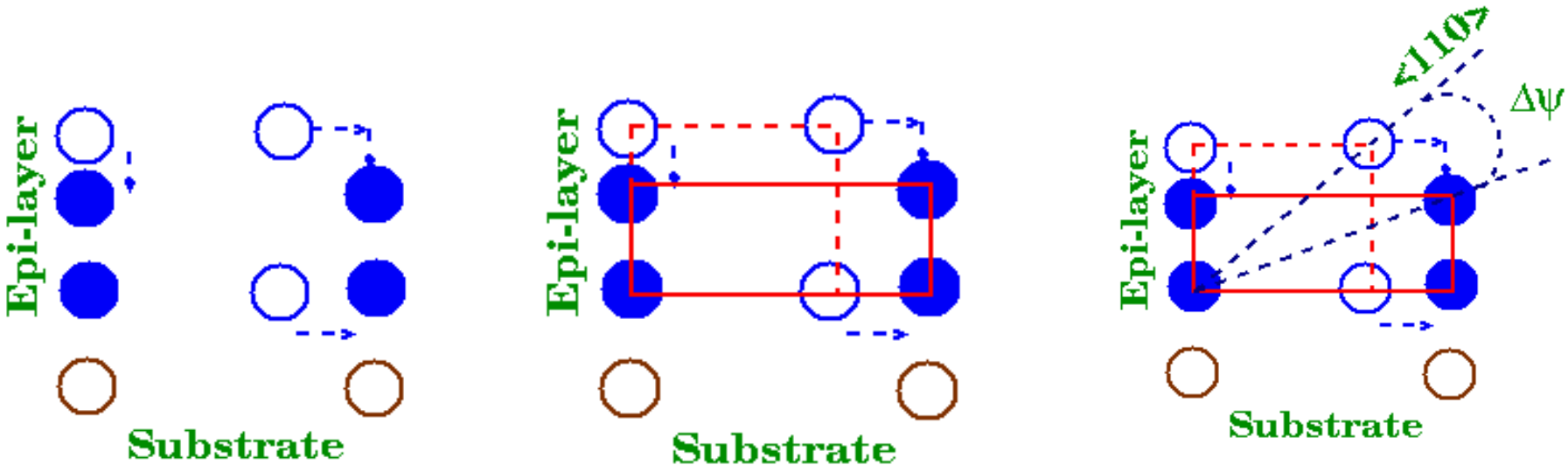

The substrate, normally GaAs is thick (microns)and thin epi-layers (about nm) of materials like In GaAs or AlGaAs are deposited. If the epi-layer has same lattice parameter,one gets lattice matched system. But, for a Lattice mismatched system, strain is generated .

- **The strain in the epilayer due to the tetragonal distortion improves the device performance and is a parameter for tailoring the device performance.**
- **Beyond a critical thickness in the epilayer, the strain relaxes giving rise to misfit dislocations which deteriorate the device properties.**

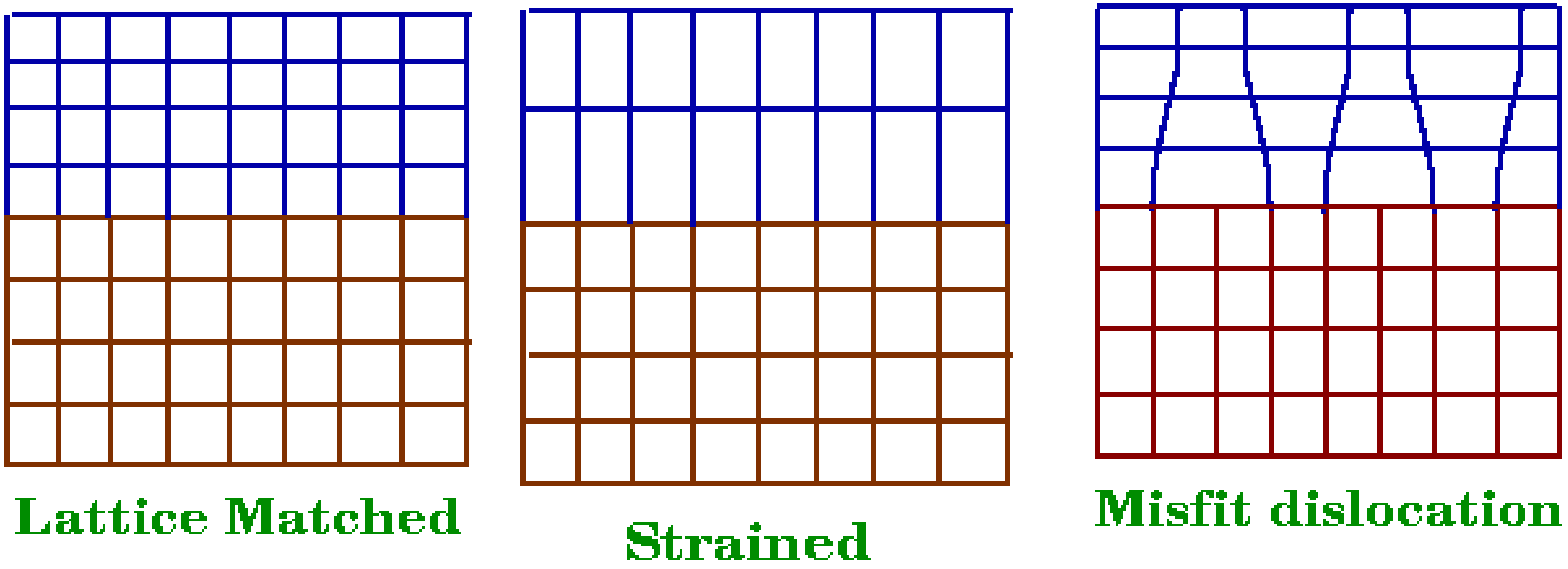

The *strain*, being key parameter is very important to study.

Strain in QWs

1.(a) Schematic representation of the band structure of an unstrained direct band gap semiconductor (b) Under biaxial compression and (c) Under biaxial tension

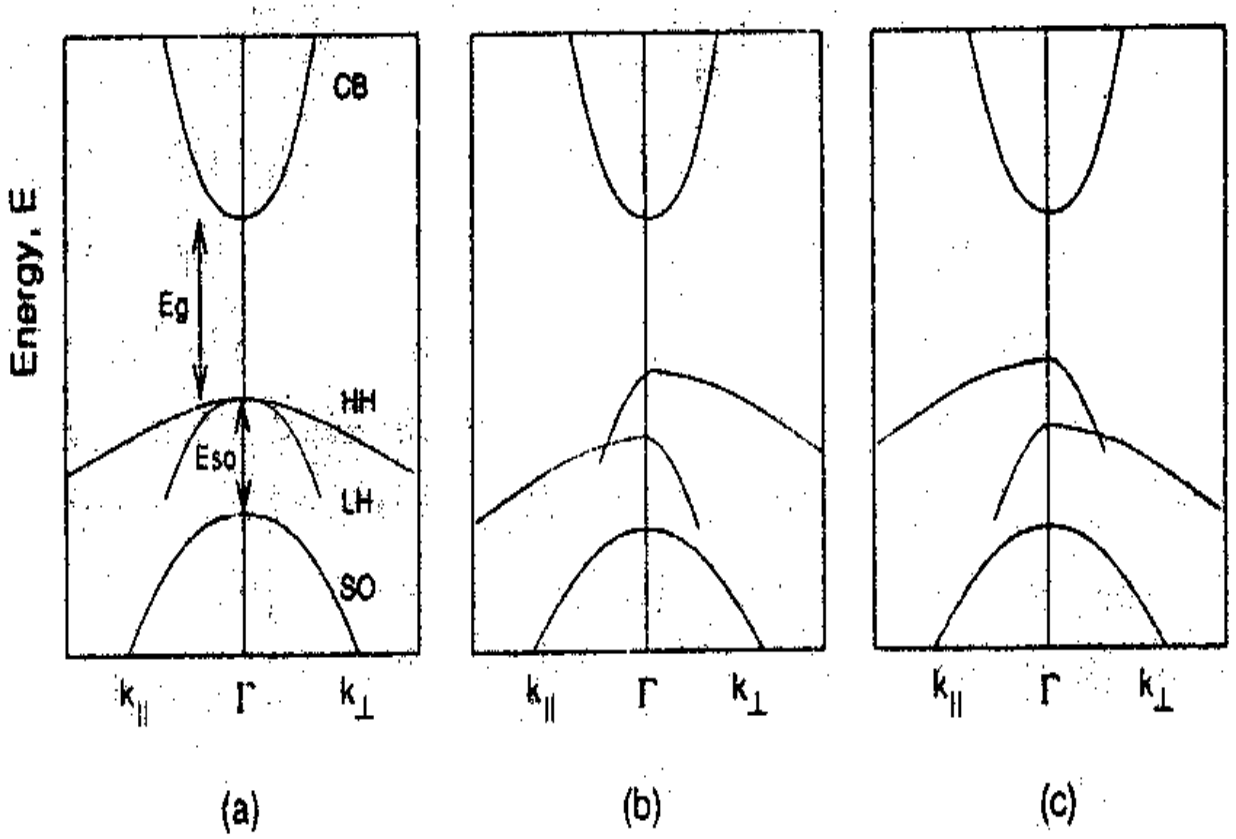

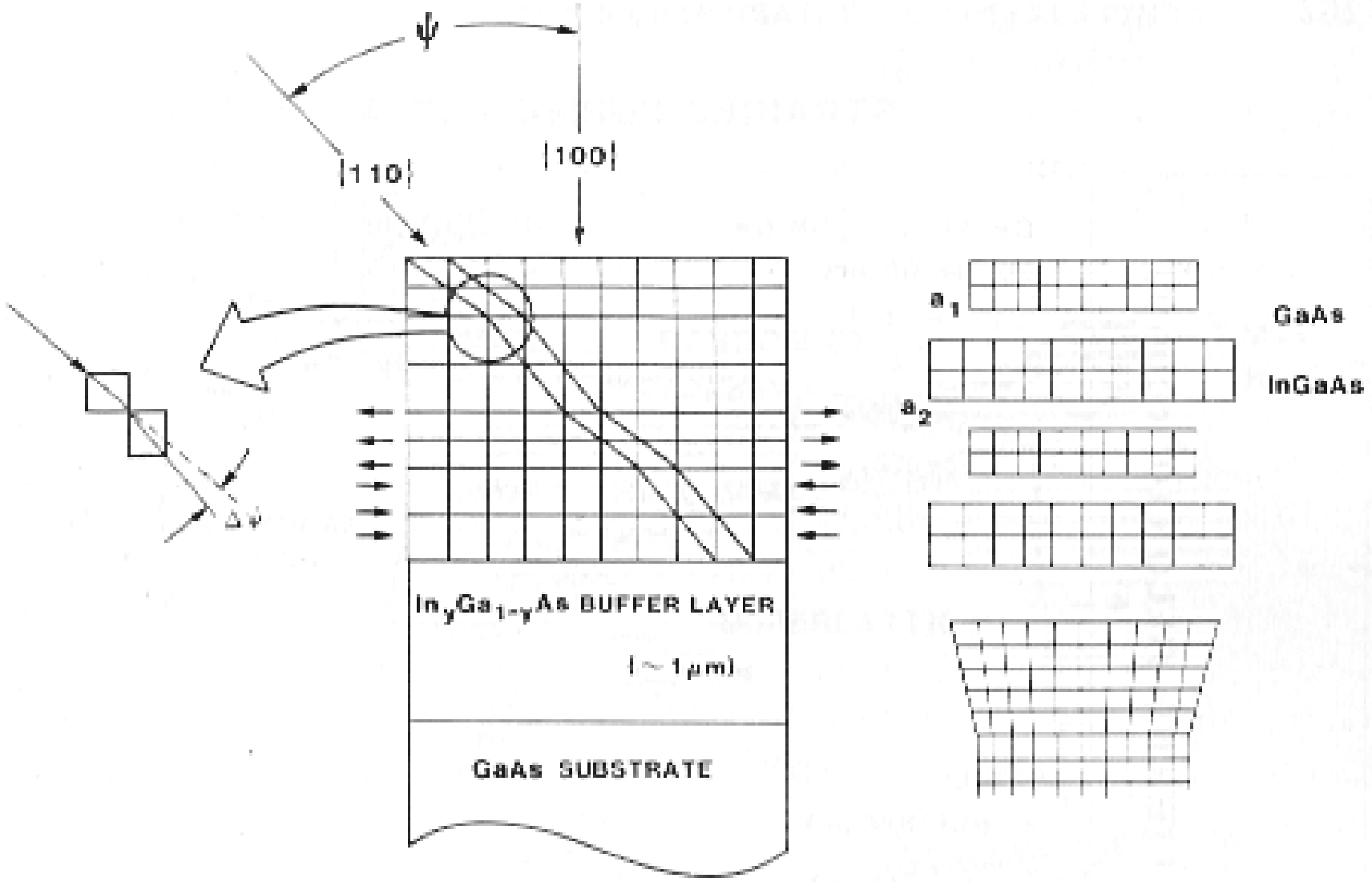
ψ
|110|
|100|
Δψ
$In_yGa_{1-y}As$ BUFFER LAYER
(~1μm)
GaAs SUBSTRATE
a_1
a_2
GaAs
InGaAs

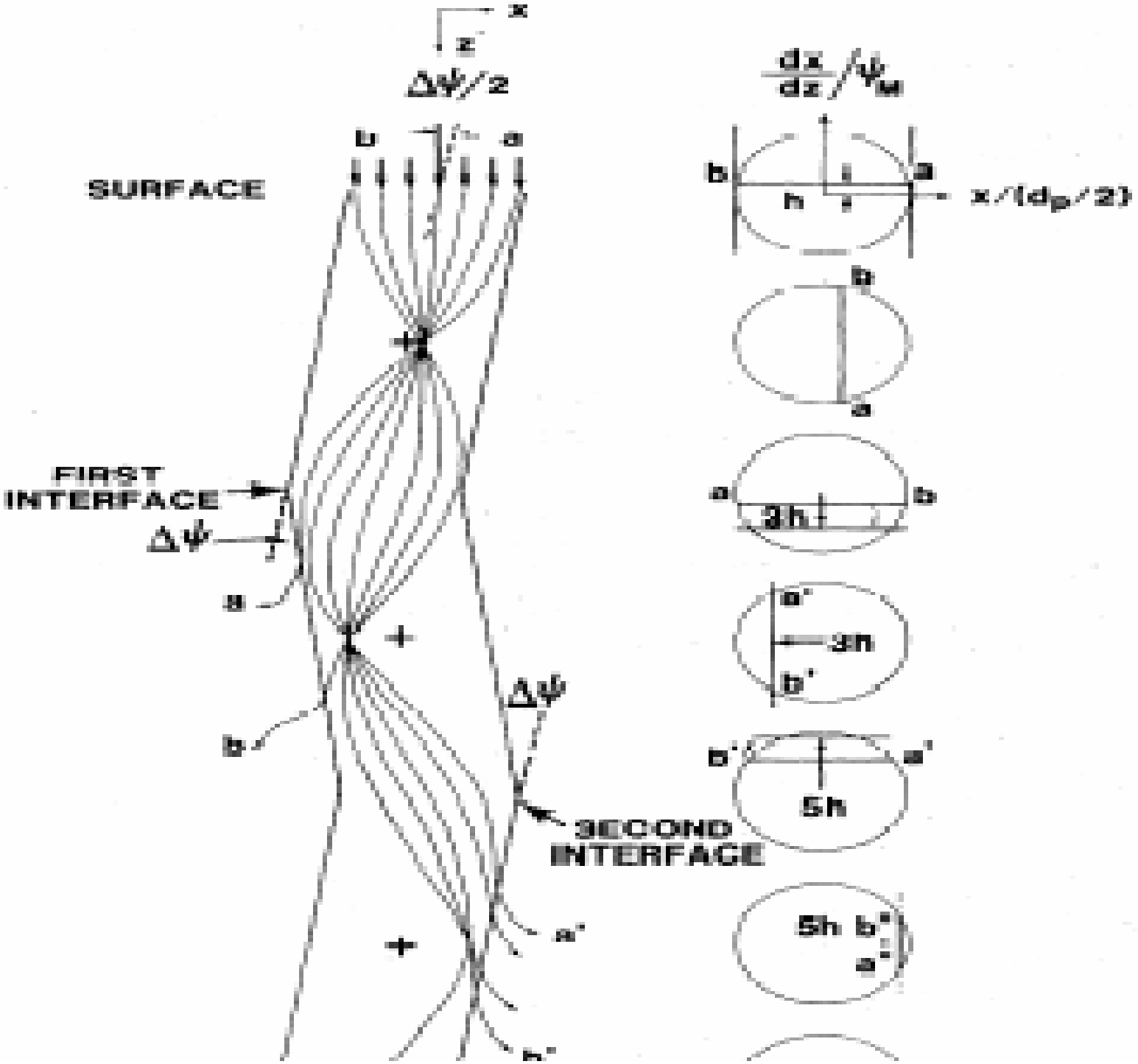
x
z
Δψ/2
SURFACE
b
a
FIRST
INTERFACE
Δψ
a
b
Δψ
SECOND
INTERFACE
a'
b'
dx/dz / ψM
b
a
h
x/(dp/2)
3h
a'
3h
b'
b'
a'
5h
5h b'
a'

$$E_{\perp} = E(dx/dz)^2 + U(x). \tag{3}$$

$$E\psi_{\mu}^2 = U(d_p/2). \tag{4}$$

Equation (3) can be simplified if the potential is approximated by a simple harmonic potential, $U(x) \propto x^2$, giving

$$\frac{dx^2/dz}{\psi_{\mu}^2} + \frac{x^2}{(d_p/2)} = r^2, \tag{5}$$

$$V_S(R) = \frac{Z_1 e^2}{R} \sum_j \frac{\omega_j}{2n_j} e^{-2\xi_j R} \sum_{k=1}^{2n_j} \frac{k}{(2n_j - k)!} (2\xi_j R)^{2n_j - k} \tag{4}$$

where n_j is the principal quantum number, ω_j is the occupation number of the jth shell and ξ_j is the optimized orbital exponent. The corresponding shell planar potential is given by

$$Y_S(y) = 2\pi N d_p Z_1 e^2 \sum_j \frac{\omega_j}{2n_j} \sum_{k=1}^{2n_j} k(2\xi_j)^{2n_j - k} \sum_{m=0}^{2n_j - k} e^{-2\xi_j y} \frac{y^m}{m!(2\xi_j)^{2n_j - k - m + 1}}. \tag{5}$$

The average continuum potential due to two planes on either side of a channel is given by

$$U(x) = Y(\tfrac{1}{2}d_p + x) + Y(\tfrac{1}{2}d_p - x) - 2Y(\tfrac{1}{2}d_p) \tag{6}$$

where $Y(x)$ is the planar potential due to a single plane (equations (3) and (5)) and x is the transverse displacement of the channelled particle and is measured from the midpoints between the planes.

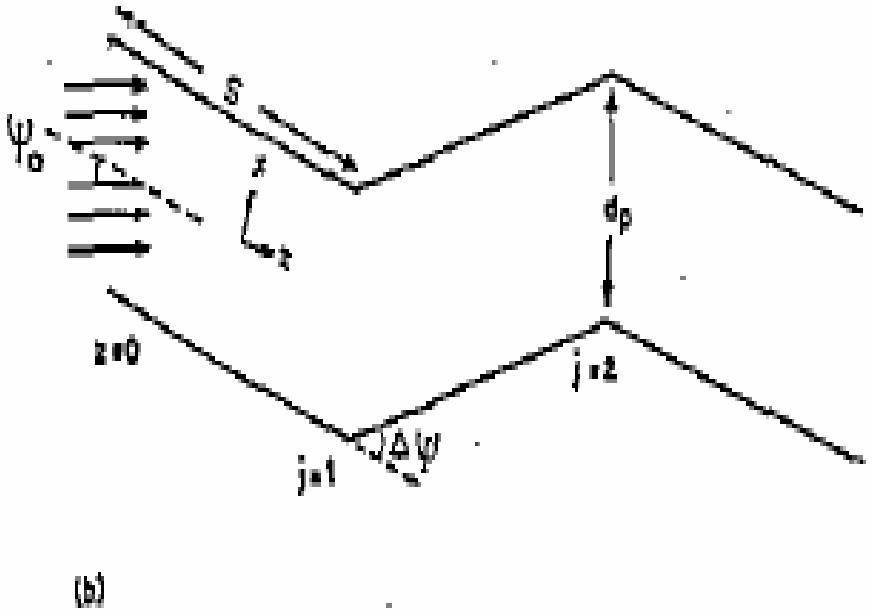

Figure 1. (*a*) Trajectory of a planar channelled particle. d_p is the interplanar spacing, r_c is the minimum impact parameter for channelling, ψ is the incident angle and a is the amplitude of the motion of a channelled particle. (*b*) Schematic diagram of a (110) planar channel of a strained layer superlattice. $\Delta\psi$ is the tilt angle, and s is the path length per layer of the SLS.

2.2. *Planar channelling in SLS*

The equation of motion for a SLS is given by

$$\frac{\mathrm{d}^2x}{\mathrm{d}z^2} + \frac{1}{2E_1}\frac{\mathrm{d}}{\mathrm{d}x}U(x) = \sum_{j=1}^{n}(-1)^j \Delta\psi\, \delta(z - js). \tag{7}$$

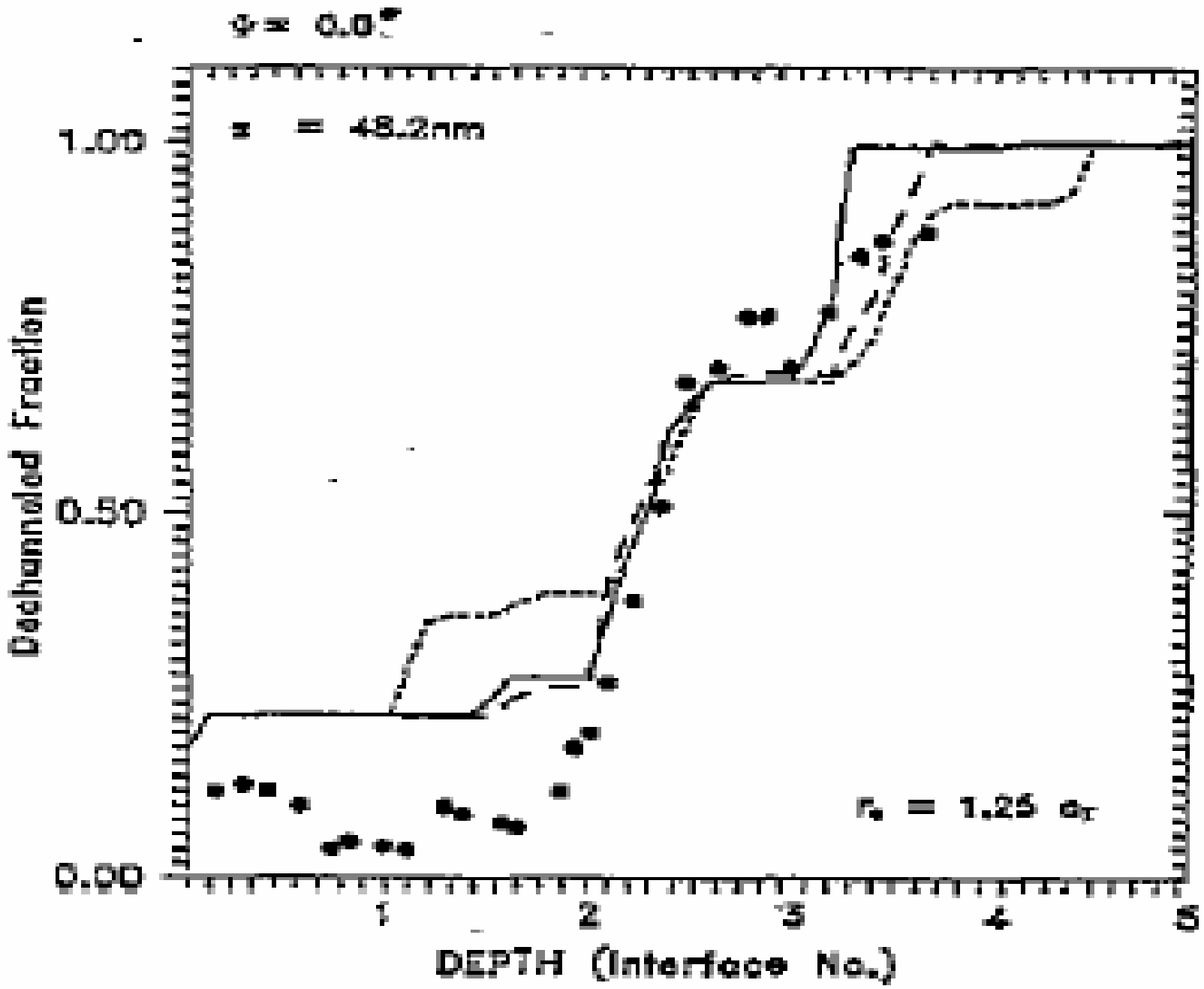
ψ = 0.0°
x = 48.2nm
1.00
0.50
0.00
Dechanneled Fraction
1
2
3
4
5
DEPTH (Interface No.)
$r_s = 1.25\ \sigma_T$

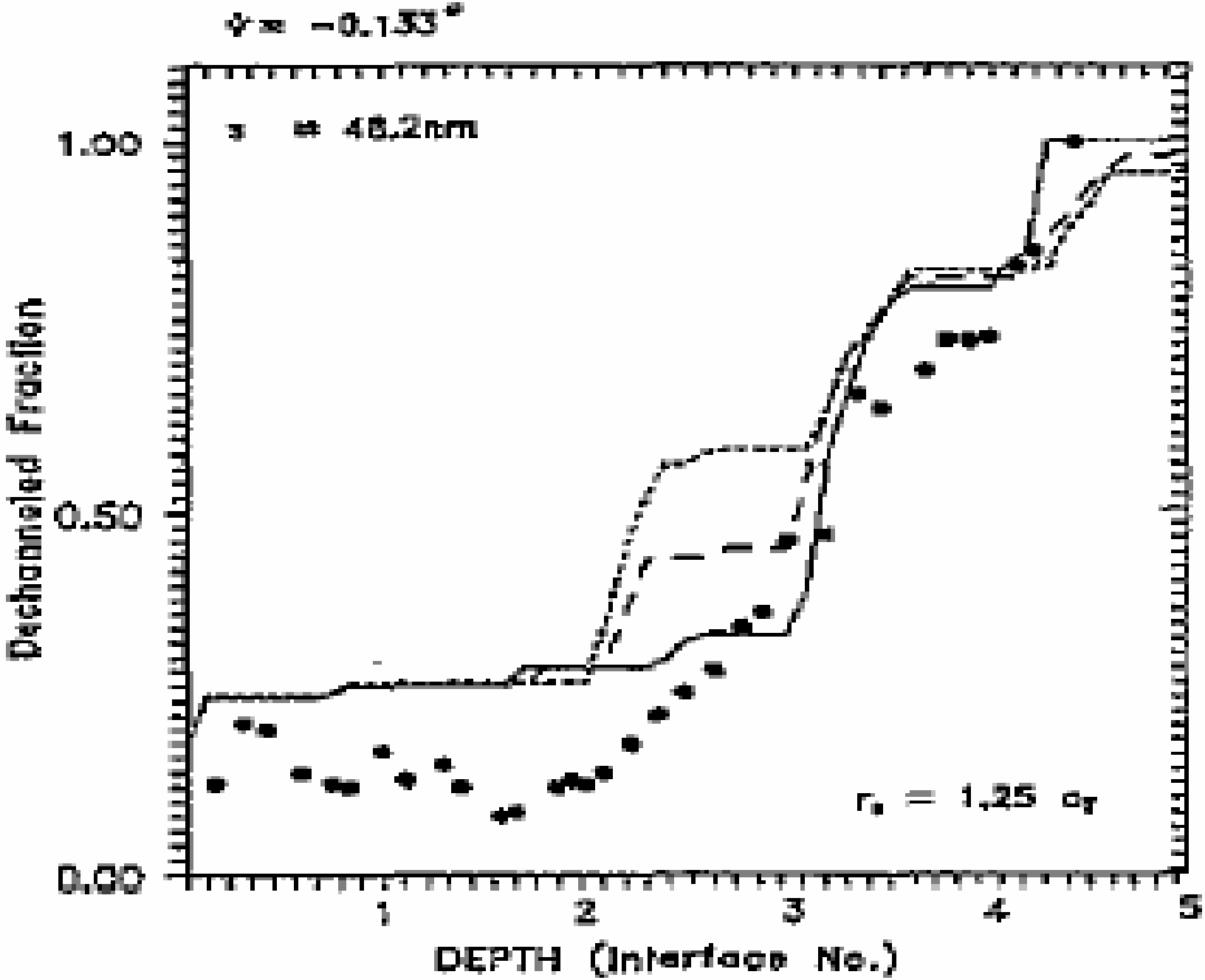
ψ = −0.133°
s = 48.2nm
1.00
0.50
0.00
Dechanneled Fraction
1
2
3
4
5
DEPTH (Interface No.)
$r_s = 1.25\ \sigma_T$

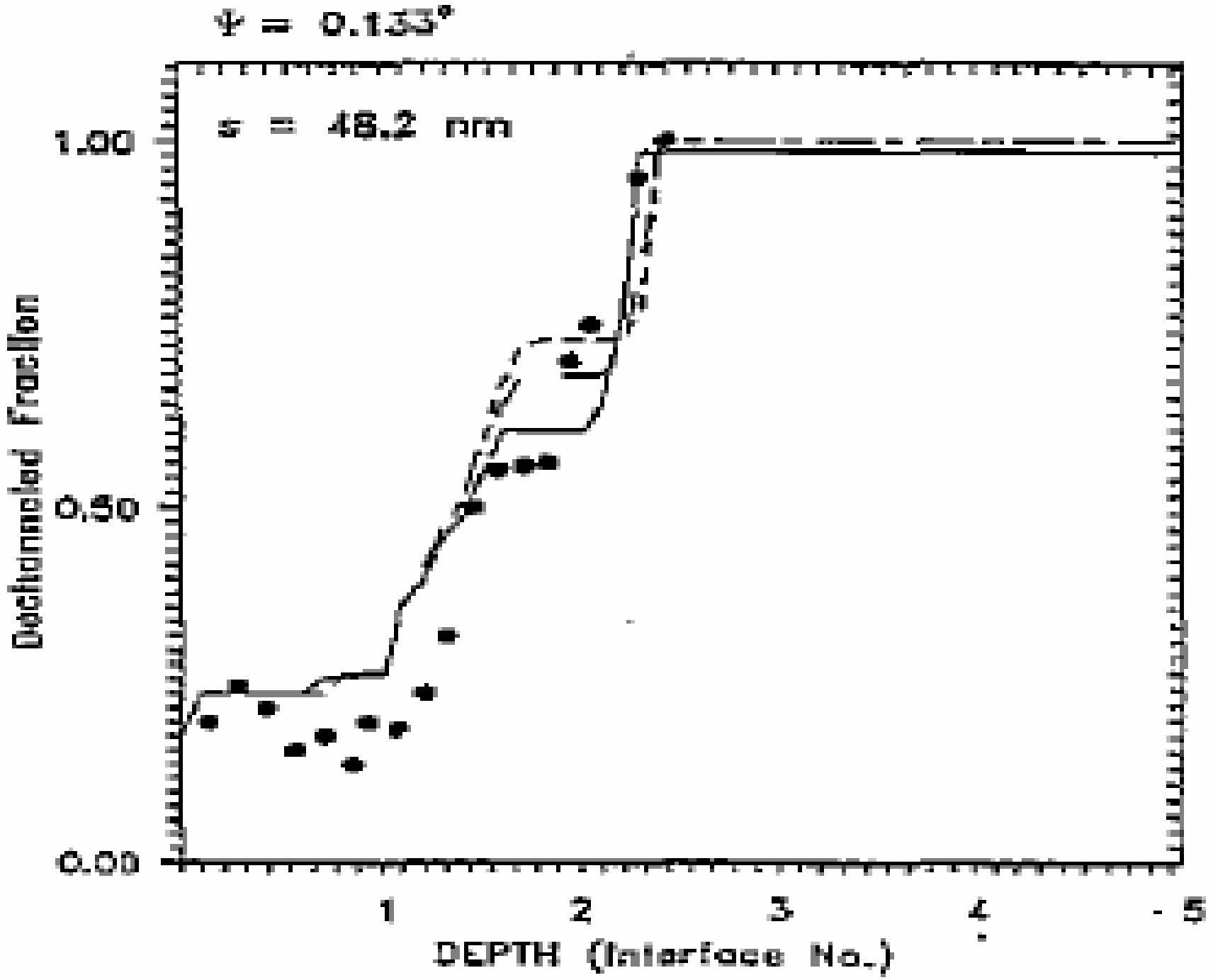
Ψ = 0.133°
s = 46.2 nm
1.00
0.50
0.00
Dechlorinated Fraction
1
2
3
4
5
DEPTH (Interface No.)

The dislocations distort the channels; the magnitude of distortion decreases with increase of distance from the dislocation core. The distortion can be modeled in terms of a transverse centrifugal force, which can be calculated in terms of dislocation and probing ion beam parameters The dechanneling coefficient is calculated by comparing transverse restoring force due to two planes or few axes surrounding the channel with centrifugal deflecting force The detailed probabilities are again calculated quantum mechanically using transverse space wave functions and their overlaps at various points along the trajectory.

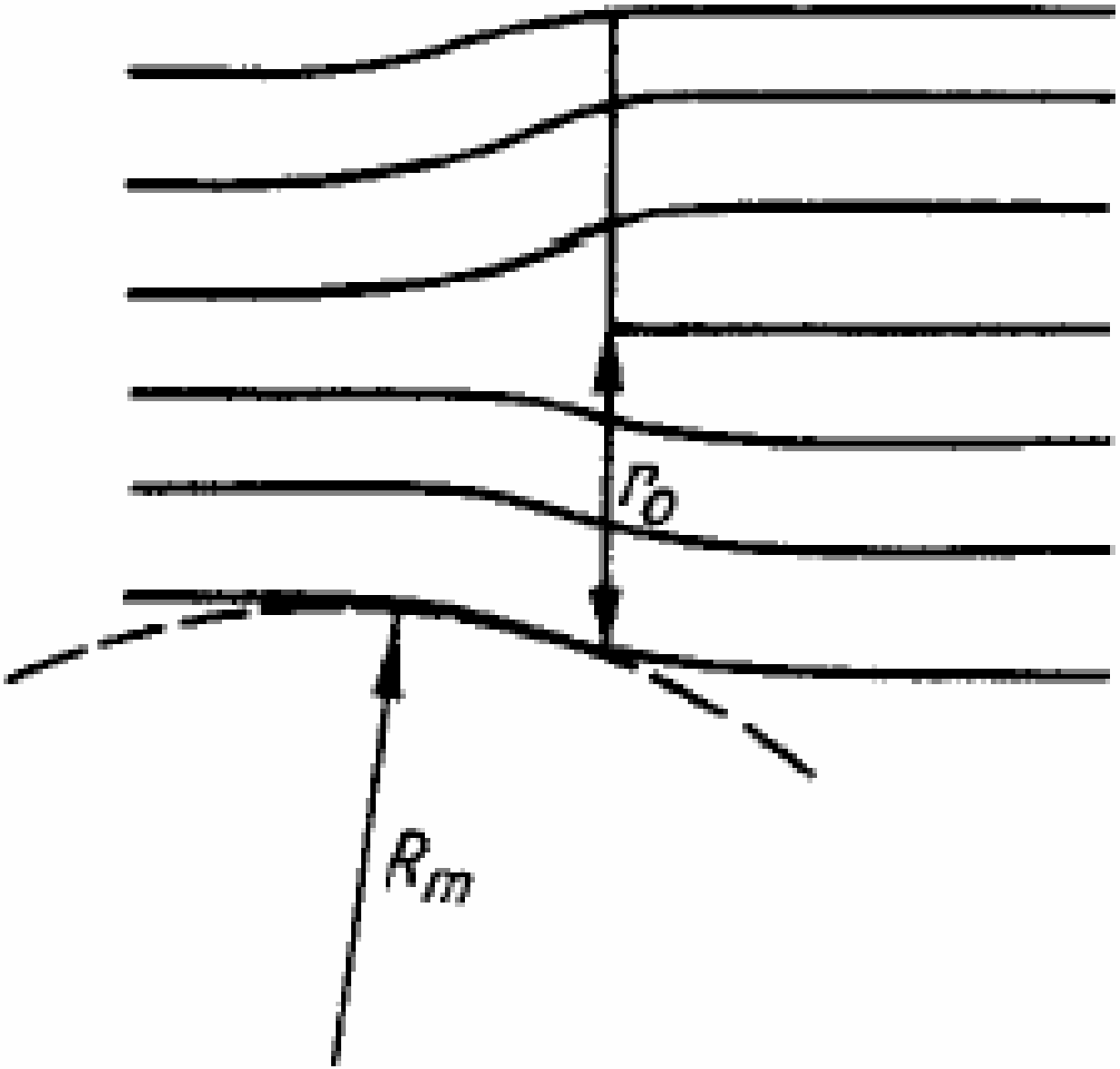
r_0
R_m

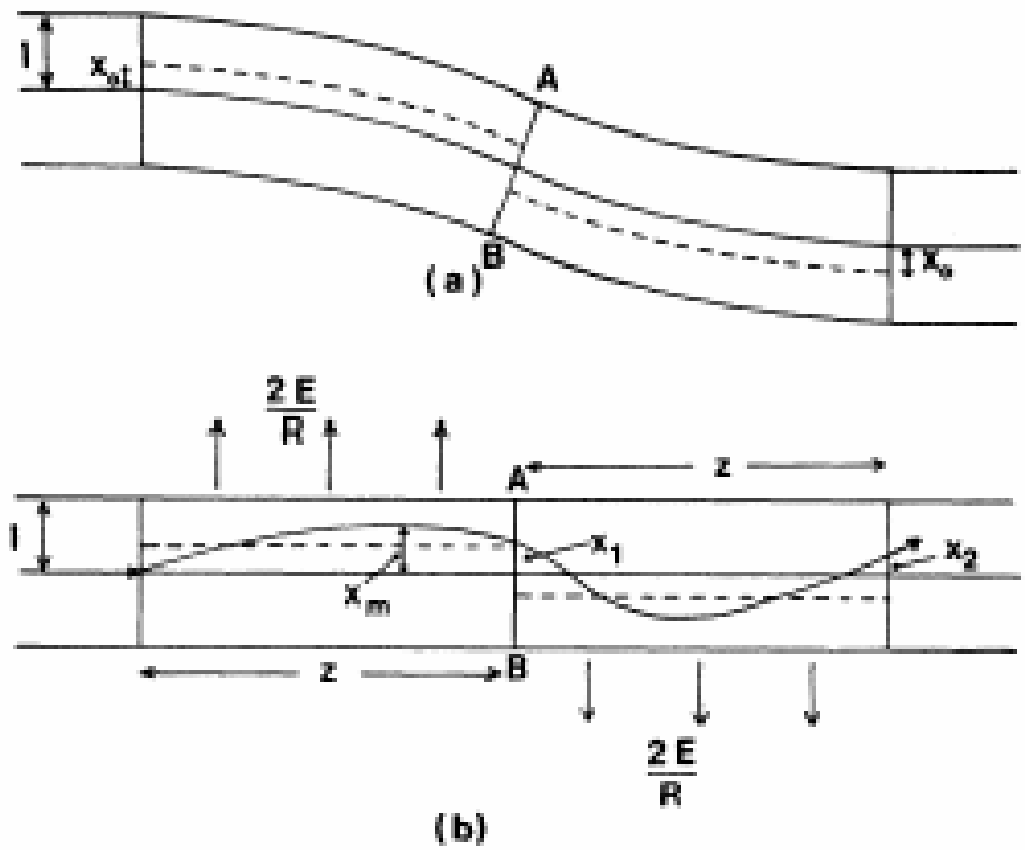

FIG. 3. (a) Typical channel at some finite distance from a dislocation. (b) Straight model channel replacing the channel of part (a) and showing the coordinates used in the text. Here, l is the half-width of the channel, x_m is the amplitude in the first part of the channel, x_0 is the equilibrium position about which the particle will oscillate, and x_1 and x_2 are the positions at which the particle arrives after having traversed the first and second parts of the channel, respectively.

$$\frac{2E}{R_m} = \frac{2Z_1 Z_2 e^2}{d r}.$$

For a given $r=r_0$, the radius of curvature R_{mc} is calculated from dislocation displacement equations and equated to restoring force to find the diameter of dechanneling cylinder,

$$\lambda(E) = \left(\frac{b d a}{x Z_1 Z_2 e^2} E \right)^{1/2}$$

So the dechanneling probability is then proportional to square root of the particle energy E

depending upon the dislocation parameter. For example, a well channeled particle (which will not emit any channeling radiation) will start oscillating after passing through a distorted channel, at distance r_0 away from dislocation core with Burger's vector b, with an average amplitude[10]

$$\bar{x}_{\text{amp}} = 0.49 L^3 Eb / 4 V_0 a \pi^2 r_0^2 \quad , \tag{6}$$

and will have a period

$$T = \left(\frac{2mL\,(L^2 - \bar{x}_{\text{amp}}^2)}{V_0 a} \right)^{1/2} F\left(\frac{\bar{x}_{\text{amp}}}{L} \right) \quad , \tag{7}$$

where F is the complete elliptic integral of the second kind. The observed additional channeling radiation frequency in the forward direction should, therefore, be

$$\omega_{\text{obs}} = 4\pi\gamma^2 / T \quad . \tag{8}$$

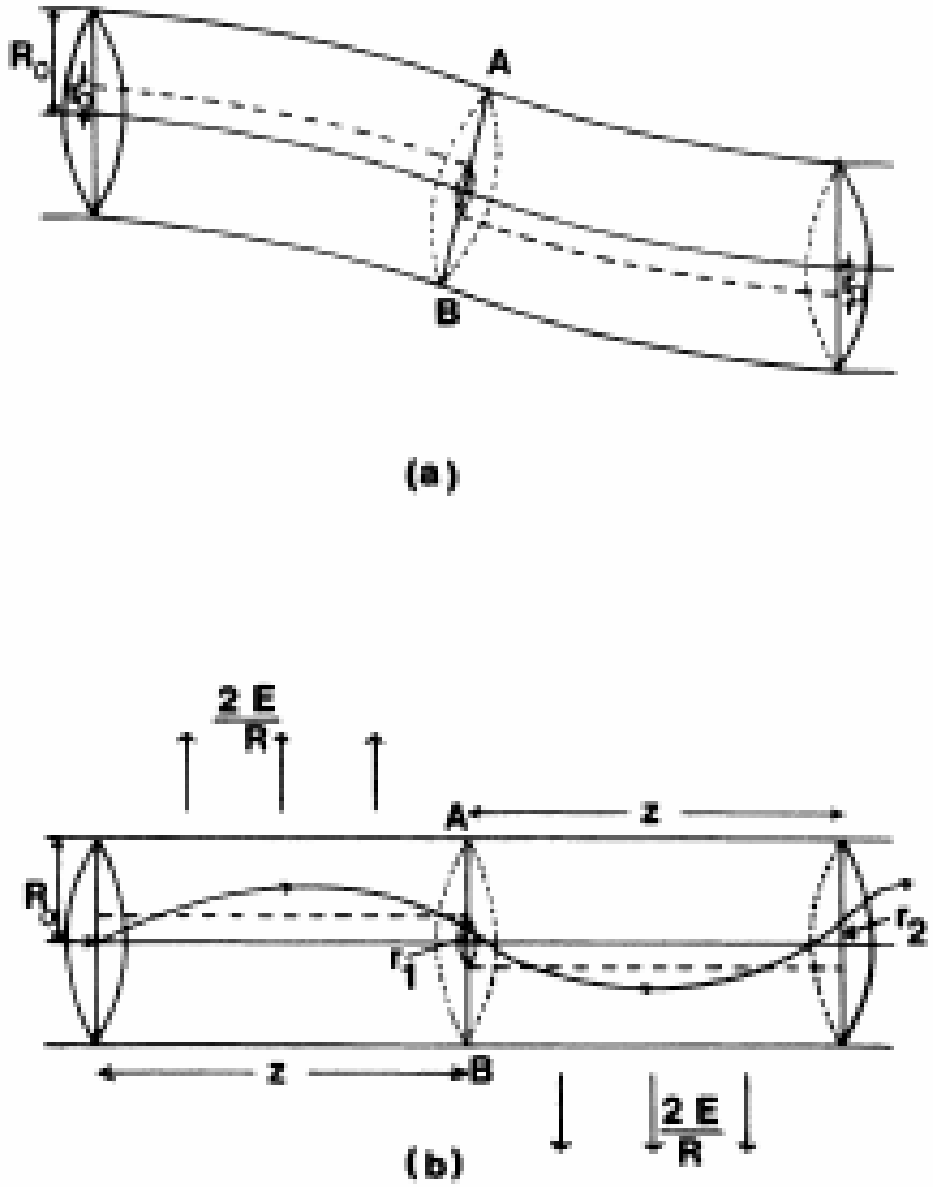

FIG. 5. (a) Typical axial channel at some finite distance d_3 from a dislocation. (b) Straight model channel replacing the channel of part (a) and showing the

The analysis for the axial situation is basically the same as for the planar case except that one has to deal with a two-dimensional, hydrogen-like model with a quantum-defect correction (for electrons) or harmonic oscillatorlike, with anharmonicity corrections (for positrons). For instance, taking the positron axial channeling case, the harmonic potential seen by the positron for not too large r has been shown to be of the form[11]

$$V(r) = U_0\left(1+\frac{r^2}{R_0^2}\right) , \tag{9}$$

where R_0 is the axial channel size, r the distance measured from the central axis, $U_0 = n_s Z_1 Z_2 e^2 C^2 a^2 / d R_0^2$ for n_s strings surrounding the channel. This problem of circular oscillator gives the energy levels

$$E_n = (n_1 + n_2 + 1)\hbar\omega , \tag{10}$$

where n_1 and n_2 are the two quantum numbers, $\omega = (2U_0/m\gamma R_0^2)^{1/2}$, and the observed radiation frequency in the forward direction is

$$\omega_{\text{obs}} = 2\gamma^{3/2}(2U_0/mR_0^2)^{1/2} . \tag{11}$$

Again, for a small concentration of dislocations of Burger's vector b, the amplitude acquired by the initially well channeled particle is calculated to be

$$\bar{r}_{\text{amp}} = 4R_0^2 Eb/3\pi^3 d_0^2 U_0 , \tag{12}$$

where d_0 is the distance of the channel from the dislocation core. The corresponding period and resulting frequency is obtained as before.

dechanneling cylinder defined by Quere,[13] which for the planar case and screw dislocations is given by

$$\left(\frac{Eb}{8.6 Z_1 Z_2 e^2 N d_p}\right)^{1/2} .$$

This has a numerical value of the order of 800 Å for 56-MeV positrons channeling in (110) planes of silicon crystals. The corresponding critical density of dislocations at which all the particles will be dechanneled and, hence, no channeling radiation, is found to be of the order of 10^{11} dislocations/cm^2.

For dislocation densities lower than this critical value, channeling radiation will still be observed but the spectra will be modified. Firstly, the particles responsible for the radiation peak are the ones which were oscillating in a perfect crystal and the majority of these (except the ones reaching distorted channel in right phase) will be dechanneled. On the other hand, the particles which were well channeled (or oscillated with a very small amplitude) will acquire an amplitude given by expression (6) and, hence, will be responsible for channeling radiation. The corresponding radiation frequency emitted by particles acquiring an amplitude $\bar{x}_{\text{amp}} = L/2$, due to a dislocation density $= 3.4\times 10^9$ per cm^2, is given by 49.2 keV [for 56-MeV positrons channeling along (110) planes in a silicon crystal]. The detailed calculation of the entire spectrum is yet to be done but the present preliminary and approximate results are expected to motivate some experiments in this direction.

The dynamics of particle motion in distorted channels

The effects of distortion on the planar potential is Embedded in the second term below, for a general Relativistic case:

distorted part of the channel the modified continuum potential as "seen" by the particle becomes $\gamma V_{\text{eff}}(x)$, which is written as

$$\gamma V_{\text{eff}} = \gamma V(x) - \gamma^2 m v_z^2 \left\{ \frac{b}{\pi} \frac{r_0(\gamma Z)}{(r_0^2 + \gamma^2 Z^2)^2} \right\} x. \qquad (2)$$

$$\psi_i = \psi_L = \left(\frac{\alpha}{\sqrt{\pi} 2^i i!} \right)^{1/2} \exp\left\{ \frac{-\alpha^2 x^2}{2} \right\} H_i(\alpha x), \qquad (4)$$

$$\psi_j^{(1)} = \psi_{\mathrm{I}} = \left(\frac{\alpha'}{\sqrt{\pi} 2^j j!} \right)^{1/2} \exp\left\{ \frac{-\alpha'^2 (x + a_r)^2}{2} \right\}$$

$$\times H_j(\alpha' x + \alpha' a_r), \qquad (5)$$

$$\psi_k^{(2)} = \psi_{\mathrm{II}} = \left(\frac{\alpha'}{\sqrt{\pi} 2^k k!} \right)^{1/2} \exp\left\{ \frac{-\alpha'^2 (x - a_r)^2}{2} \right\}$$

$$\times H_k(\alpha' x - \alpha' a_r), \qquad (6)$$

$$\psi_f = \psi_R = \left(\frac{\alpha}{\sqrt{\pi} 2^f f!} \right)^{1/2} \exp\left\{ \frac{-\alpha^2 x^2}{2} \right\} H_f(\alpha x). \qquad (7)$$

The channeling probability of the particle with an initial state $|i\rangle$ to cross the first interface and to be in the state $|j\rangle$ in the distorted part can be defined as

$$p_{i\to j}=|\langle\psi_j^{(1)}|\psi_i\rangle|^2, \tag{9}$$

where the subscript 1 in the state denotes the relevant wave function that corresponds to the distorted channel after the I interface. The corresponding probability of occupying any one of the states $|j\rangle$ ($j_{\max}<i_{\max}$) is

$$p_i^1=\sum_{j=0}^{j_{\max}}|\langle j^{(1)}|i\rangle|^2. \tag{10}$$

Variation of distortion parameter with distance of the Channel from dislocation core. Inset is the shift of Equilibrium axis from the middle position

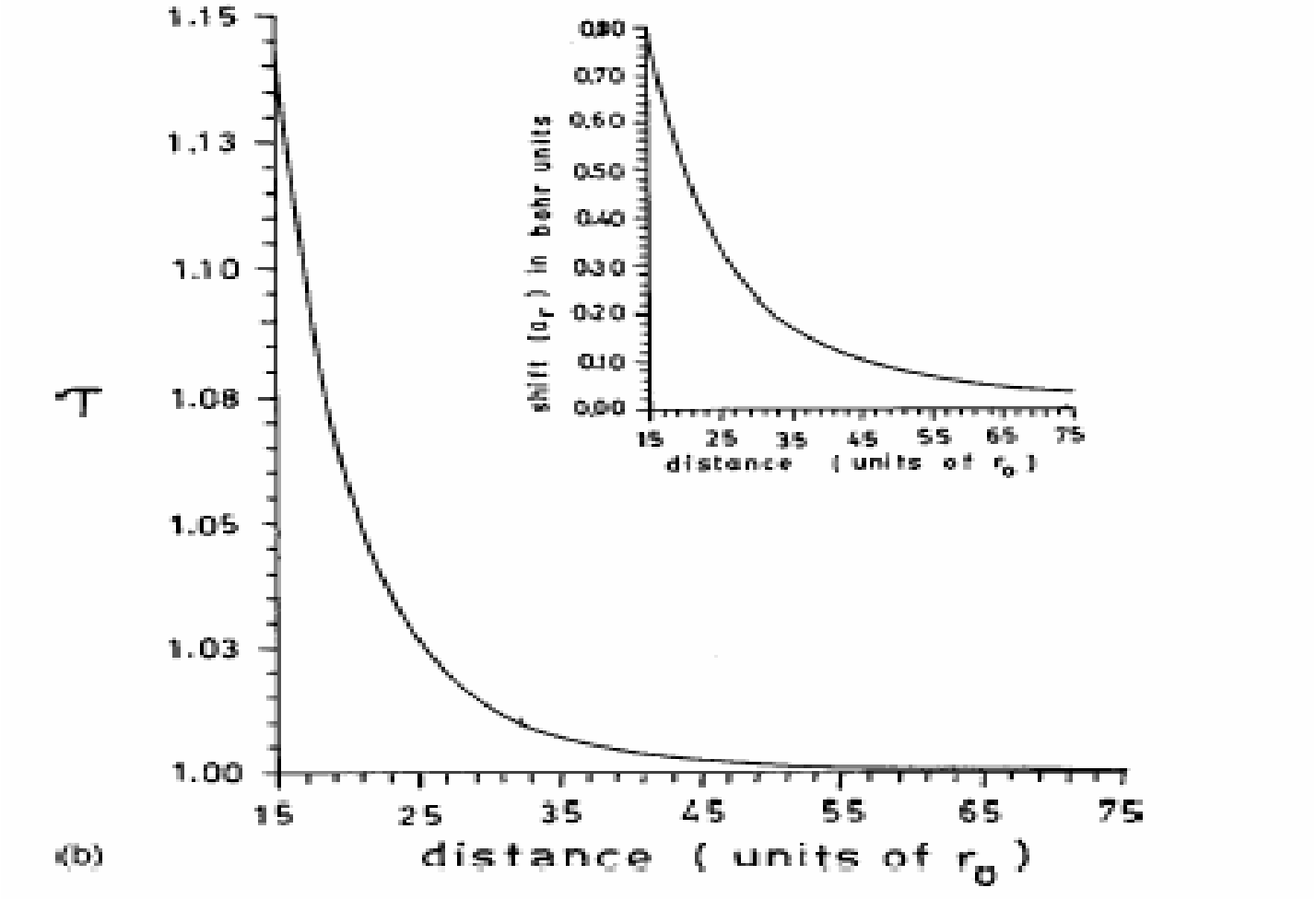

$$a' = Ta$$

J_{max} is the maximum number of bound states supported By the contimuum potential.

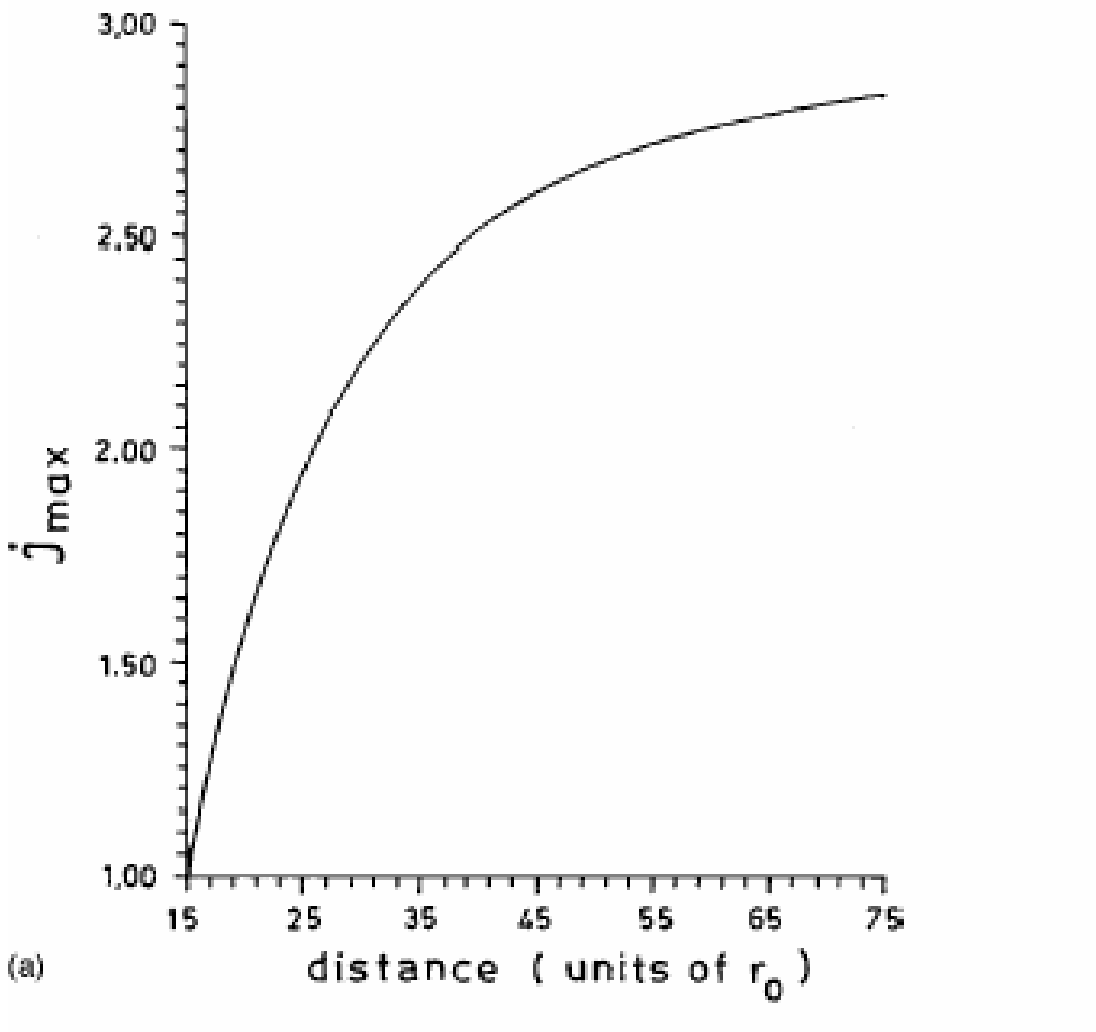

The channeling probability of the particle with the intermediate state $|j\rangle$ to cross the second interface and to occupy a state $|k\rangle$ can be defined as

$$p_{j\to k}=|\langle\psi_k^{(2)}|\psi_j^{(1)}\rangle|^2. \tag{11}$$

Here the subscript 2 denotes the wave function in the second part of the distorted channel after crossing the II interface.

Corresponding the probability of the particle to occupy any one of the states $|k\rangle$ ($k_{\max}<i_{\max}$) is

$$p_{j(1)}^{\mathrm{II}}=\sum_{k=0}^{k_{\max}}|\langle k^{(2)}|j^{(1)}\rangle|^2;\quad \chi_{j(1)}^{\mathrm{II}}=1-p_{j(1)}^{\mathrm{II}}. \tag{12}$$

To evaluate the various matrix elements in this case, we make use of the general expression obtained for $\langle j|k\rangle$ in our recent work,[3] and one may easily verify that $|\langle k^{(2)}|j^{(1)}\rangle|^2=|\langle j^{(2)}|k^{(1)}\rangle|^2$.

C. Channeling probabilities across the (III) interface

The channeling probability of the particle with intermediate state $|k\rangle$ to cross the third interface and to occupy any one of the states $|f\rangle (f \leqslant i)$ is

$$p_k^{\mathrm{III}} = \sum_{f=0}^{3} |\langle f|k^{(2)}\rangle|^2; \quad \chi_k^{\mathrm{III}} = 1 - p_k^{\mathrm{III}}, \tag{13}$$

with

$$p_{k^{(3)}\to f} = |\langle f|k^{(2)}\rangle|^2. \tag{14}$$

For example,

$$p^{(3)}_{0^{(2)}\to 0} = |\langle 0|0^{(2)}\rangle|^2 = 2\beta Ex = |\langle 0^{(1)}|0\rangle|^2.$$

$$p_{i\to f}=\sum_{k^{(2)}=0}^{k^{(2)}_{\max}}\left\langle p_{k^{(2)}\to f}\left[\sum_{j^{(1)}=0}^{j^{(1)}_{\max}} p_{i\to j^{(1)}}\times p_{j^{(1)}\to k^{(2)}}\right]\right\rangle = p_{f\to i}\,. \tag{15}$$

The total channeling probability for an initially well-channeled particle to find itself again in the straight channel after passing through various portions of the distortions is given by

$$p_0=\sum_{f=0}^{f_{\max}=3}(p_{0\to f}); \quad \chi_0=1-p_0\,. \tag{16}$$

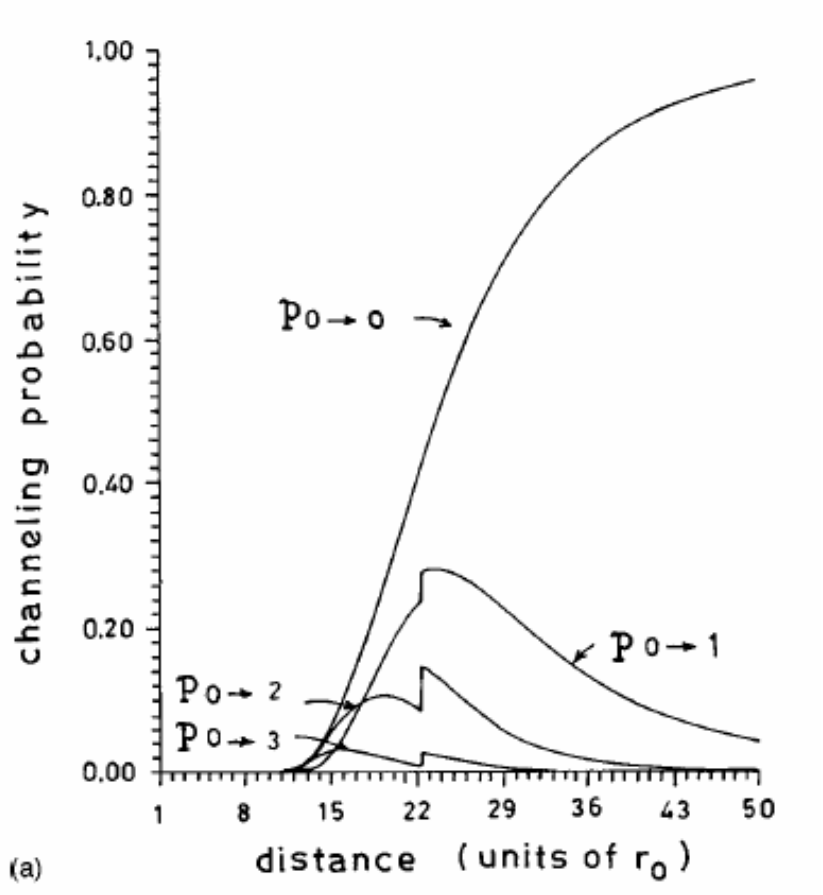
1.00
0.80
0.60
0.40
0.20
0.00
channeling probability
P0→0
P0→1
P0→2
P0→3
1
8
15
22
29
36
43
50
distance (units of r0)

(a)

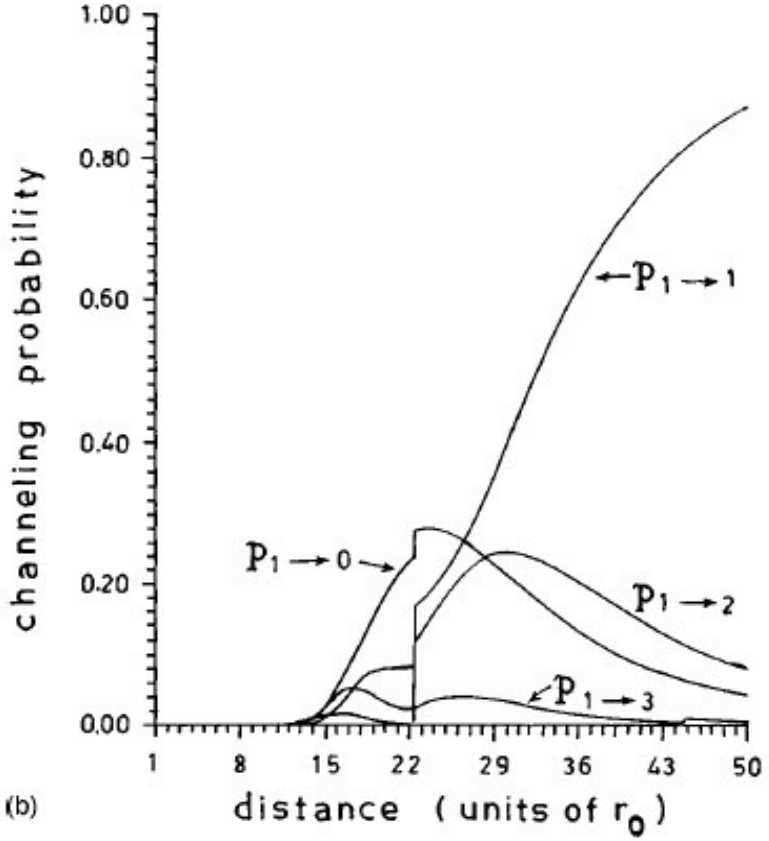
1.00
0.80
0.60
0.40
0.20
0.00
channeling probability
P1→1
P1→0
P1→2
P1→3
1
8
15
22
29
36
43
50
distance (units of r0)

(b)

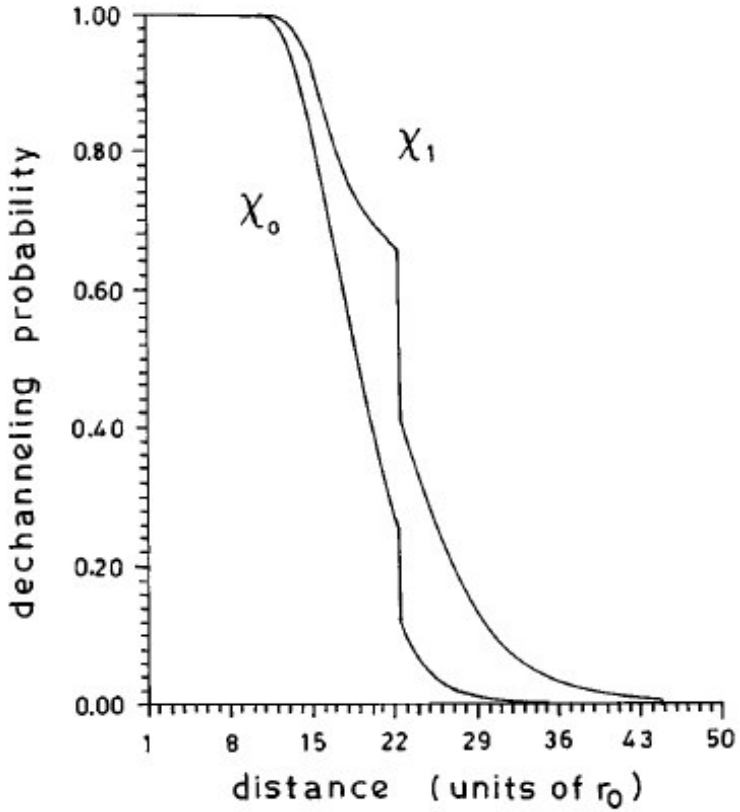
dechanneling probability
1.00
0.80
0.60
0.40
0.20
0.00
χ_1
χ_o
1
8
15
22
29
36
43
50
distance (units of r_0)

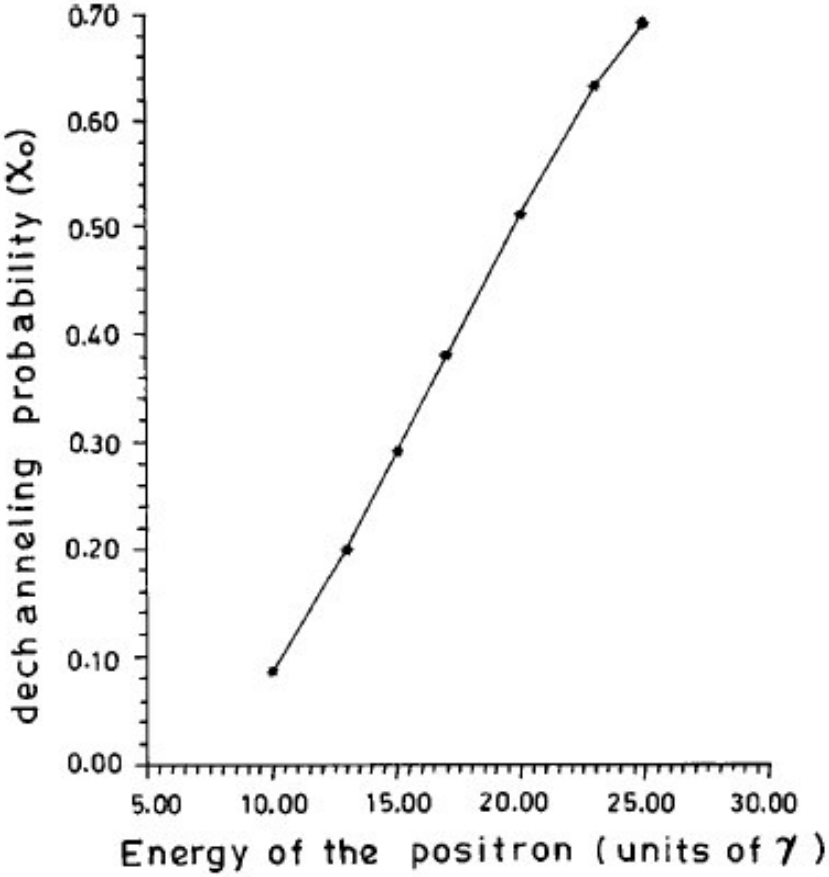
dechanneling probability (χ_o)
0.70
0.60
0.50
0.40
0.30
0.20
0.10
0.00
5.00
10.00
15.00
20.00
25.00
30.00
Energy of the positron (units of γ)

Ion Beam Mixing

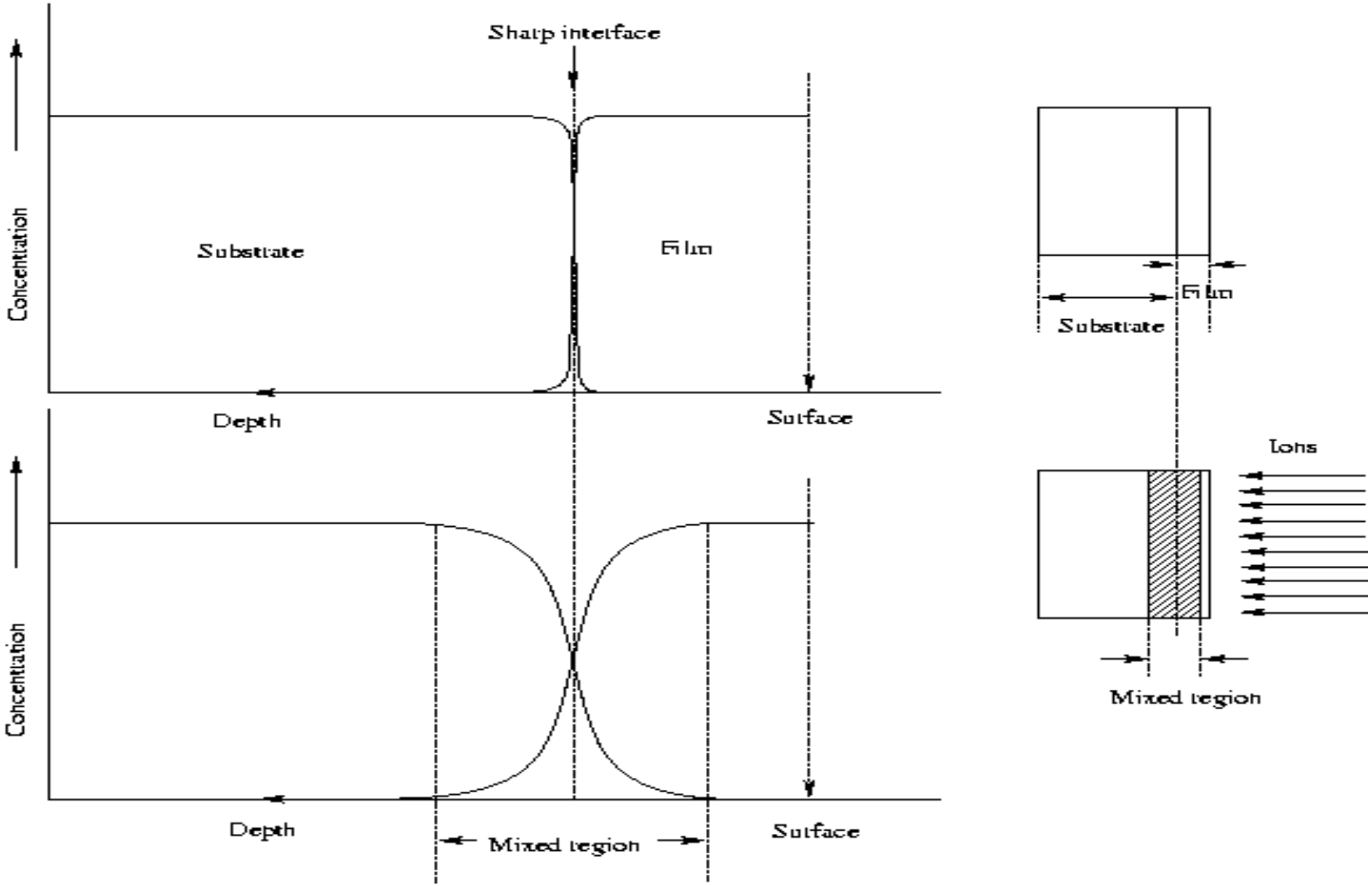

Using proper masks, defects are introduced over selective areas and then annealed at 600^0 C (NIMB 106 (1995) 457-460)

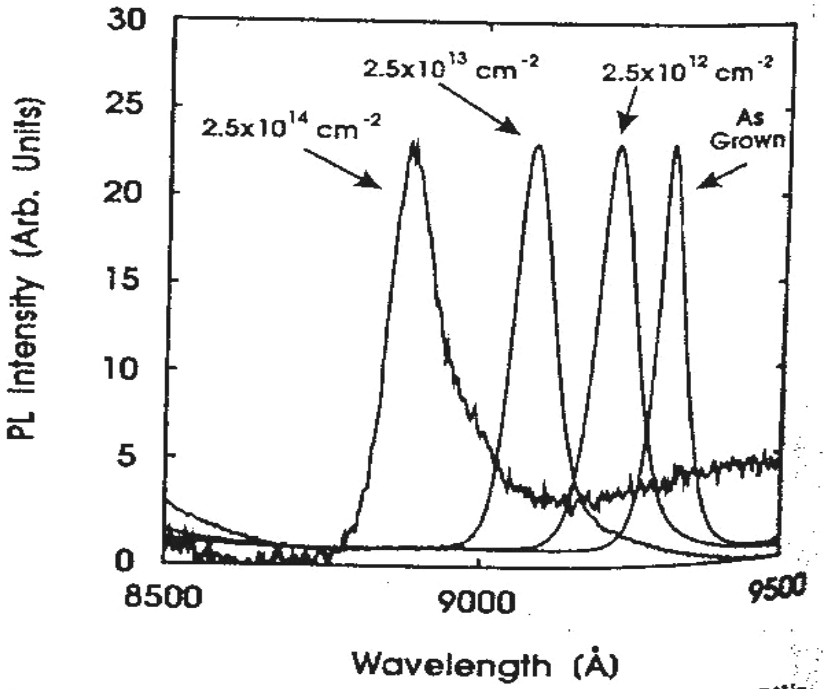

Fig. 2. Low temperature PL spectra of InGaAs/GaAs QWs in the laser diode, after ion implantation and RTA as a function of dose.

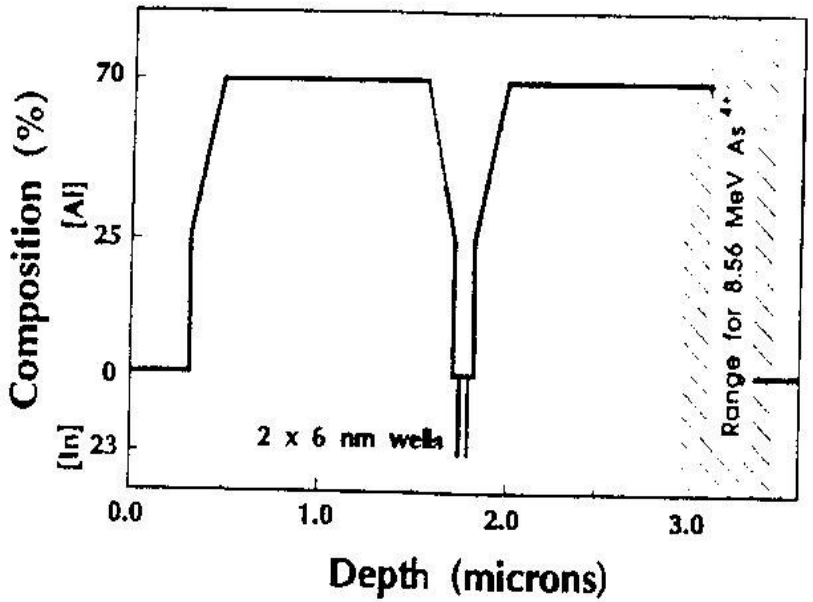

Fig. 1. Schematic diagram of the InGaAs/GaAs/AlGaAs QW laser structure studied in this paper. The expected range for 8.56 MeV As^{4+} ions, as calculated by TRIM, is also shown.

CRYSTALLINE QUALITY RETAINS AS IT IS

Ion beam modification in low energy region is well understood(Binary collisions) and has been applied rigorously in semiconductor science

Swift Heavy Ions in Matter (SHIM)

Passage of Ion through material causes excitation / ionization of atoms

$\lesssim 10^{-17}$ s 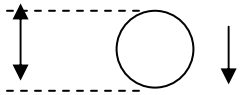 v = 1cm/ns

Simultaneous / Competing process

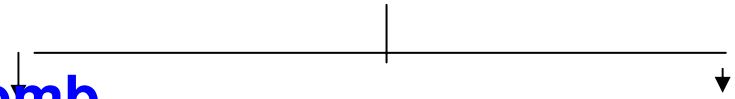

Coulomb explosion

Thermal Spike

⇐+ + ⇒
+ +
+ +
⇐+ + ⇒

Electrons emitted in secondary process & delta electrons cause heating of narrow cylindrical zone ~ 1000 K in 10^{-12} s region

Preferred in insulators

Transfer of electronic energy to lattice by electron phonon coupling, Temperature & time profile

APPLICATIONS of ION BEAMS=====➔

Ion beam - monitoring modifying

- **Should not modify while monitoring**

Dose (Fluence ~ Number of ions per cm^2) plays a major role

No modification below a certain dose (critical dose)

Critical value depends on material and the ion

e.g.: ~ 10^{12} ions/cm^2 for Au in GaAs.

If we want to just characterize a material	Should not modify a material so experiment should be completed before reaching the critical value
If we want to monitor and control the modifications	Above the critical dose

Sample ID	Specification	Growth technique	Source
4201	$In_{0.1}Ga_{0.9}As$(100 A^0)/GaAs	MBE	SSPL, Delhi
2701	$In_{0.1}Ga_{0.9}As$(150 A^0)/GaAs	"	"
2601	$In_{0.1}Ga_{0.9}As$(250 A^0)/GaAs	"	"
4101	$In_{0.1}Ga_{0.9}As$(400 A^0)/GaAs	"	"
4401	$In_{0.14}Ga_{0.86}As$ (75 A^0)/GaAs (~200 A^0)....x 10 /GaAs	"	"
MQW5	$In_{0.12}Ga_{0.88}As$ (75 A^0)/GaAs (150 A^0) .....x 20 /GaAs	"	"
P520 & P523	$In_{0.53}Ga_{0.47}As$ (150 A^0)/InP(150 A^0).....x 10 /InP (Lattice matched)	MOCVD	Warsaw, Poland

Sample ID	Irradiation Details		New name
	Energy (MeV)	Fluence (ions/cm^2)	
4201	150	1 X 10^{13}	4201113
2701	150	1 X 10^{13}	2701113
2601	150	5 X 10^{12} 1 X 10^{13} & 2 X 10^{13}	2601512, 2601113 & 2601213
4101	150	1 X 10^{13}	4101113
4401	200	5 X 10^{12}	4401 I
MQW5	130	5 X 10^{12}	MWQ5I
P523	130	5 X 10^{12} & 5 X 10^{13}	P523I & I2

3.5 MeV He Channeling in P523U & I; NIMB, 193 (2002) 319

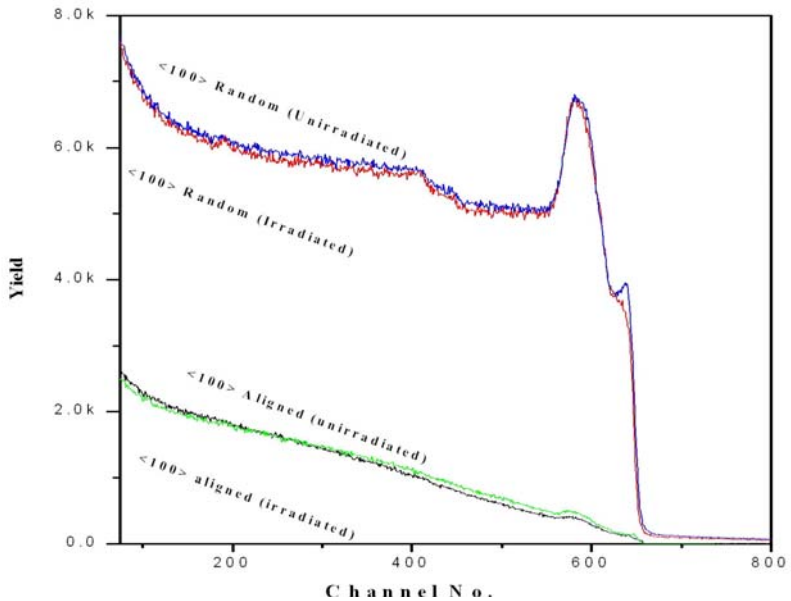

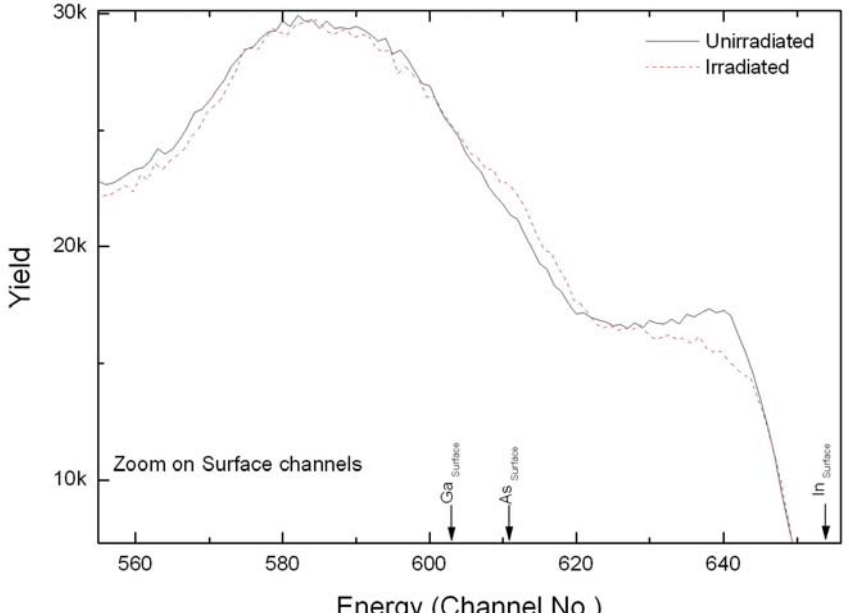

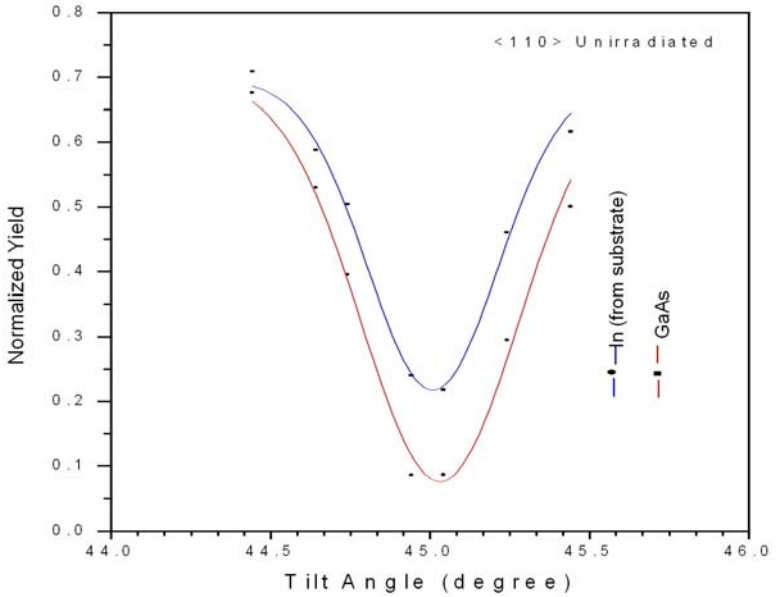

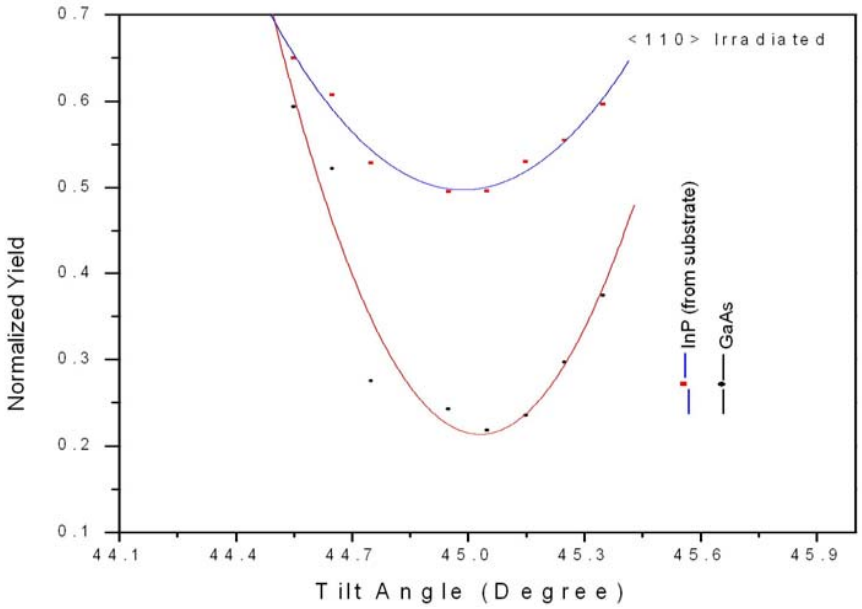

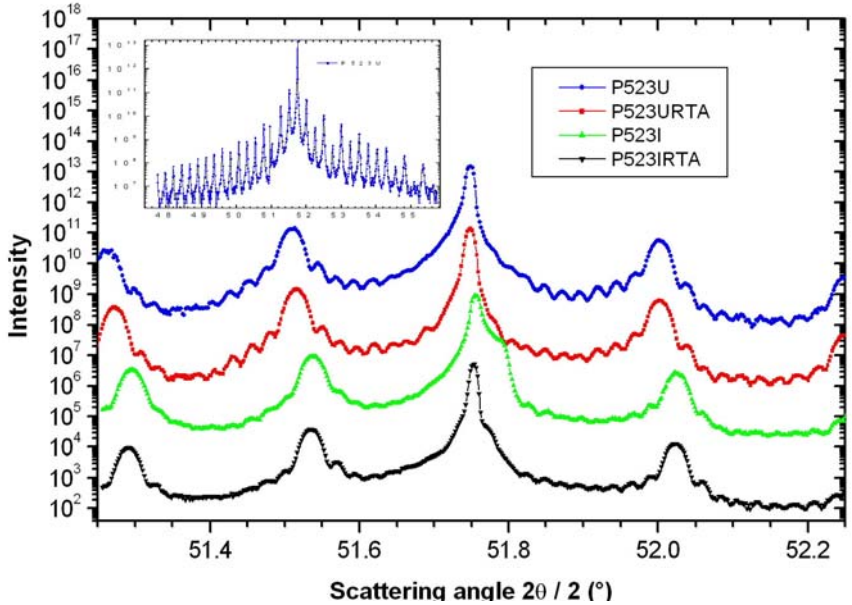
P523U
P523URTA
P523I
P523IRTA
Intensity
Scattering angle 2θ / 2 (°)

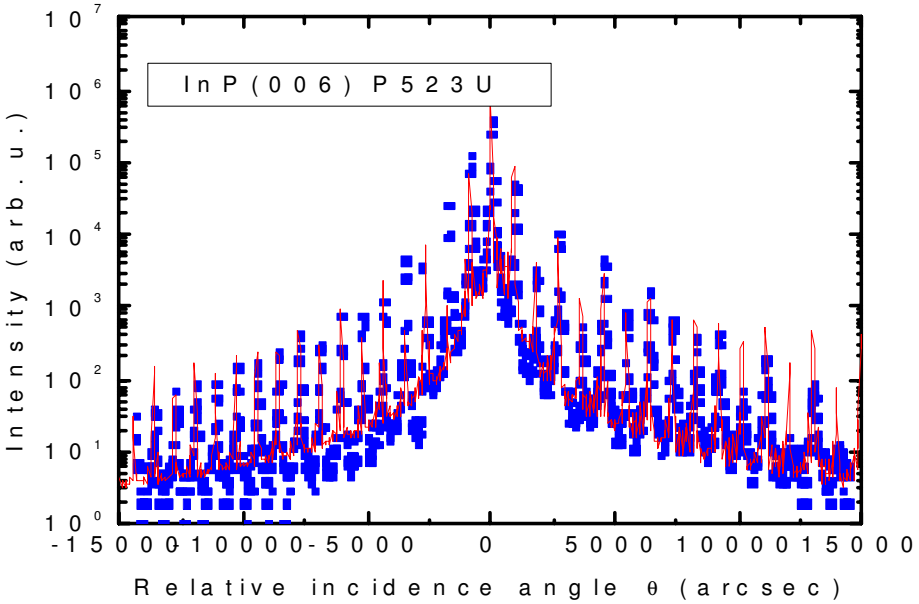
InP (006) P523U
Intensity (arb. u.)
Relative incidence angle θ (arcsec)

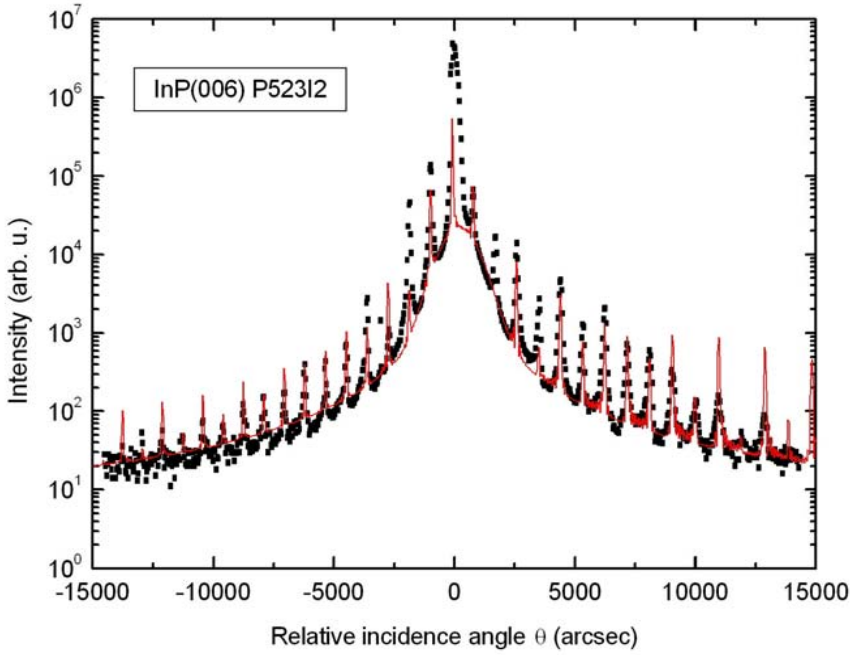
InP(006) P523I2
Intensity (arb. u.)
Relative incidence angle θ (arcsec)

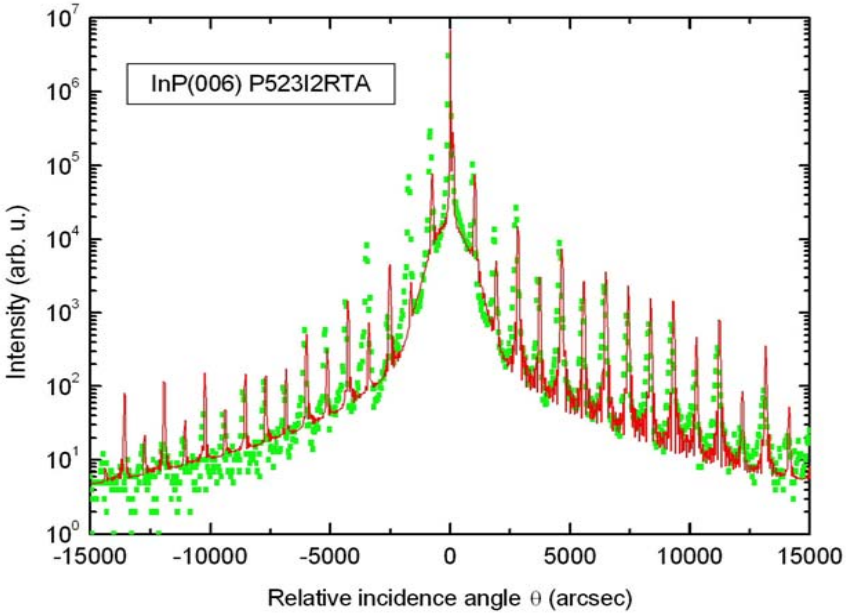
InP(006) P523I2RTA
Intensity (arb. u.)
Relative incidence angle θ (arcsec)

Sample	s (nm) (Nominal 30nm)	$(\Delta d/d)_{\perp}$
P523 U	28.90	-1.10×10^{-4}
P523 URTA	29.08	-1.44×10^{-4}
P523 I	29.01	-3.46×10^{-4}
P523 IRTA	28.93	-3.59×10^{-4}
523 I2	29.69	-
523 I2RTA	28.59	-6.92×10^{-4}

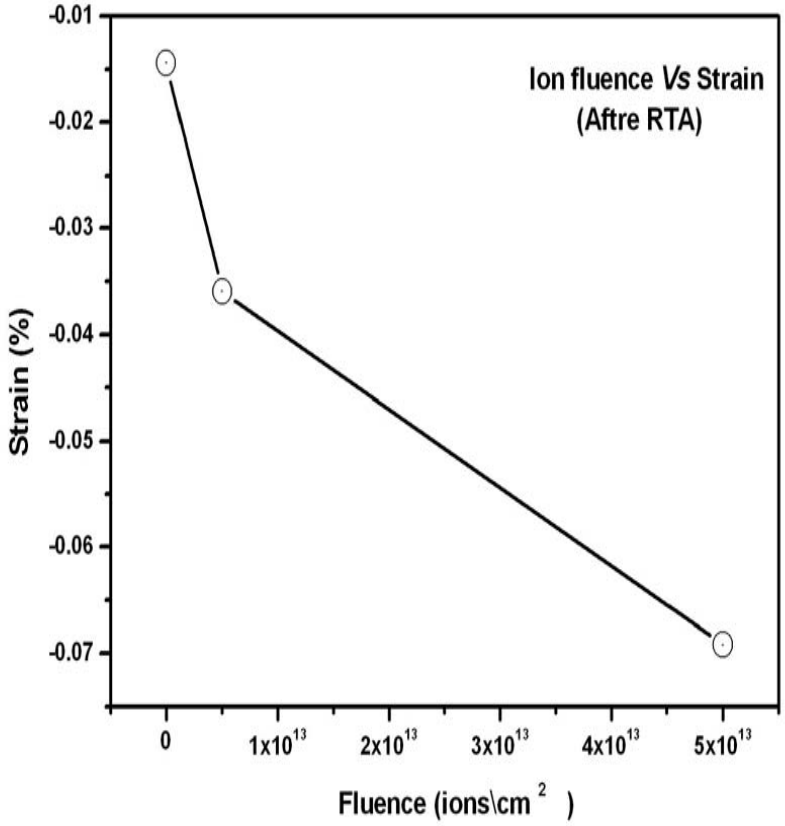

Sample Name	Structure Details	P523U		P523I2		P523I2RTA	
		X	Y	x	y	x	y
$In_xGa_{1-x}As_yP_{1-y}$	x 10 Layers	0.248	0.349	0.321	0.442	0.668	0.471
InP		-	-	-	-	-	-
$In_xGa_{1-x}As_yP_{1-y}$		0.258	0.180	0.407	0.124	0.668	0.348
$In_xGa_{1-x}As$		0.513	-	0.548	-	0.516	-
$In_xGa_{1-x}As_yP_{1-y}$		0.407	0.631	0.233	0.499	0.524	0.544
InP	Substrate	-	-	-	-	-	-

Sample treatment	Multilayer period(λ) (Aº)	d_{InP} (Aº)	d_{InGaAs} (Aº)	$d_{InGaAsP}$ above InP (Aº)	$d_{InGaAsP}$ below InP (Aº)	Sum thickness of diffusion layers / λ
P523U	289.8	151.5	131.3	6.8	0.2	0.024
P523I2	289.9	152.7	121.6	8.3	7.3	0.054
P523I2RTA	289.1	137.8	116.0	7.9	27.4	0.122

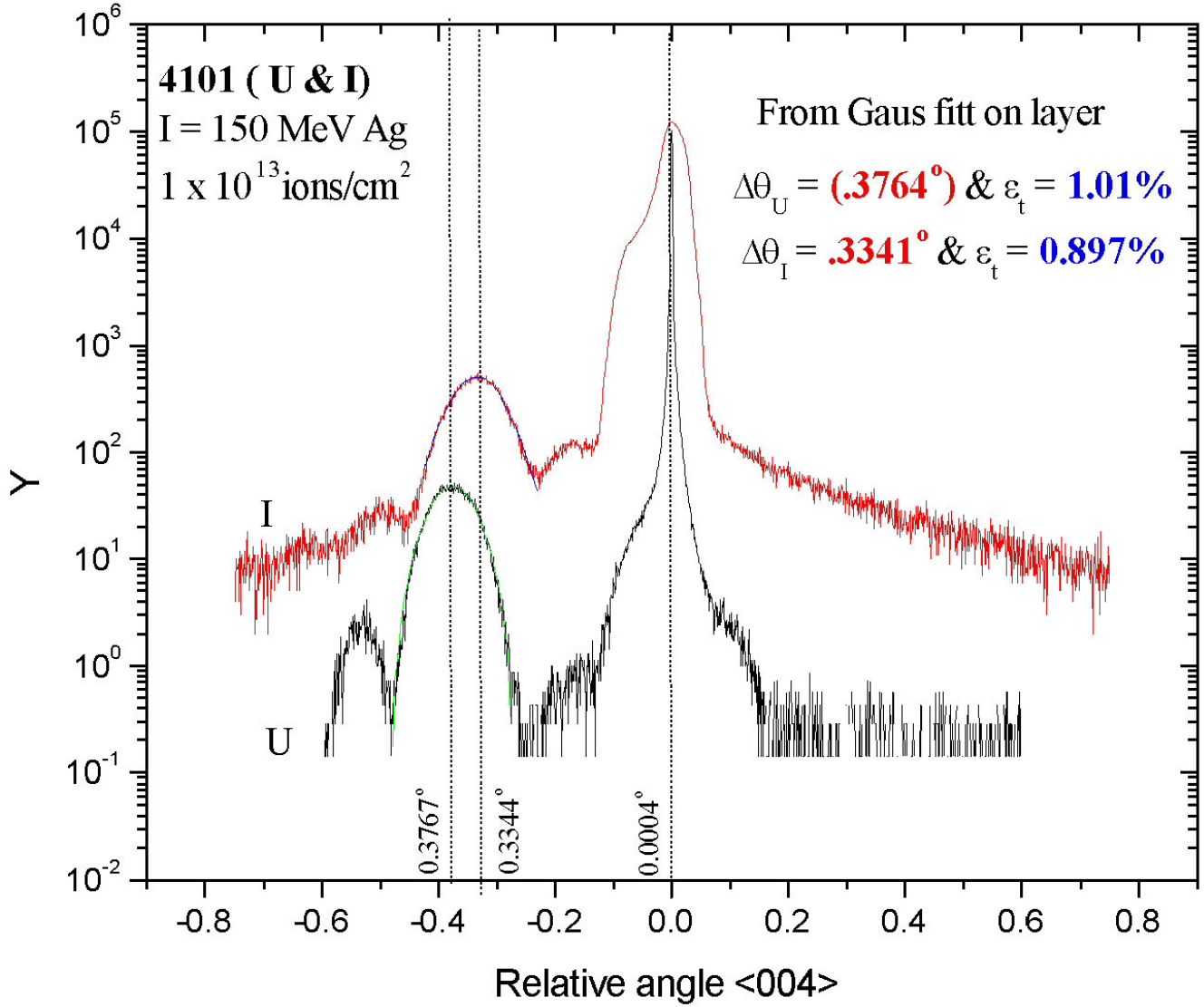
4101 (U & I)
I = 150 MeV Ag
1 x 10^13 ions/cm^2
From Gaus fitt on layer
Δθ_U = (.3764°) & ε_t = 1.01%
Δθ_I = .3341° & ε_t = 0.897%
I
U
0.3767°
0.3344°
0.0004°
Y
Relative angle <004>

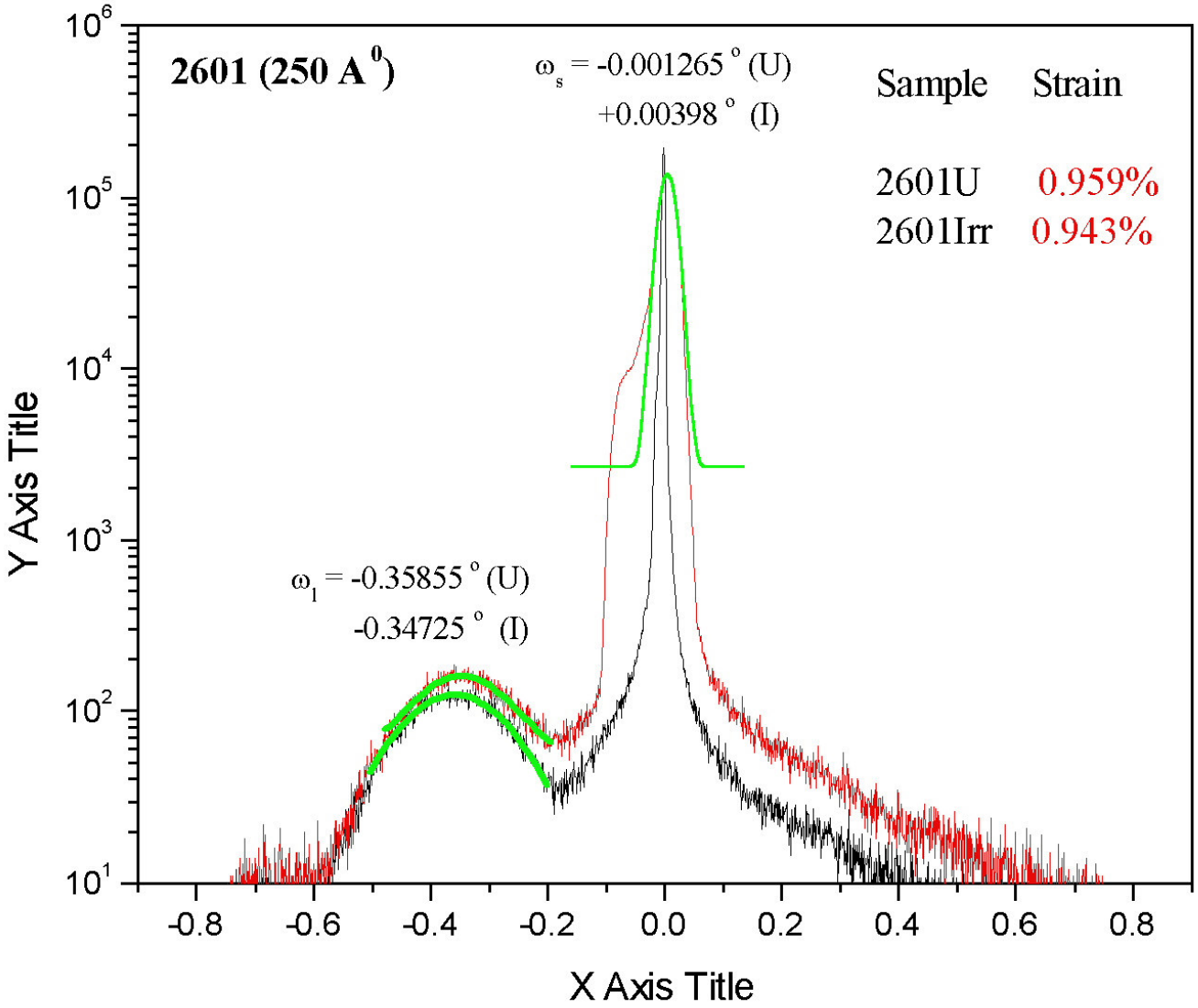
2601 (250 A 0)
ωs = -0.001265 ° (U)
+0.00398 ° (I)
Sample Strain
2601U 0.959%
2601Irr 0.943%
ω1 = -0.35855 ° (U)
-0.34725 ° (I)
Y Axis Title
X Axis Title
10^6
10^5
10^4
10^3
10^2
10^1
-0.8
-0.6
-0.4
-0.2
0.0
0.2
0.4
0.6
0.8

2601

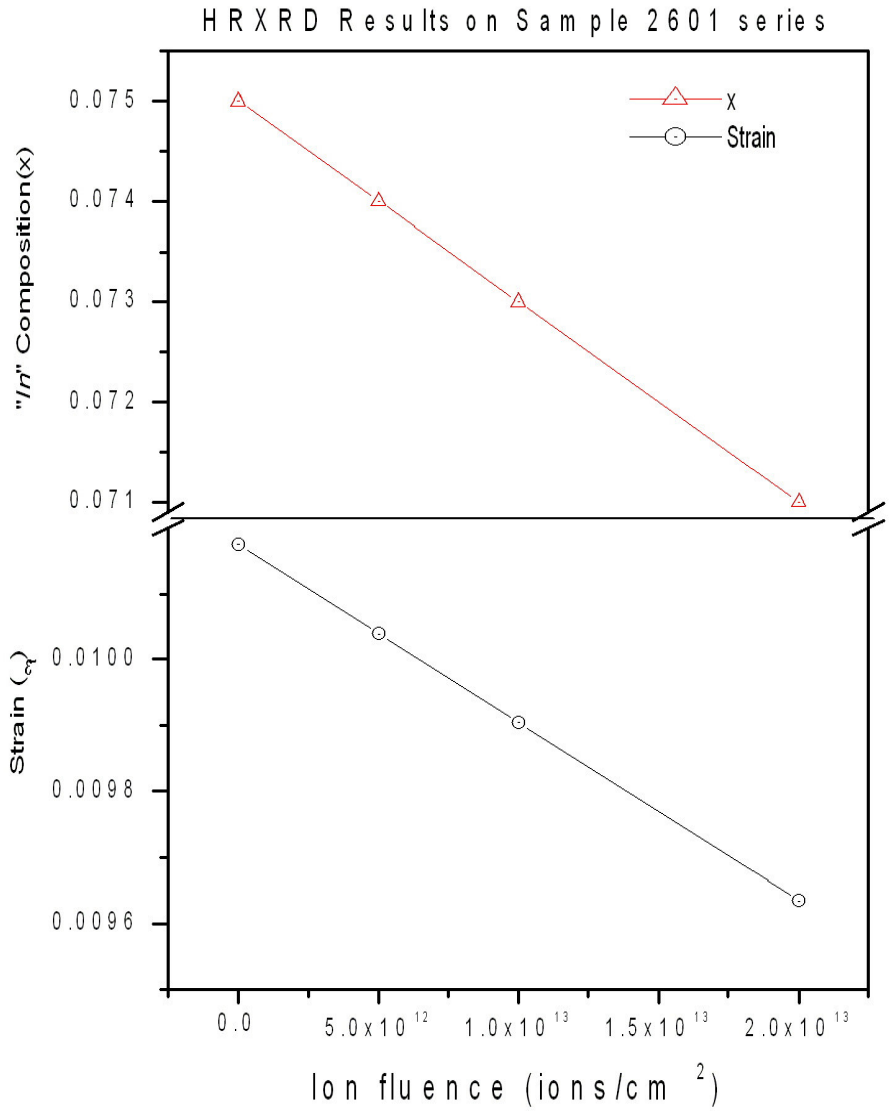

P523

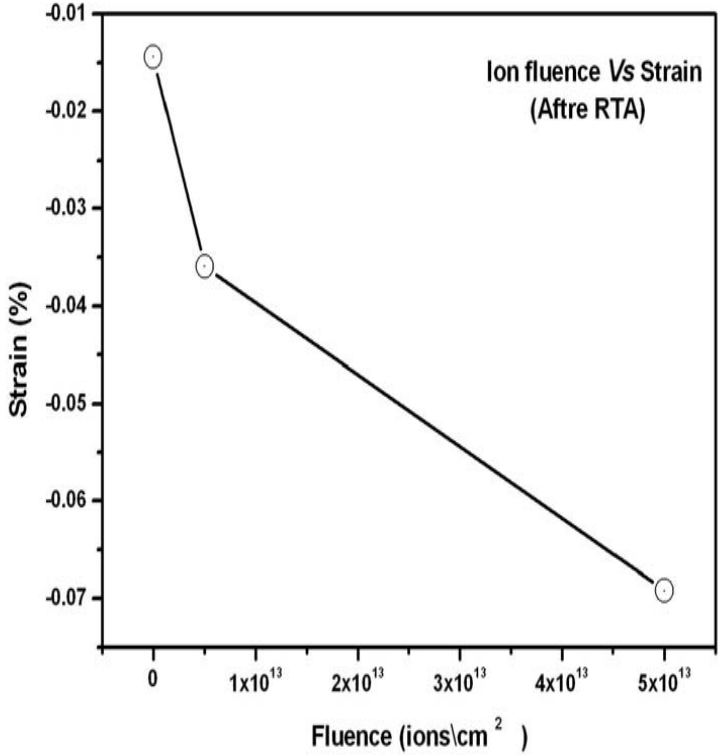

Compressive strain decreases with Increase in fluence

Tensile strain is induced in lattice matched system and it increases with fluence

Slope changes after a critical fluence

Experimental

The details of the samples used in this experiment are described in Table-1. The irradiation of the samples were done at room temperature by 150 MeV Ag ions with the fluence of $5x10^{12}$ and $1x10^{13}$ ions/cm^2 at the Nuclear Science Centre, New Delhi. The current was maintained low (0.5 – 2 pna) to avoid heating of the samples, which has been oriented at an angle of 5^0 with respect to the beam axis to minimize channeling. The samples were studied by ion channeling experiments at Alabama A&M University, Alabama, using 3.5 MeV He^{++} ions.

Table - 1

Sample ID	Irradiation Details Fluence (Ions/cm^2)	Nominal Composition and Thickness	Growth Technique & Source
4201U	Unirradiated	$In_{0.1}Ga_{0.9}As$ (100 Å)/GaAs	MBE, SSPL, Delhi
4201I	$1x10^{13}$	$In_{0.1}Ga_{0.9}As$ (100 Å)/GaAs	MBE, SSPL, Delhi
2601U	Unirradiated	$In_{0.1}Ga_{0.9}As$ (250 Å)/GaAs	MBE, SSPL, Delhi
2601I1	$5x10^{12}$	$In_{0.1}Ga_{0.9}As$ (250 Å)/GaAs	MBE, SSPL, Delhi
2601I2	$1x10^{13}$	$In_{0.1}Ga_{0.9}As$ (250 Å)/GaAs	MBE, SSPL, Delhi

Table – 2

Sample ID	Strain* $\varepsilon_{\perp}$(%)	'In' Content* (%)	FWHM of channeling dip** (Degrees)	$(a_{\perp}/a_{\parallel})$**	Alpha**	Strain** $\varepsilon_{\perp}$ (%)
4201U	0.9769	7.2	0.812	1.01005	0.9482±0.1506	0.50766
4201I	0.8418	6.2	0.832	1.01004	1.2579±0.1503	0.50720
2601U	1.0174	7.5	1.1228	1.01086	1.0296±0.1748	0.54836
2601I1	1.0039	7.4	1.413	1.01007	0.8993±0.1512	0.50866
2601I2	0.9904	7.2	1.8208	1.01005	0.9482±0.1506	0.50766

*** HRXRD Results From [12]**

**** Results of Present Ion Channeling Work**

Channeling Angular Scans

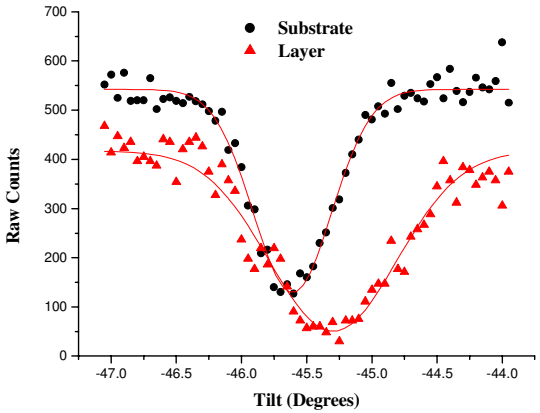

(a)

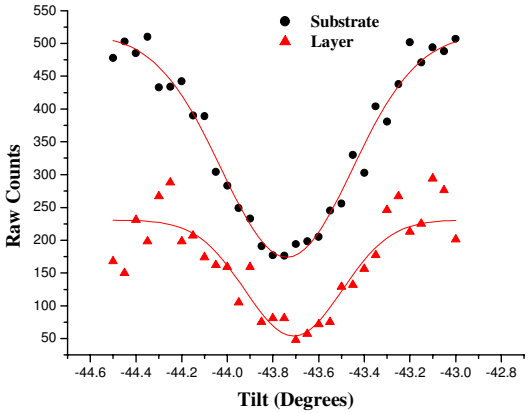

(b)

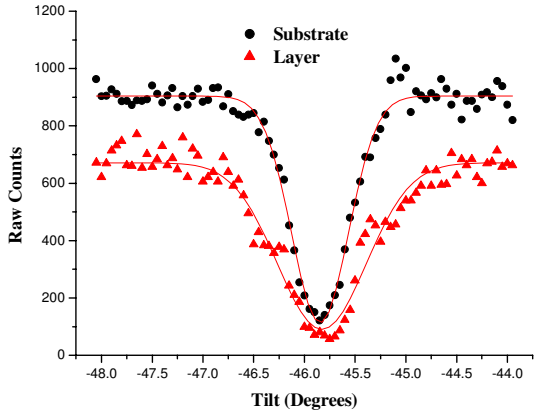

(c)

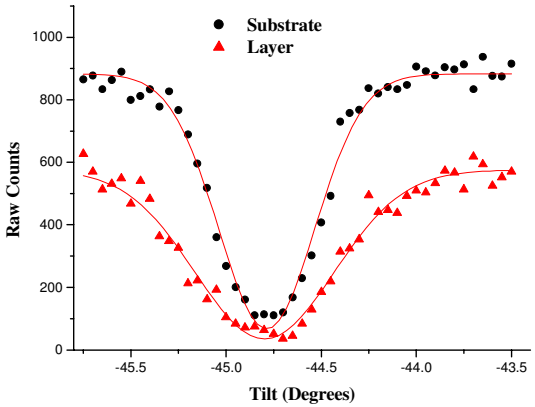

(d)

(a) & (b) Angular Scans of 2601U and 2601I1, (c) & (d) Angular Scans of 4201U and 4201I, Data Points with Gauss Fittings.

Fluence Dependence

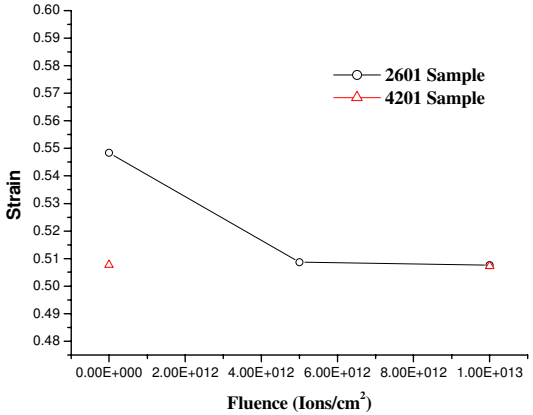

(a)

(b)

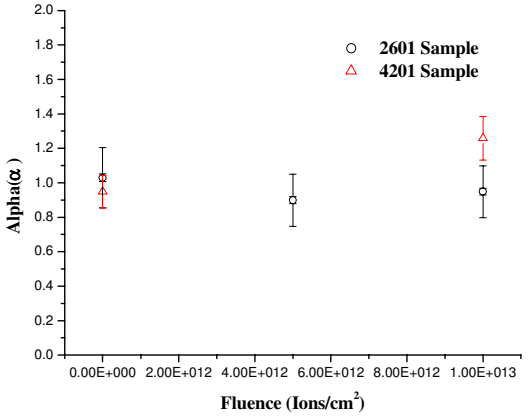

(c)

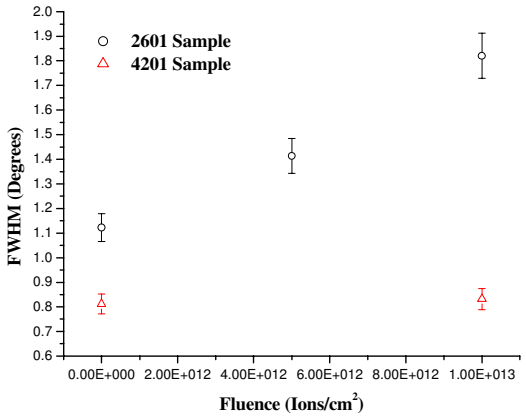

Fluence Dependence of (a) Strain, (b) Alpha and (c) FWHM of Layer Dip

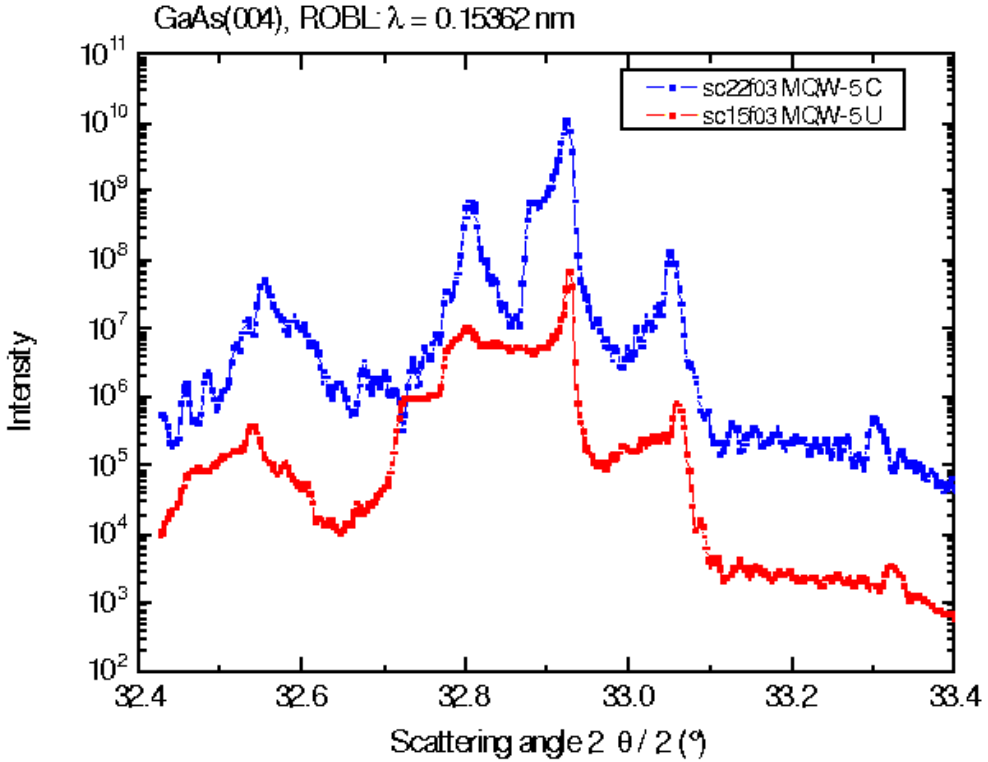

Sample	Double layer thickness (nm)	Main system		Secondary system	
		$(\Delta d/d)_{\perp}$	In content	$(\Delta d/d)_{\perp}$	In content
MQWU	20.15±. 08	0.325%	7%	0.164%	4%
MQWI	21.18± . 08	0. 298%	6%	0.120%	3%

The common trend in all the samples indicates the gradual diffusion of *In* from surface and the migration of *Ga or As* like atoms to the surface regions due to the SHI irradiation and/or annealing processes. The compressive strain is found to decrease in the initially compressive strained samples and tensile strain is induced in an initially lattice matched system. General trend indicates the increase in the superlattice period after the irradiation. Effect increases linearly with in crease in fluence and slope changes at a critical fluence.

Strain Relaxation

The $In_{0.18}Ga_{0.82}As/GaAs$ heterostructures were grown by Molecular Beam Epitaxy (MBE) with layer thicknesses of 12, 36, 60 and 96nm, at a growth temperature of 500^0C and at a rate of 0.2nm/Sec.

- The SHI irradiations were done at room temperature by 150 MeV Ag^{12+} ions with a fixed fluence of $1x10^{13}$ ions/cm^2 from 15MV Tandem Van de Graff – type electrostatic accelerator (pelletron) at NSC, New Delhi. The beam current was maintained low (0.5 – 2 pnA) to avoid heating of the samples, the samples were oriented at an angle of 5^o with respect to the beam axis to minimize channeling.

RBS/Channeling experiments were performed by varying the incident He+ ion energy from 1.7MV pelletron accelerator at IGCAR, Kalpakkam. <001> axis channeling was carried out for dechanneling analysis varying the energy between 2 and 4.1MeV. The dechanneling parameter is calculated from the normalized the back scattering yield to see the energy dependence for defect analysis. The dechanneling parameter (DP) is calculated using the formula,

$$DP = -\log\left\{\frac{1-\chi_D}{1-\chi_V}\right\} \quad \text{--------- (1)}$$

Where DP = $n_D\sigma_D$, n_D is the defect density and σ_D is the dechanneling cross section χ_D is the minimum yield in the defected crystal and χ_V is the minimum yield of the defect free crystal at the same depth.

In the present study χ_D was obtained from the experimental RBS spectra from the GaAs buffer layer (i.e. below the interface) and χ_v was taken as 3% approximately. DP Vs $E^{0.5}$ plot with linear fit and its slope was used for the calculation of dislocation density,

$$n_D = \frac{Slope \times \sqrt{E}}{\sigma_D} \quad \text{--------- (2)}$$

Where σ_D is given by,

$$\sigma_D = K \times \sqrt{\frac{a\,b\,d\,E}{Z_1 Z_2 e^2}} \quad \text{--------- (3)}$$

K is constant = 0.471, a is Thomas Fermi screening radius = 0.127366 Å, b is the burger vector ≅ 4 Å.

Table-I

InGaAs/GaAs (001) sample details and calculated parameters.

Sample Id#	Layer Thickness (nm)	Indium Composition (%)	χ_{min}		Energy Dependence of DP		Dislocation Density (10^5 cm^{-1})	
			U	I	U	I	U	I
0903	36	18	0.221	0.169	$E^{0.42}$	$E^{0.45}$	4.643	3.859
1003	60	18	0.304	0.287	*	*	*	*
1103	96	18	0.441	0.380	$E^{0.51}$	$E^{0.54}$	9.602	9.431

* Not reported in the present study. # Sample Ids in text with U & I refers to unirradiated and irradiated.

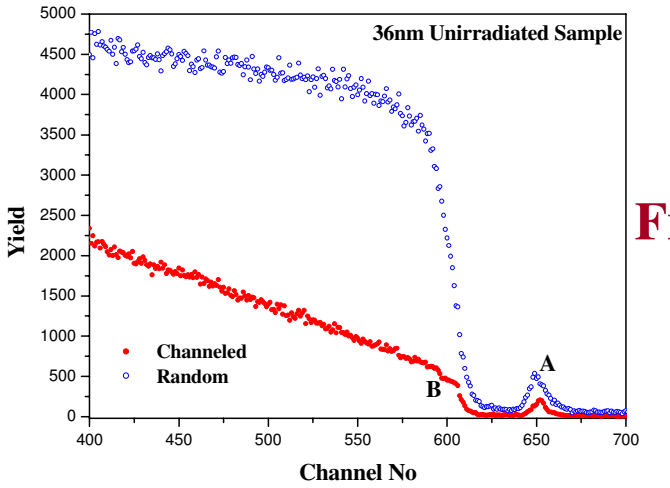

Fig:1

Fig:2

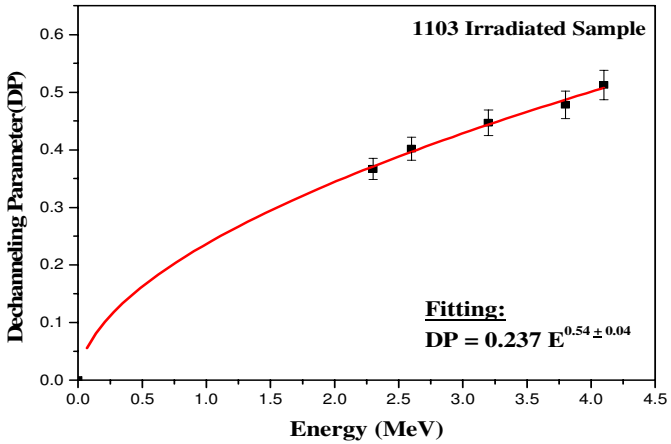

Fig.1: Random and Channeling spectra of 0903U sample. Fig.2: Energy dependence of DP for 1103I Sample. Fig.3: DP Vs $E^{0.5}$ for 1103U sample data points with linear fit. Fig.4: Experimental RBS Spectra of 1003 U&I Sample with Gisa3 fittings.

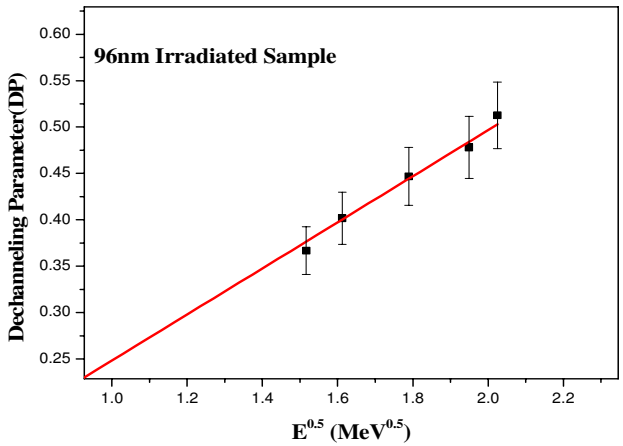

Fig:3

Fig:4

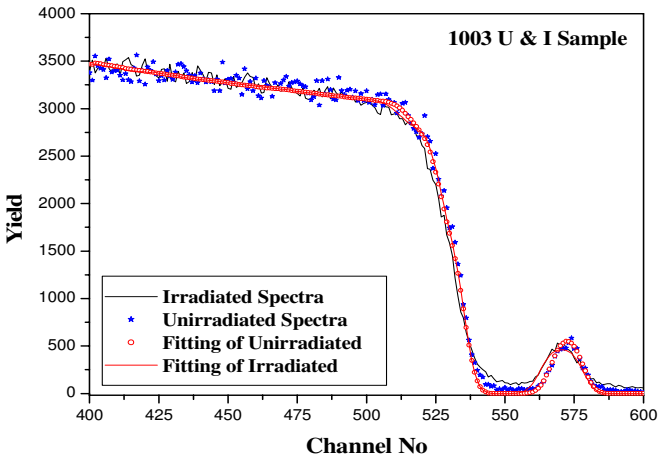

In conclusion the DP shows E0.5 dependence which is attributed to the presence of dislocations. The dislocation density calculated shows that it has been reduced after irradiation. The reduction in dislocation density is probably due to the formation of intermediate layer $In_xGa_{1-x}As/In_yGa_{1-y}As/GaAs$ (with y<x), where the intermediate layer would act as a buffer for the over-layer and at this interface the strain would be relatively less. Though in irradiated samples y and x values could not be determined the intermediate layer formation is clearly observed from the indium diffusion which is confirmed in other complementary studies also. This is proposed as the possible mechanism for the observed reduction in dislocation density, further analysis is in process to confirm this mechanism.

- **The Raman scattering measurements were made at room temperature and in backscattering geometry with argon-ion laser of 514.5nm. Surface morphology of these structures has been characterized using AFM (DFM mode).**
- **Under strained conditions LO phonon frequency of the InGaAs layer depends on the strain induced according to the following equation (1) [2, 7&8], $\Delta\Omega_H$ is shift due to hydrostatic component of the stress and**

$$\omega = \omega_0 + 2\Delta\Omega_H - \frac{2}{3}\Delta\Omega \qquad \text{-------- (1)}$$

$$\Delta\Omega_H = \frac{p + 2q}{6\omega_0^2}\left(\frac{S_{11} + 2S_{12}}{S_{11} + S_{12}}\right)\omega_0\varepsilon \qquad \text{-------- (2)}$$

$$\Delta\Omega = \frac{p - q}{2\omega_0^2}\left(\frac{S_{11} - S_{12}}{S_{11} + S_{12}}\right)\omega_0\varepsilon \qquad \text{-------- (3)}$$

$\Delta\Omega$ is difference between the singlet and doublet components of optical phonons.

Where the term involving p and q is deformation potential and S_{11} and S_{12} is the elastic constants. The values of $(p+2q/6\omega_0^2)$ and $(p-q/2\omega_0^2)$ are (-)0.891 and 0.185, the values of $(S_{11}+2S_{12}/ S_{11}+S_{12})$ and $(S_{11}-S_{12}/ S_{11}+S_{12})$ are 0.028 and 0.047. These values are obtained from Ref [7] assuming Veggard's law for $In_{0.18}Ga_{0.82}As$. Negative sign for compressive strain is the convention used here. Replacing the values of these terms in equation (1) we obtain a simple relation,

$$\omega = \omega_0 - 1.293\omega_0\varepsilon \quad \text{.....(4)}$$

with ω and ω_0 in units of cm^{-1}. This equation predicts the shifts due to the strain (ε) in the layer.

Table-II

Strain Measured from the Raman Spectra

$In_{0.18}Ga_{0.82}As/GaAs$ Samples (Layer Thickness)	Shift in GaAs LO Mode (cm^{-1}) (Unirradiated)	Shift in GaAs LO Mode (cm^{-1}) (Irradiated)	Strain (%) (Unirradiated)	Strain (%) (Irradiated)
12 nm	4.64	6.12	1.248	1.646
36 nm	4.26	5.36	1.194	1.442
60 nm	4.06	2.73	1.092	1.005
96 nm	1.30	0.38	0.350	0.122

Figures

Fig. 1&2: Raman spectra of 12 and 60nm thick samples

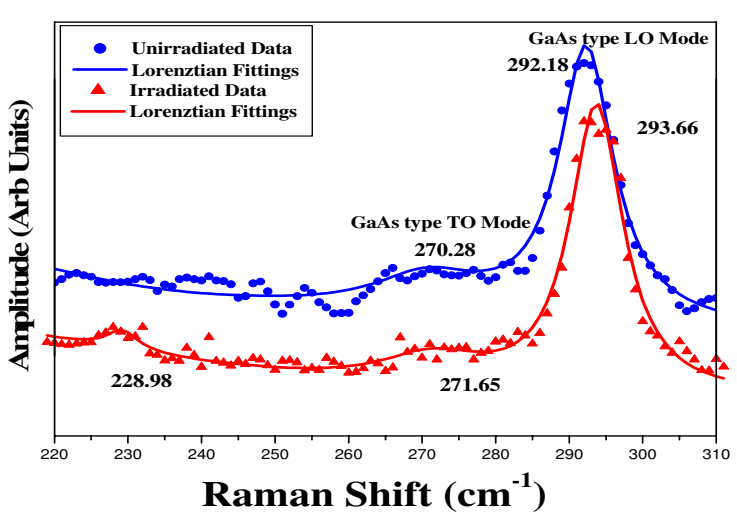

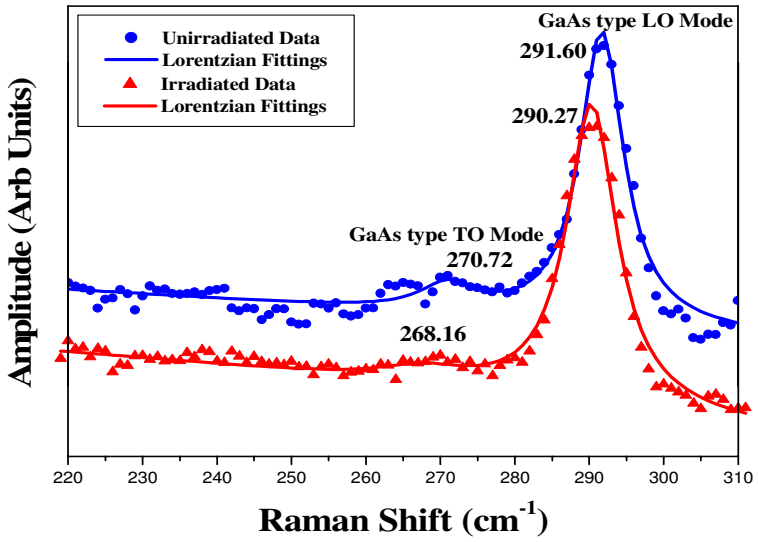

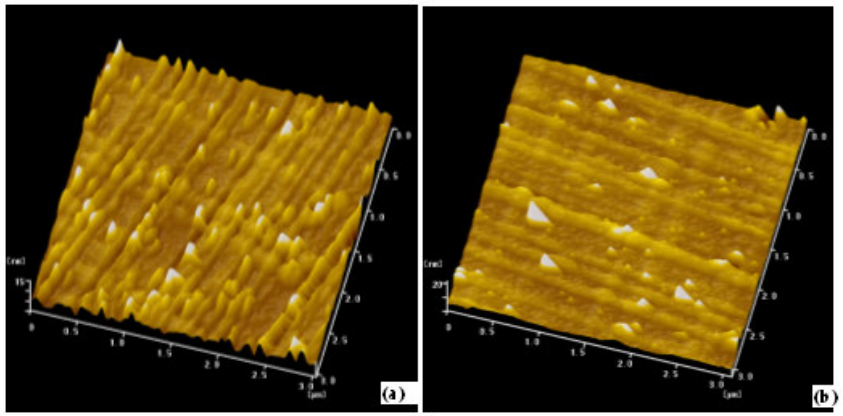

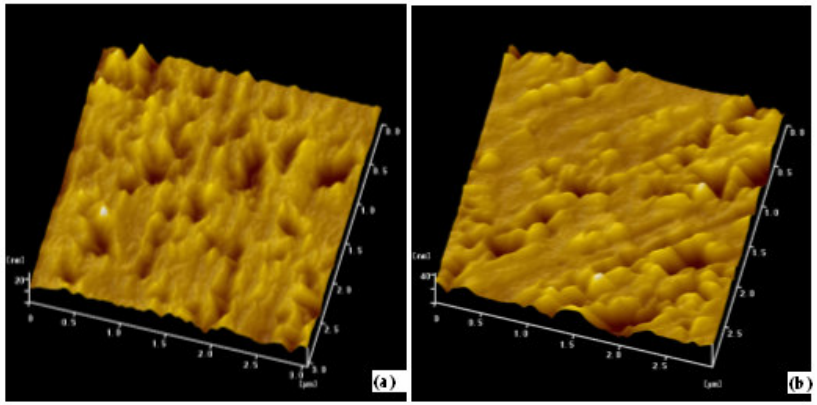

Fig. 3&4: AFM of 36 and 60nm thick (a) Unirradiated and (b) Irradiated samples

Conclusions

- **In conclusion, strain modification of SHI irradiated InGaAs/GaAs heterostructures using Raman spectroscopy has been reported for the first time.**
- ***The Raman results are discussed in the light of penetration depth of the probe beam. Different effects of heavy ion irradiation are observed near the surface and at the interface. The role of initial strain energy for different irradiation effects is highlighted.***
- **A diffusion mechanism is proposed to explain the modifications, which is comparable with other complementary techniques namely HRXRD and RBS/Channeling.**
- **AFM results on surface morphologies are correlated with Raman results and the different relaxation regimes were identified.**

Channeling Radiation

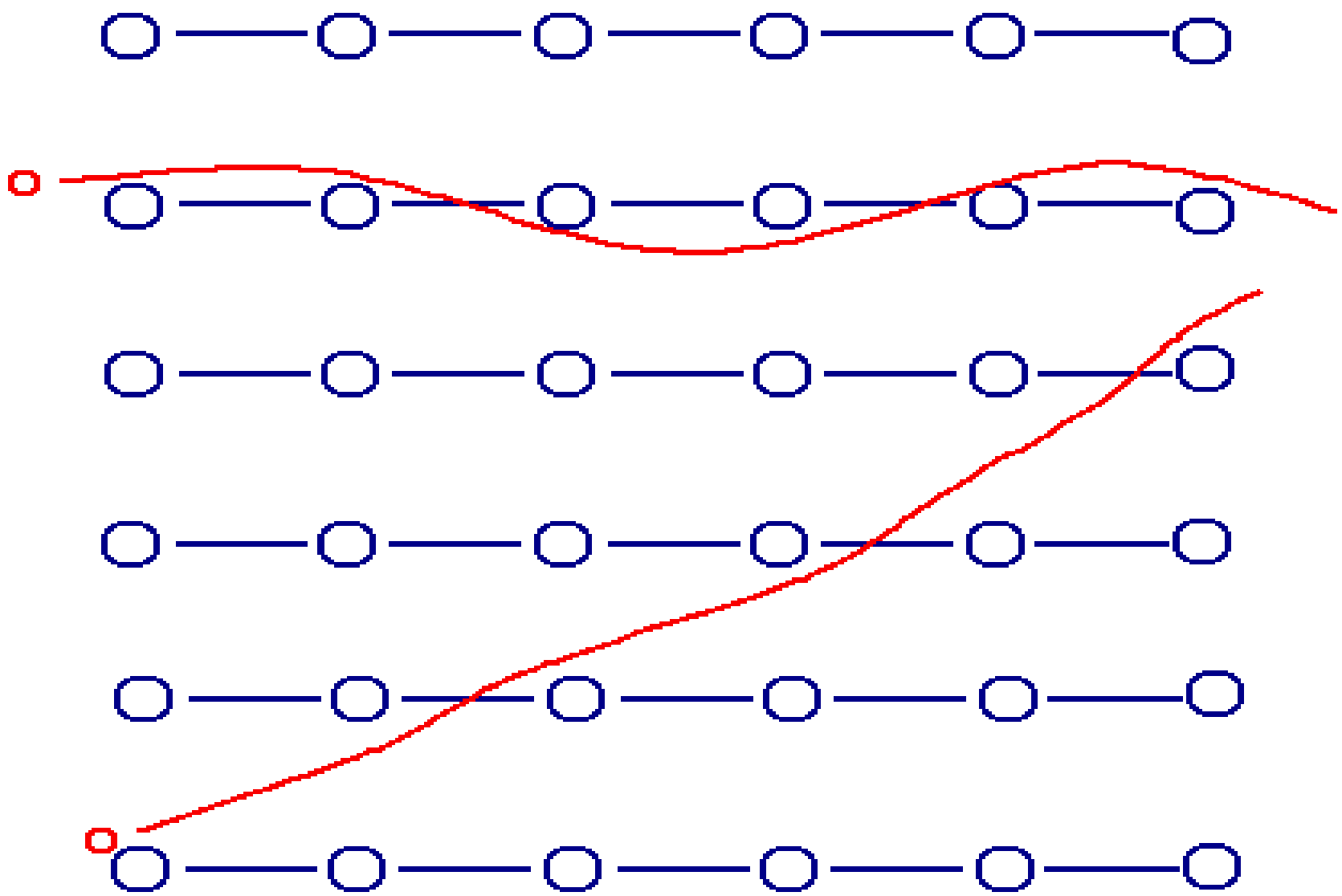

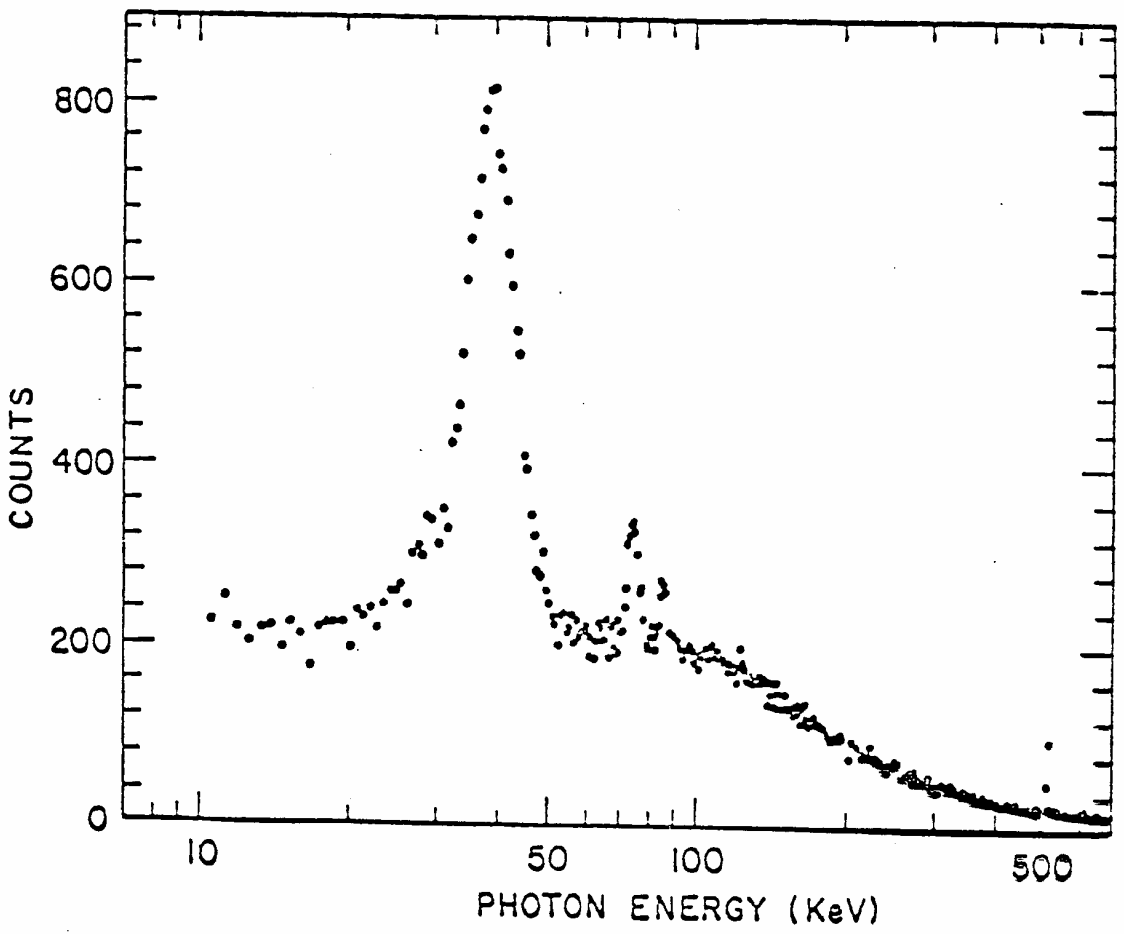

Figure 1. Radiation from $\gamma = 107$ positrons channeled by (110) planes in Si. The crystal thickness is 9 μm. Channeling produces the large peak near 40 keV photon energy; the two peaks near 80 keV are fluorescence from Pb bricks near the detector; and the 511 keV peak is from positron annihilation.

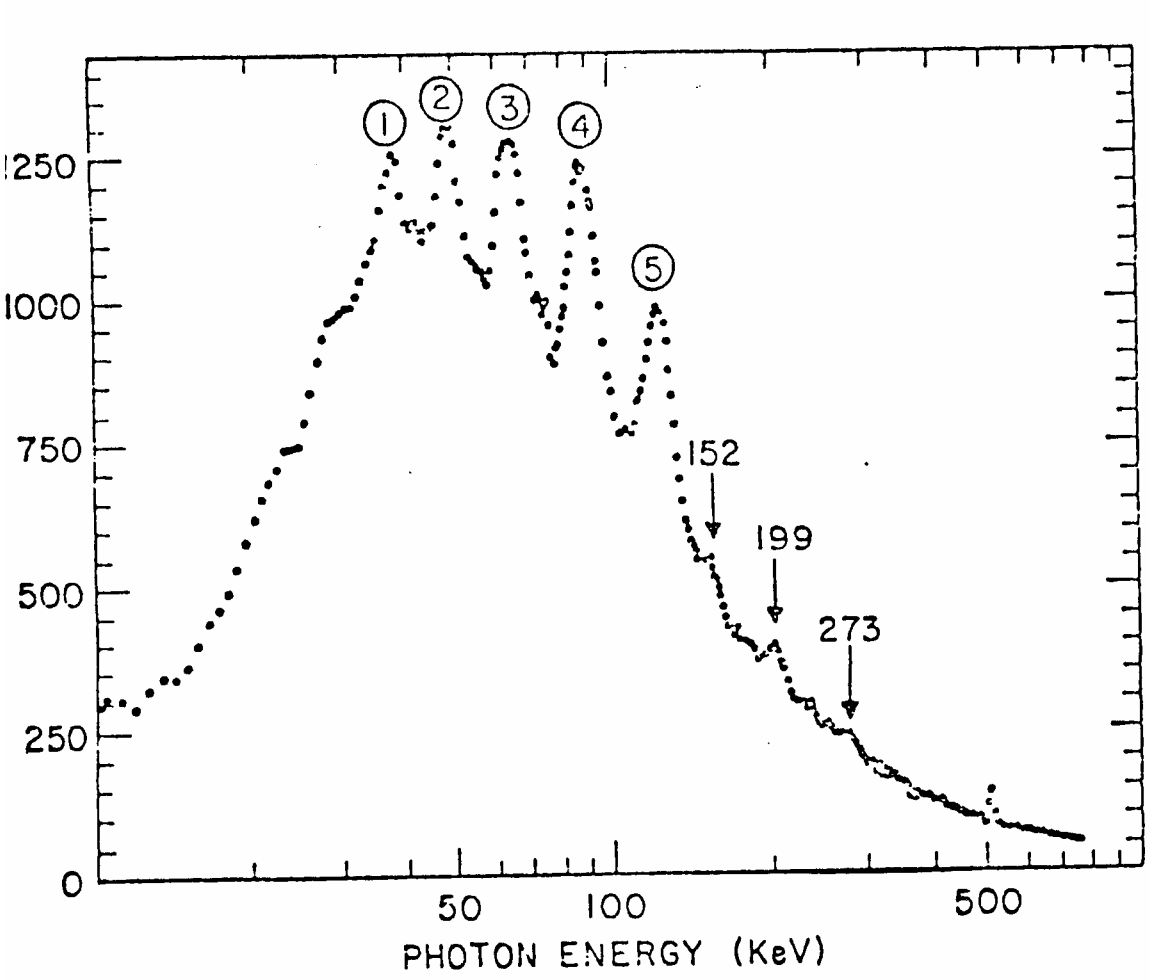

ıre 2. Radiation from γ = 107 electrons channeled by (110) planes in Si. The crystal thickness is 20 μm. Peaks labelled (1) - (5) result from Δn = 1 transitions and the peaks at 152, 199 and 273 keV are Δn = 3 transitions.

- **The realization that relativistic effects will shift the photon energy into keV or even MeV region was a turning point in this field.**

- **The radiation was in fact observed for both positrons and electrons**

Motion and Potentials

Lab frame

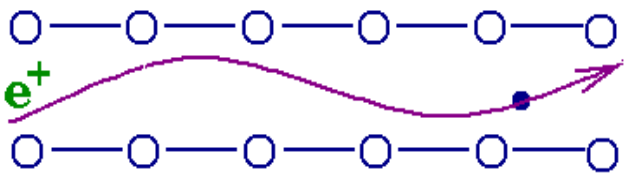

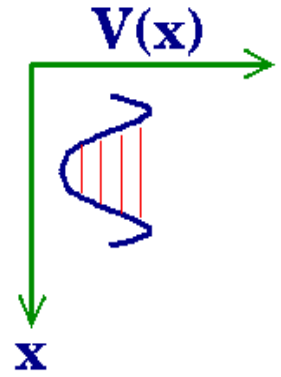

Rest frame

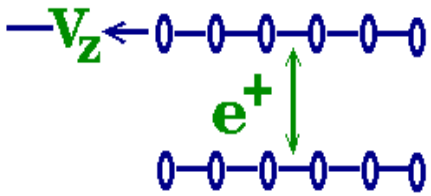

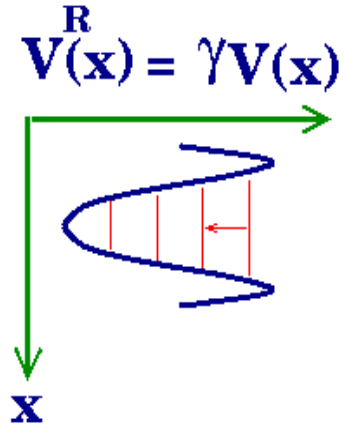

Intensity and Frequencies

Rest frame

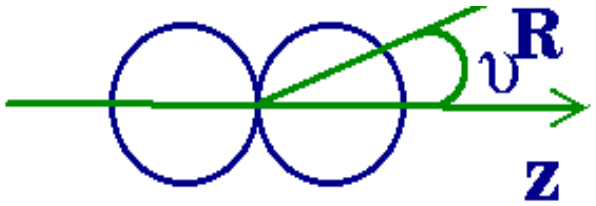

$$\varpi^R = \Delta E_\perp^R / \hbar = \gamma\omega_o$$

Lab frame

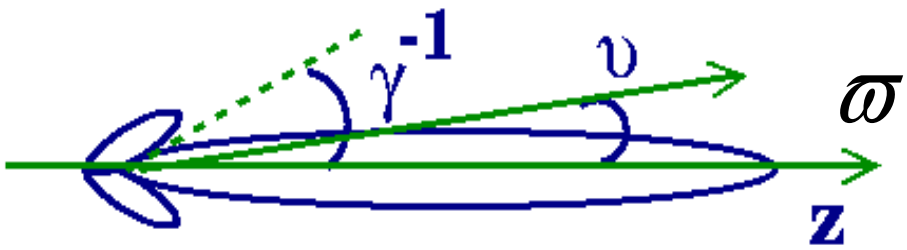

$$\varpi = \frac{\varpi^R}{\gamma(1-\beta\cos\nu)} \approx \frac{2\gamma^2\varpi_o}{1+\gamma^2\nu^2}$$

The planar potential due to both the planes is given by

$$V(x) = V_0'/(L^2 - x^2), \qquad (1)$$

where $V_0' = 4\pi Z_1 Z_2 e^2 CNd_p La^2$, Z_1 and Z_2 are the projectile and target charge numbers, N is the target atomic concentration, $d_p\,(=21)$ is the interplanar spacing, $L = 1 + a$,

The frequency of Channeling radiation in normal perfect channel is given by

$$\omega_{\text{chan}} = 2\gamma^{3/2}\sqrt{k_1/m_0},$$

where $k_1 = 2V_0'/L^4$ and m_0 is the positron rest mass. The corresponding linewidth due to anharmonic effects, determined by using the first order perturbation theory, was found to be proportional to $n_{max}\epsilon\omega_{obs}$, where n_{max} is the maximum number of bound states supported by the transverse continuum potential and ϵ is given by

$$\epsilon = \frac{3\hbar}{4\sqrt{m_0\gamma}} \frac{k_2}{k_1^{3/2}}, \tag{3}$$

where $k_2 = 4V_0'/L^6$. As discussed earlier,[4] this simple anal-

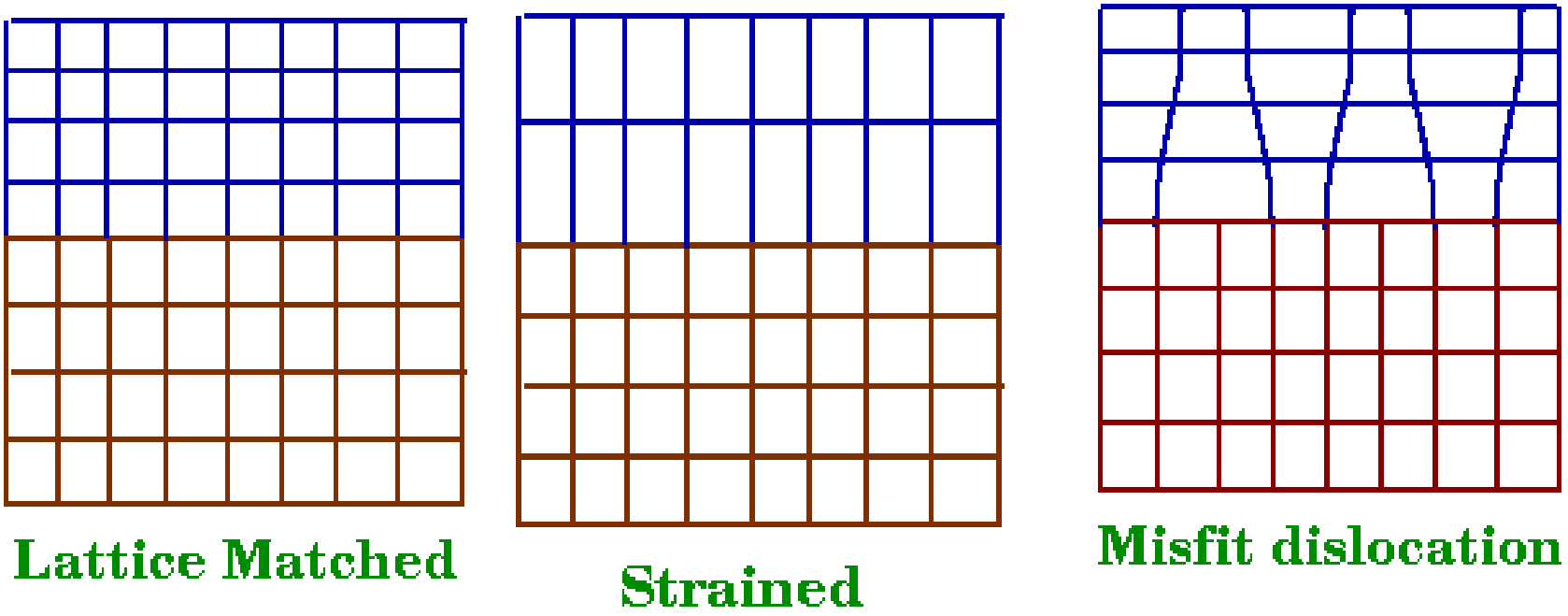

- These SLS have potential device applications for high performance detectors, high speed and high frequency digital and analogue circuits.

- The strain, being key parameter is very important to study.

At each interface the particle sees a tilted channel and hence a modified force constant $k_1 \cos\theta$ and also an-harmonicity factor so that frequency and the linewidth both change (DECREASE) as against increase due to dislocation affected curved channels

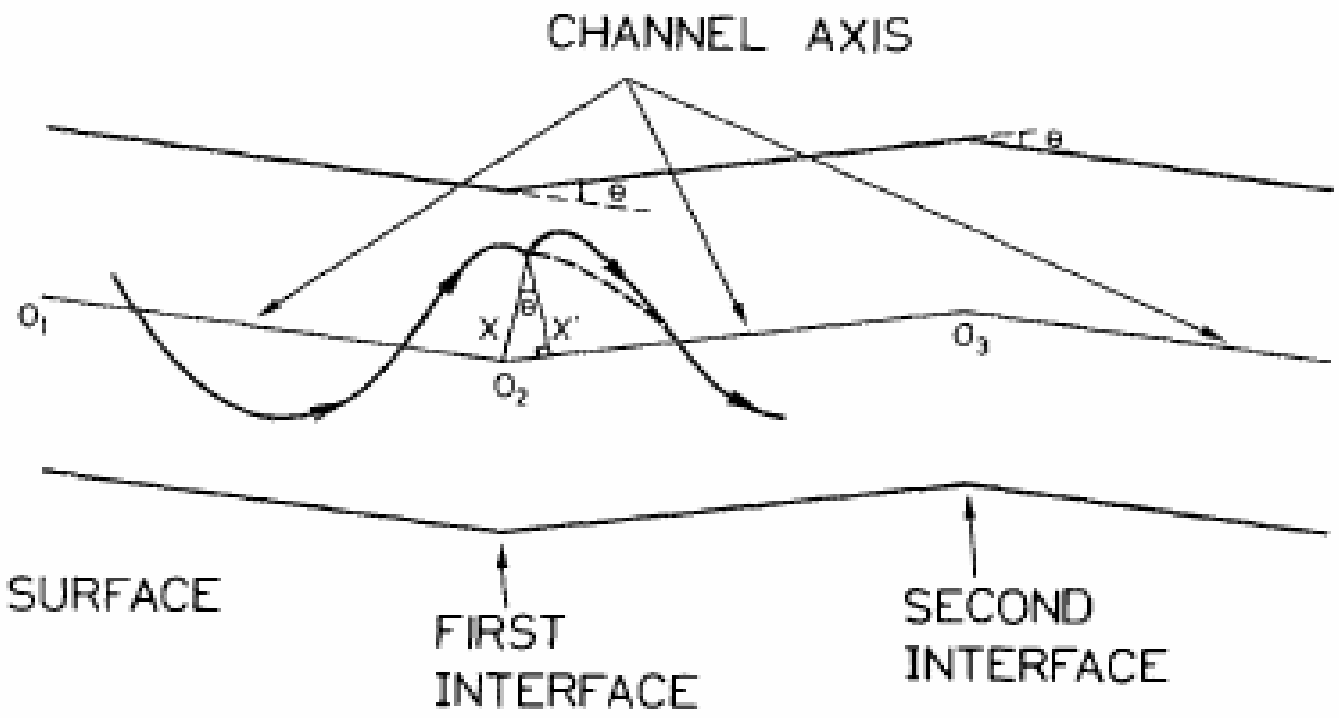

The planar potential due to both the planes is given by

$$V(x) = V_0'/(L^2 - x^2), \qquad (1)$$

where $V_0' = 4\pi Z_1 Z_2 e^2 C N d_p L a^2$, Z_1 and Z_2 are the projectile and target charge numbers, N is the target atomic concentration, $d_p\,(=21)$ is the interplanar spacing, $L = 1 + a$,

The frequency of Channeling radiation in normal perfect channel is given by

$$\omega_{\text{obs}} = 2\gamma^{3/2}\sqrt{k_1/m_0},$$

where $k_1 = 2V_0'/L^4$ and m_0 is the positron rest mass. The corresponding linewidth due to anharmonic effects, determined by using the first order perturbation theory, was found to be proportional to $n_{\max}\epsilon\omega_{\text{obs}}$, where $n_{\max}$ is the maximum number of bound states supported by the transverse continuum potential and ϵ is given by

$$\epsilon = \frac{3\hbar}{4\sqrt{m_0\gamma}}\,\frac{k_2}{k_1^{3/2}}, \qquad (3)$$

where $k_2 = 4V_0'/L^6$. As discussed earlier,[4] this simple anal-

where $V_0 = V_0'/L^2$. By absorbing the cosine factor in the force constants k_1 and k_2, we get the new peak frequency

$$\omega' = 2\gamma^{3/2}\sqrt{k_1 \cos^2\theta/m_0} = \omega_{\text{obs}} \cos\theta \tag{5}$$

and the new anharmonic (first order perturbation) constant, according to Eq. (3), becomes

$$\epsilon' = \epsilon \cos\theta \tag{6}$$

because k_2 changes to $k_2 \cos^4\theta$ and k_1 to $k_1 \cos^2\theta$. Therefore, the linewidth becomes proportional to $n_{\max}$ $\epsilon'\omega' = n_{\max}\epsilon\omega_{\text{obs}} \cos^2\theta$. For a superlattice having n layers, θ is replaced by $\sqrt{n}\theta$ (for small θ). This is because using Eq. (5) and (6) repeatedly n times, we get a $\cos\theta$ factor every time so that finally ω' (after n layers) $= \omega_{\text{obs}} \cos^n\theta$ $\simeq \omega_{\text{obs}} \cos\sqrt{n}\theta$. Because for small θ (less than channeling critical angles) the replacement $\cos\theta \simeq 1 - \theta^2/2$ and $\cos\sqrt{n}\theta \simeq 1 - n\theta^2/2$ are fairly accurate. Hence the net fractional decrease of peak frequency is $\cos\sqrt{n}\theta$ and the net fractional decrease in the linewidth is $\cos^2\sqrt{n}\theta$.

The effects of the tilt and / or the obstruction on the channeling radiation at the tilted interface of SLS has been studied in quantum mechanical framework. Channeling angular scans have been obtained using simple quantum concepts.

Quantum Description of Electron and Positron Channeling

- **The transverse potential for planar channeled positron varies as x^2 (Harmonic type) and 1/|x| for planar channeled electrons (One dimensional H atom type) with corresponding energy spectrum.**

- **Hence the wave function of planar channeled positron is that of one dimensional harmonic oscillator.**

$$\psi_n^+ = A_n \exp(-\alpha^2 x^2) H_n(\alpha x)$$

- **The wave function of planar channeled electron is given by**

$$\psi_n^- = \sqrt{\frac{2}{a_0^3 n^5 (n!)^2}} \exp(-|x|/na_0)\{x\} L_n^1(2|x|/na_0)$$

- **Where the function {x} is defined as x for even states and |x| for odd states.**

- **The electrons corresponding to lower transverse energy states, oscillate around the atomic planes with a smaller amplitude so that overall they spend larger fraction of their time in the vicinity of atomic planes.**

- **Hence in electron channeling, the electrons in the ground state of**

INITIAL POPULATION

- When high energetic electron / positron beam is injected into the crystal, depending upon the angle of incidence and beam divergence the particle flux gets populated among various quantized energy leve

- The initial value of quasi momentum (q_x) is defined by matching the Bloch wavefunction to the incident plane wave at the crystal surface.

- By matching the wavefunction at the crystal entry face, we obtain an expression for the initial population of the energy levels as

$$\Pi_n = \left| \int_{-d_P/2}^{d_P/2} \exp(iq_x x)\psi_n(x)dx \right|^2$$

- **For positron case this is obtained in terms of *Hermite polynomial* index and coupling constant ‘α’**

$$\Pi^{+}{}_{n} = \frac{\sqrt{\pi}}{\alpha n! 2^{n-1}} \exp\left\{-\frac{q_x^2}{\alpha^2}\right\} \left| H_n\left(\frac{q_x}{\alpha}\right)\right|^2$$

- **Similar integral for electron case was evaluated numerically due to the complicity caused by Laguerre polynomials.**

- **These incident angle vs population graphs represent the famous channeling angular scans.**

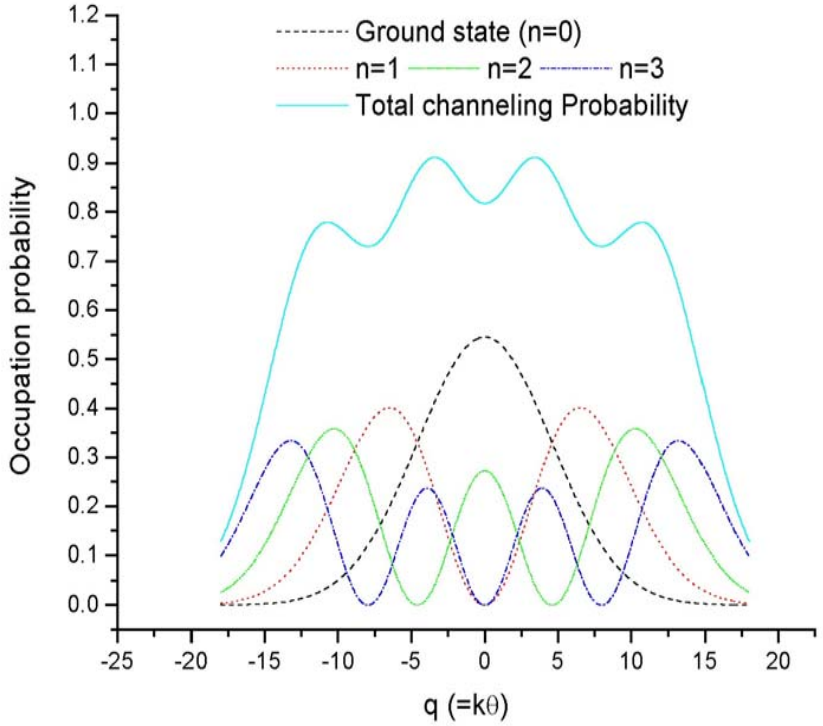

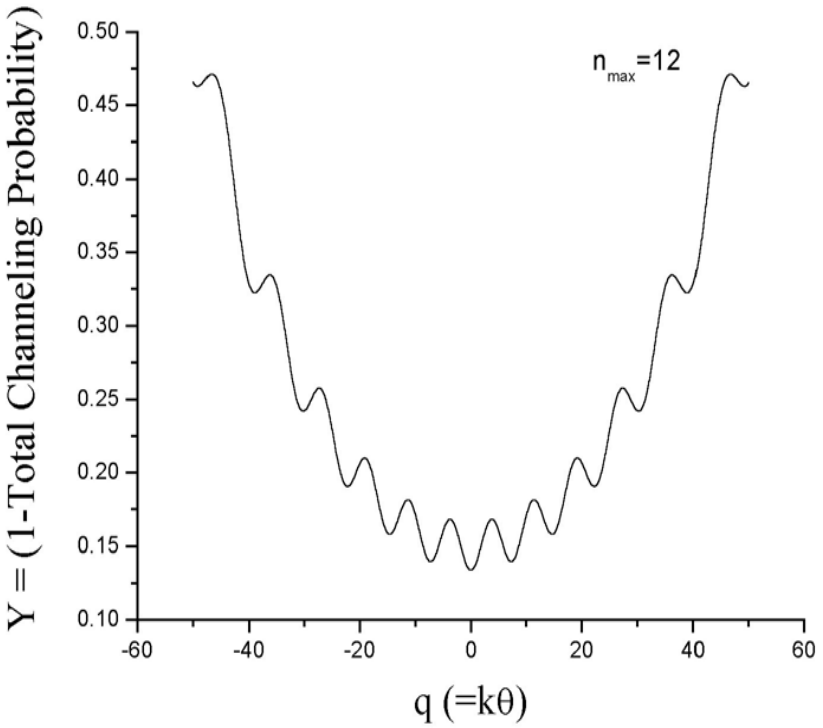

We have obtained the channeling angular scans, quantum mechanically in a more natural way.

- It is clear from the figure that the lower states have more probabilit while excited states are less populated.
- As expected, the ground state shows a Gaussian distribution aroun center of the channel.
- Higher states are populated if the incident angle is increased.
- Total channeling probability shows the wiggles that are generally observed in the experiments with planar-channeled positrons.

EFFECTS OF STRAINED LAYER SUPER LATTICE ON CHANNELING RADIATION

- Some of the particles will dechannel while crossing the tilted inter
- This beam attenuation depends on initial phase at the entry surfa

- **The dechanneling is attributed partly to**
  (i) the abrupt shift (a_s) in the atomic planes (denoted by) an
  (ii) their relative orientation angle 'θ'.

Case 1

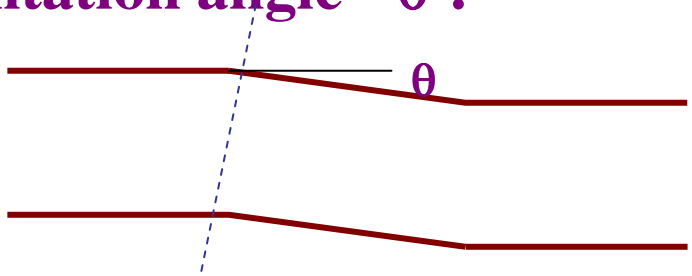

Case 2

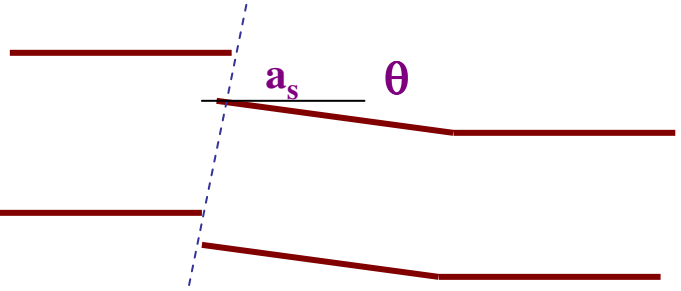

- **If the layers are less strained and the shift $a_{sls} \sim a_{TF}$, majority of tl particles are expected to survive during their passage through th strained portion between the multi-layers.**

- **The wave function describing these survived particles will b similar to that of the usual channeled states with modified argume containing a_s and 'θ'.**

- **The expression for population re-distribution after passing the tilt interface, is obtained by matching the wave functions across t boundary, near the strained portion.**

$$\prod_{SLS} = \sum_{n=0}^{n_{max}} \left| \int e^{ik\theta_x} \phi_n(x) \phi_m(x + a_s) dx \right|^2$$

- **The analytical expression for e^+ case is obtained in terms of Laguer polynomials.**

$$\Pi^{+}_{SLS} = e^{-r^2/2} \left(\sum_{n=0}^{n_{max}} \frac{(\min\{m,n\})!}{(\max\{m,n\})!} \left(\frac{r^2}{2} \right)^{|n-m|} \left[L^{|n-m|}_{\min(m,n)} \left(\frac{r^2}{2} \right) \right]^2 \right)$$

Here $b^2 + \beta^2 = r^2$ with $b = \alpha s$, $\beta = K\theta / \alpha$ and 'K' being the longitudi momentum.

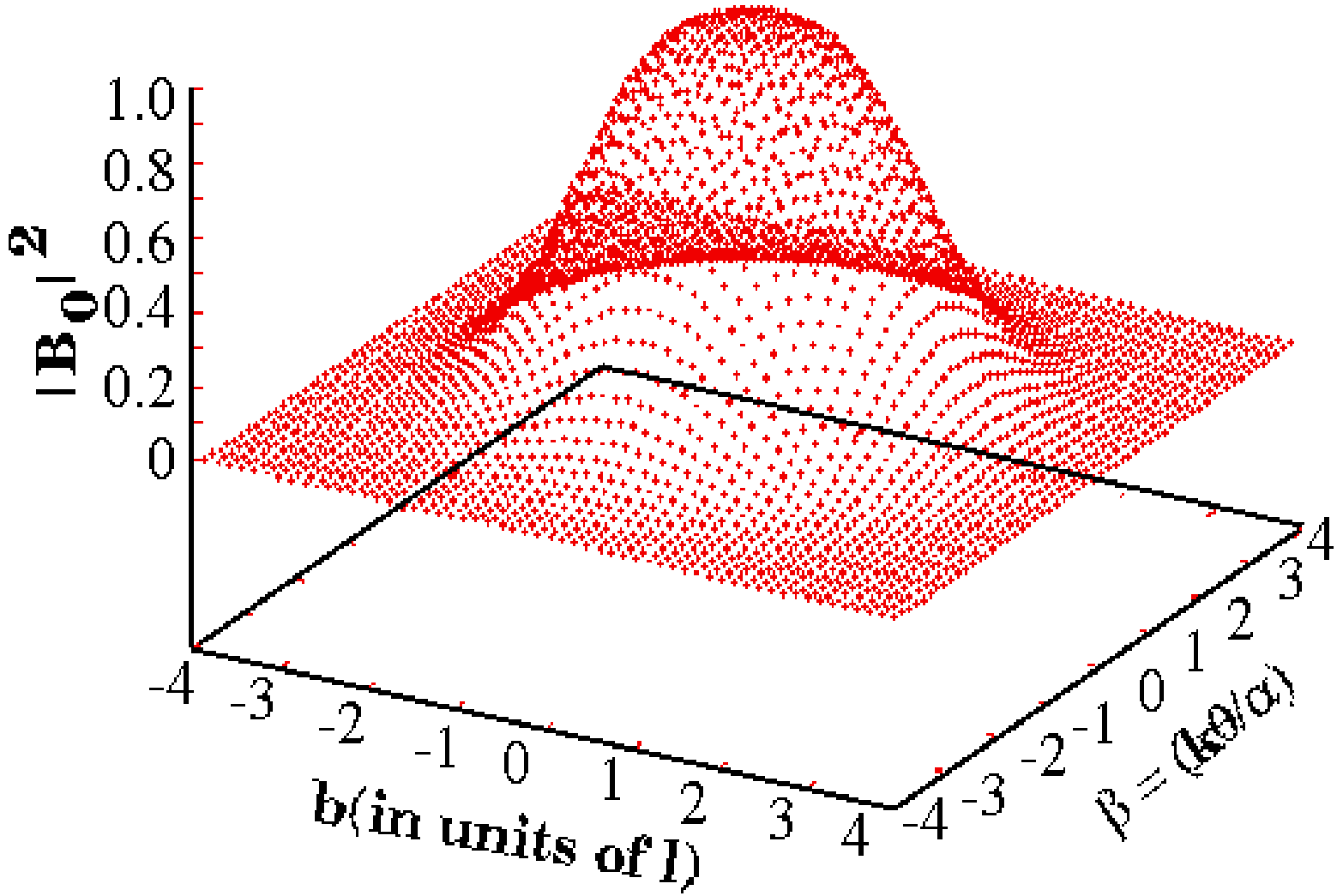
1.0
0.8
0.6
0.4
0.2
0
$|B_0|^2$
-4
-3
-2
-1
0
1
2
3
4
b(in units of l)
-4
-3
-2
-1
0
1
2
3
4
$\beta = (k\theta/\alpha)$

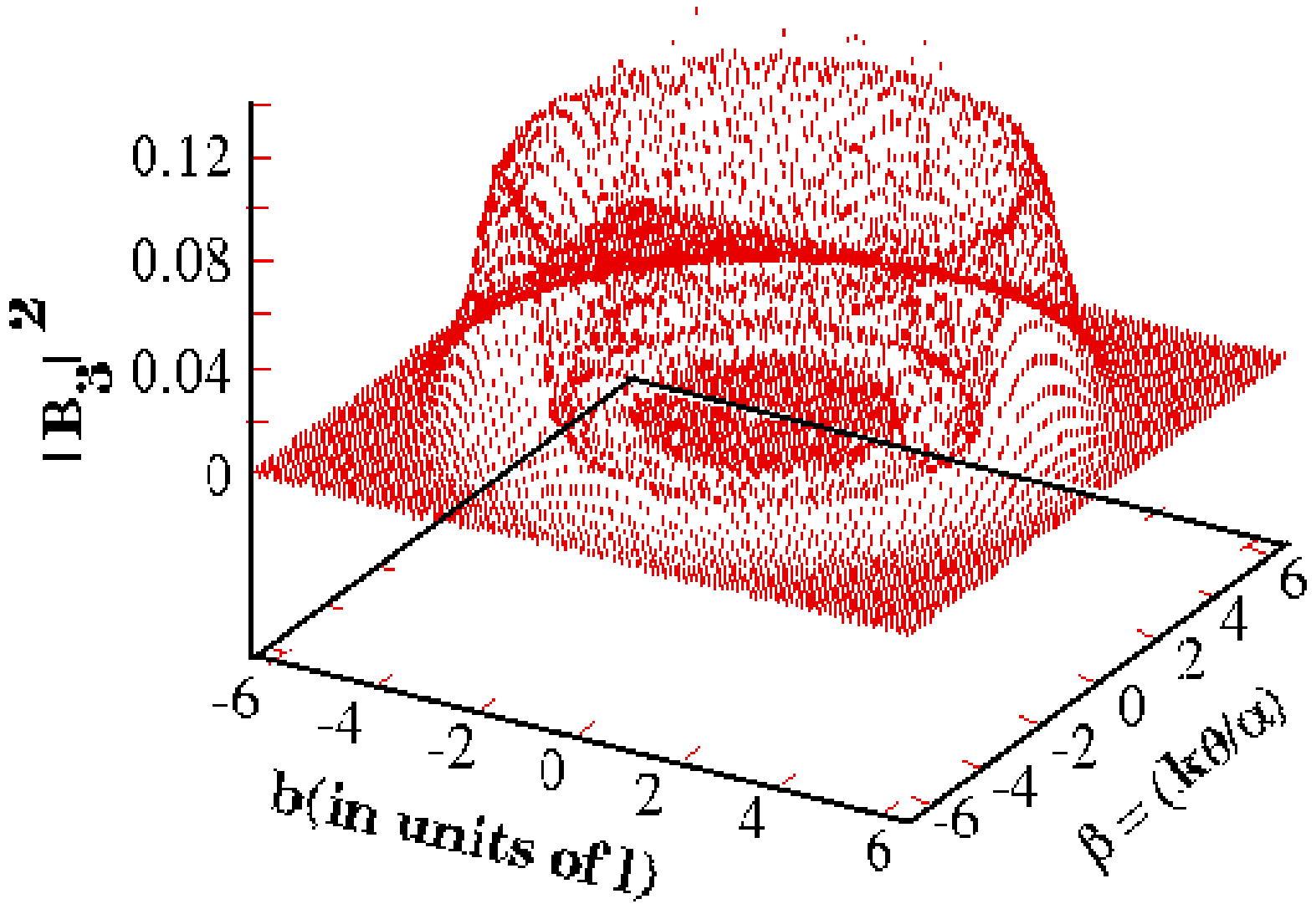
0.12
0.08
0.04
0
$|B_{-3}|^2$
-6
-4
-2
0
2
4
6
b(in units of l)
-6
-4
-2
0
2
4
6
$\beta = (k\theta/\alpha)$

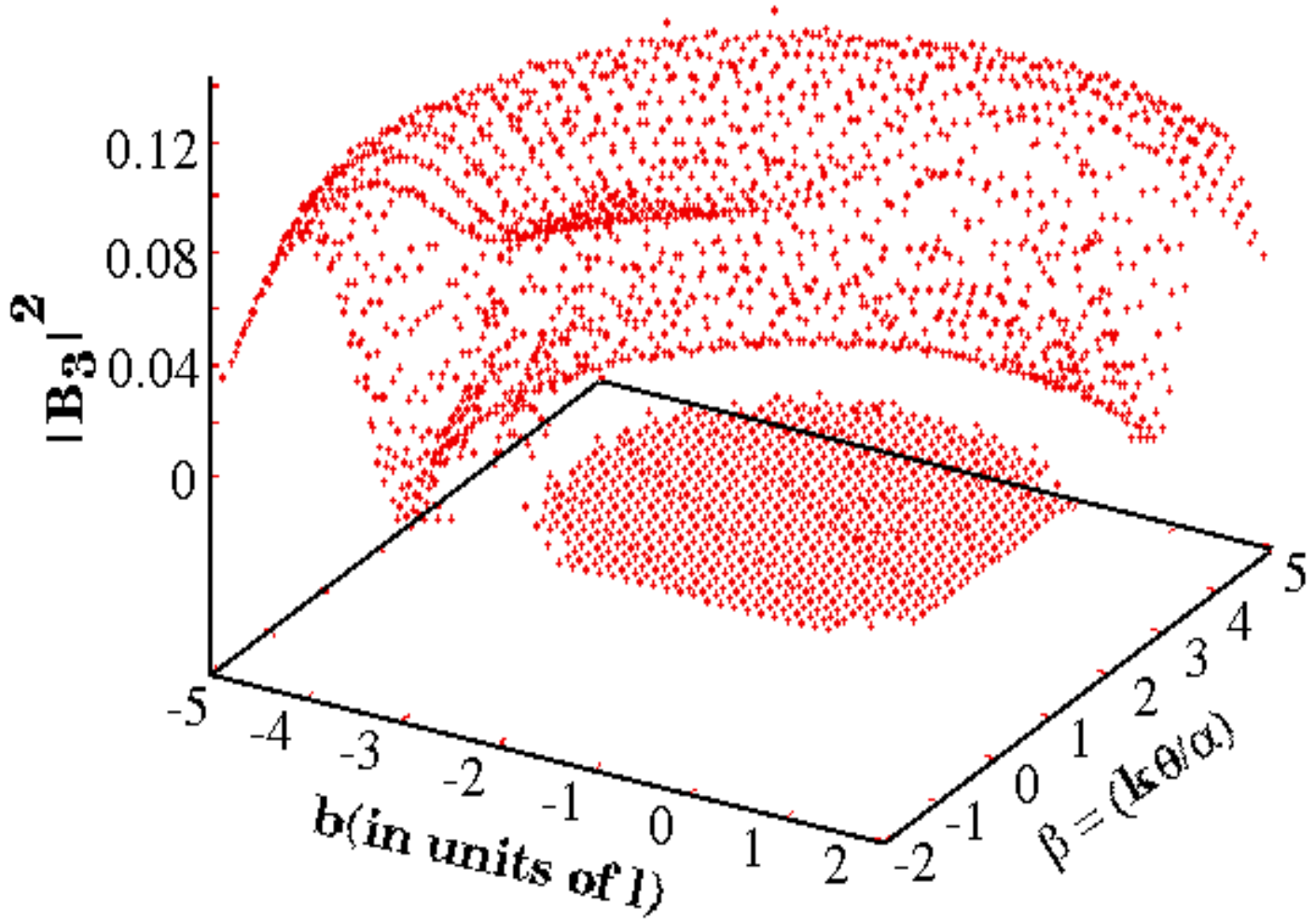
0.12
0.08
0.04
0
$|B_3|^2$
-5
-4
-3
-2
-1
0
1
2
b(in units of l)
-2
-1
0
1
2
3
4
5
$\beta = (k\theta/\alpha)$

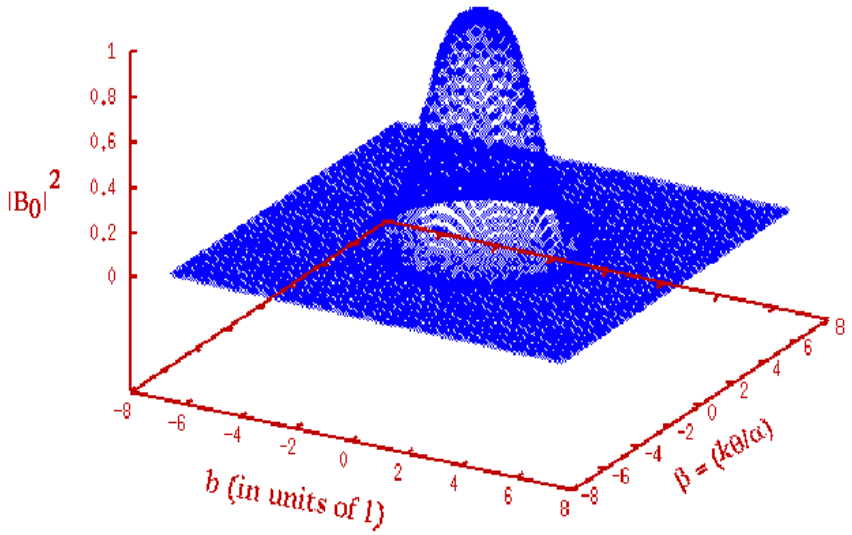
$|B_0|^2$
b (in units of l)
β = (kθl/α)

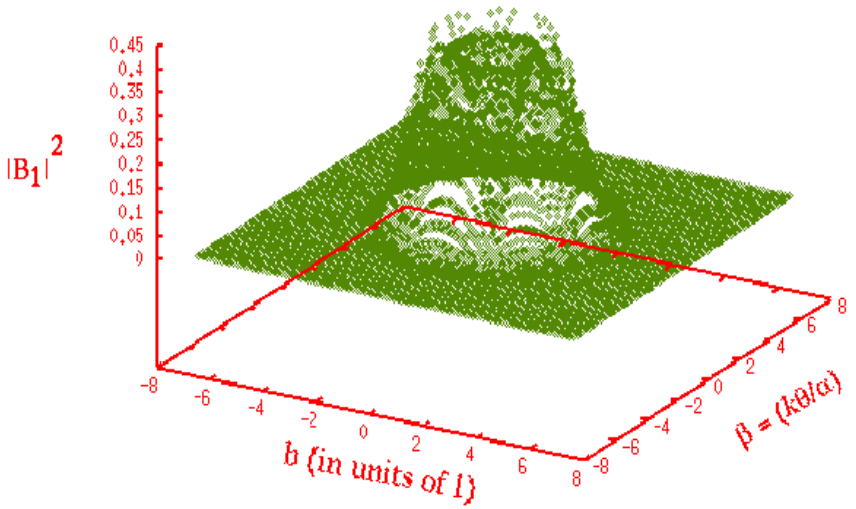
$|B_1|^2$
b (in units of l)
β = (kθl/α)

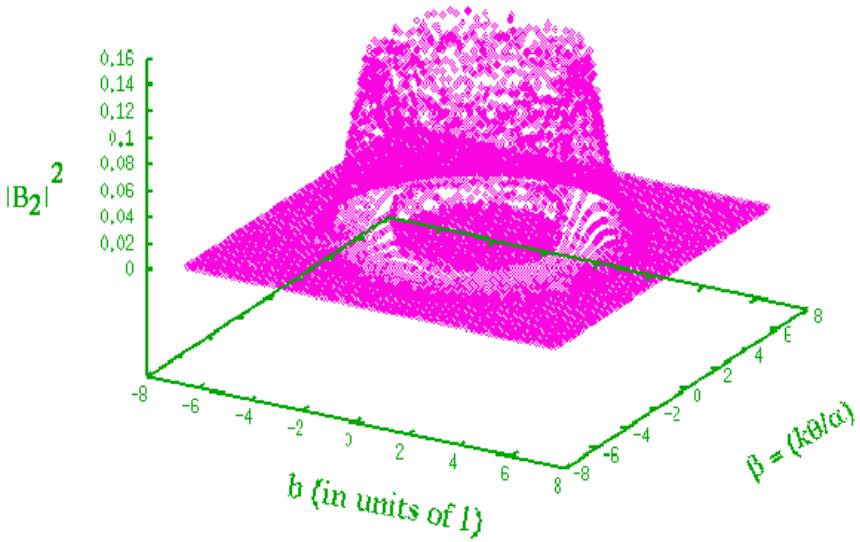
$|B_2|^2$
b (in units of l)
β = (kθl/α)

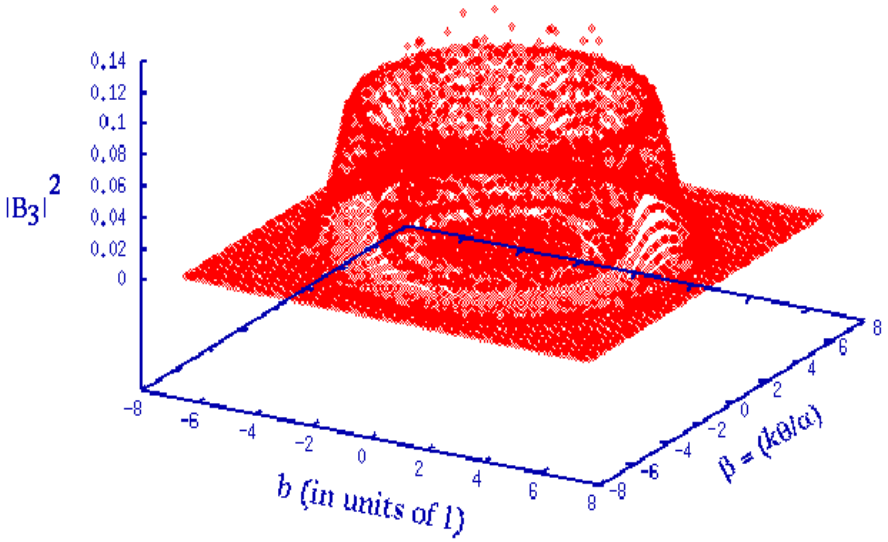
$|B_3|^2$
b (in units of l)
β = (kθl/α)

- Maximum probability is observed when both shift and tilt is zero as exp because ground is most populated in the case of positron channeling.

- However excited states have lower occupation probability even after pas the defected region also. For the higher states, it is observed that the channeling is enhanced if the shift and /or tilt is grater than zero.

- Hence the tendency of occupying higher states is more in the presence o defects.

- Such transitions between the states contributes to the intrinsic channelin radiation caused by spontaneous transitions.

- Hence it is necessary to take these effects in to account while calculating radiation intensity and other radiation characteristics.

The complexity involved in the electronic wave functions, reflects on the analytical approach to obtain the equivalent expression and these calculations are carried out using *Mathematica* ™.

These expressions obtained for population redistribution can be used for calculating the radiation intensities as well as the angular scans.

CONCLUSIONS

Expressions for the initial population of different states at the surface of an SLS and for the population re-distribution due to the strain/shift preset at the interfaces are obtained quantum mechanically.

The expression for initial population reveals the channeling angular scans that are generally performed and on the other hand the expression for population re-distribution helps in determining the tilt or shift existing in the system.

The tendency of occupying higher states is more in the presence of defects.

Thank You

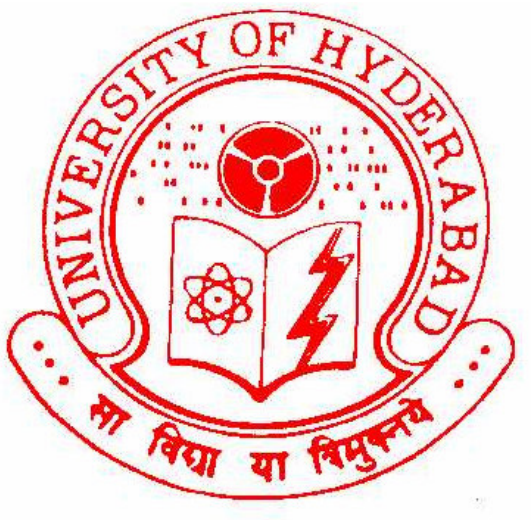

HCU, Hyderabad

NSC, New Delhi

India

IOP, Bhubaneswar

IGCAR Kalpakkam

SSPL, Delhi